BI-AXIAL TESTING OF ZINC AND ZINC ALLOY SHEETS UNDER SUPERIMPOSED HYDROSTATIC PRESSURES

BI-AXIAL TESTING OF ZINC AND ZINC ALLOY SHEETS UNDER SUPERIMPOSED HYDROSTATIC PRESSURES

by

HARJEET S. SANDHU, B.Eng. (Mech.)

A Thesis

Submitted to the School of Graduate Studies

in Partial Fulfilment of the Requirements

for the Degree

Master of Engineering

(Production)

McMaster University

July 1973

MASTER OF ENGINEERING (1973) McMaster University
(Production) Hamilton, Ontario.

TITLE: Bi-Axial Testing of Zinc and Zinc Alloy Sheets under Superimposed Hydrostatic Pressures.

AUTHOR: Harjeet S. Sandhu, B.Eng. (Govt. College of Engineering and Technology, Raipur, India.)

SUPERVISOR: Dr. R. Sowerby

NUMBER OF PAGES: viii, 133.

SCOPE AND CONTENTS:

The effects of pressurization on the properties of metals has long been of interest to scientists. Bridgman found that in general, the ductility (ability of the metal to deform without fracture) increased with superimposed hydrostatic pressure. Pugh et al. confirmed similar findings.

The effects of hydrostatic pressure on the mechanical properties of thin anisotropic zinc, heat treated and non heat treated zinc alloy sheets subjected to biaxial tension (via the circular bulge test) is investigated in this project.

A brief look is taken into the generalized conditions for the onset of tensile plastic instability in a thin circular diaphragm bulged under superimposed hydrostatic pressure. The material is assumed to obey Hill's theory of yielding for anisotropic materials. These predictions are verified by conducting bulge tests using back pressures up to 10,000 nsi. It is concluded that within the pressure range of investigation there is no detectable changes in the properties of the materials tested.

In the appendix section a brief look is taken into the microstructure of the materials tested.

Acknowledgement

The author would like to express his sincere gratitude to Dr. R. Sowerby for his advice and encouragement throughout the course of this work. Thanks are also due to the Department of Mechanical Engineering, University of Waterloo for loaning the equipment thereby saving considerable time and effort.

In addition the author gratefully acknowledges the help offered by Mr. Hodgeson, Material Sciences, McMaster University and Mr. Piercy of Cominco in helping with the micro analysis of the material. Mr. Whitehouse who helped start the project in the initial stages and others who have directly or indirectly helped in completing this work.

Last but not the least Miss BettyAnne Bedell for so cheerfully typing the thesis. Most of the work reported here was supported by grants from the National Research Council of Canada and is gratefully acknowledged.

TABLE OF CONTENTS

NOTATION

x_1, x_2, x_3	=	Directions of principal axes of anisotropy in the sheet. x_1 being in the direction of rolling, x_2 transverse to the rolling direction and x_3 perpendicular to the plane of the sheet.
$\bar{x}_1$, $\bar{x}_2$, $\bar{x}_3$	=	Cartesian coordinate axes of reference.
θ or α	=	Angle measured anticlockwise to the rolling direction.
ℓ_0, w_0, t_0	=	Original length, width and thickness respectively.
ℓ, w, t	=	Current length, width and thickness respectively.
σ, ε, $d\varepsilon$	=	Stress, strain and strain increments.
$\bar{\sigma}$, $\bar{\varepsilon}$, $d\bar{\varepsilon}$	=	Representative stress, strain and strain increments.
A, n	=	Constants in the empirical stress-strain relation $\bar{\sigma} = A\,\bar{\varepsilon}^{\,n}$.
F, G, H, N	=	Anisotropic constants for the material, Hill's notation.
I	=	F + G + H
Q	=	FG + GH + HF
P	=	Load
R	=	Normal anisotropy
ΔR	=	Planar anisotropy
$\bar{R}$	=	Average normal anisotropy

$d\lambda$	=	is the ratio of proportionality in the Levy-mises equation.
h	=	Height of the bulge at the pole.
ρ	=	Radius of curvature.
p_i	=	Pressure on the inner side of the bulge.
p_o	=	Pressure on the outer side of the bulge.
W	=	Work done
a	=	Die radius

CHAPTER I

INTRODUCTION

1.1. Introduction

The art of sheet metal forming stretches back to times immemorable. In this present era of space age technology, sheet metal forming is playing an ever increasing important role. Every day millions of components are pressed from sheet metal under varying conditions, and small changes in material properties can make the difference between success or scrap metal. Scientists are continuously on the look out for different and better means of changing the shape of sheet metal into intricate forms and there have been a lot of brilliant achievements. The once thought of concept "This is impossible to do" applies no more.

The principal purpose of sheet metal testing is to determine the forming characteristics (limits) under varying conditions of temperature, pressure and techniques. The theory of plasticity has given a better insight into the nature of deformation but, the existing theories in general have not been able to adequately describe the rheological behaviour of materials.

From the sheet forming point of view, the situation is not very different. In a large number of forming operations, the process is essentially one of plane stress (at least over certain sections of the deforming sheet) and hence one of the principal stresses can be regarded as zero. Although in principle, this

should simplify the problem, sheet metal forming is still a complicated combination of stretching, drawing, bending, shearing, piercing, etc. [1]. Certain formability tests have been devised to determine the limit to which the metal can be strained during any specific operation. Since most forming operations are a complex combination of stretching and drawing, the applicability of tests such as the simulative test (Erichsen and Olsen test, Swift draw test, etc.) are designed to represent one or more important features of the forming operation. The non-simulative tests on the other hand, used for assessing such material properties like strain hardening, degree of anisotropy, measure of ductility, etc. are not too helpful in understanding the material behaviour under complex stress systems encountered in practical problems. The generalized strain at instability as a measure of the "effective ductility" seems to be the most general and rational so far. It is valid for all stress systems; and for simple geometric configurations can often be calculated quite easily.

It is recognized that ductility is not just a property of the material but, is controlled by the stress system which in turn is induced by the forming operation. Goodwin [2] examined the principal strains at the failure site in biaxially stretched sheet by measuring the dimensions of the actual fracture surface. He found that the maximum tensile strain at the fracture site was least for a process of approximately plane strain and greatest for one of nominal equal biaxial tension as shown in Fig. (1.1).

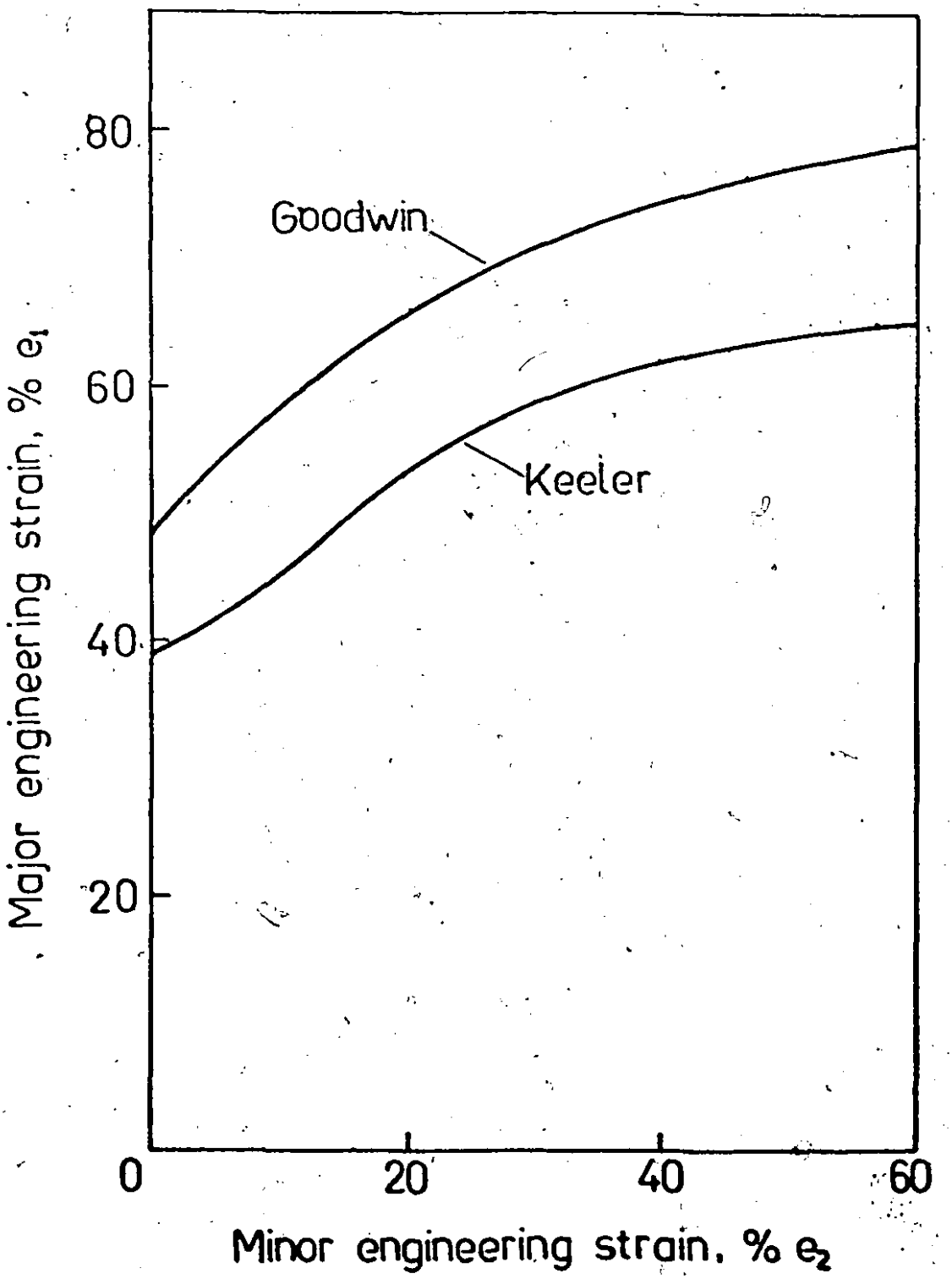

FIG. 1.1 KEELER-GOODWIN FORMABILITY CURVE

Keeler and Backofen [3] examined limit strain* in sheet metal subject to varying amounts of biaxial tension and plotted a similar diagram. Fig. (1.1) shows that there is a significant difference between the maximum strain at the fracture site - the Goodwin curve - and the limit strain - the Keeler curve - this suggests that there is some very localized deformation process which precedes actual fracture in a biaxial stretching process. It is unlikely, therefore, that the maximum useful strain in a process - the limit strain - can be predicted theoretically either by consideration of fracture alone or simply from a stability or diffuse necking analysis. This work has recently been extended by Marciniak [4] and Sowerby and Duncan [5] who showed that it was possible to obtain the forming limit diagrams theoretically. The analysis assumes an initial inhomogeneity in the sheet at which fracture finally takes place by forming a localized neck. The theory is capable of covering all stress states from plane strain ($\sigma_1/\sigma_2 = 2$) to balanced biaxial tension ($\sigma_1/\sigma_2 = 1$) and to include such material parameters as the n and R-value in the analysis.

---

* It is convenient to use the term "limit strain" to describe the strain in a fractured sheet near to the rupture but measured in a region clear of any zone of localized plastic deformation associated with fracture or a localized neck.

1.2. Choice of Problem

The work presented in this thesis uses an instability analysis approach similar to the one used by Kular [6]. The main problem investigated was the effect of hydrostatic pressure on the instability strain (stress-strain characteristic) in a biaxial stress system. The work extends a familiar two-dimensional forming operation, that of forming a clamped circular diaphragm with hydraulic pressure, by introducing a back pressure. A brief discussion of the bulge test follows in the next section.

Bridgman [7] has shown that plastic deformation without fracture may be significantly increased with the co-operation of hydrostatic pressure or sometimes other forms of stress. Similar results were reported by other workers for extrusion of metals under pressure. Starting from a work principle Hillier [8, 9] derived the conditions for instability under complex stresses for isotropic as well as for orthotropic materials. Hillier [10] also showed that for simple forming processes the instability strain increases with hydrosatic pressure. There were two remarkable points about his calculations: firstly, they seemed to explain the increase in plasticity with pressure as qualitatively demonstrated by Bridgman, and secondly, the effect predicted could be checked experimentally even at relatively easily attainable pressures.

From the practical point of view the study of instability is important because the onset of instability can be regarded as the limit of useful plastic deformation in forming process. From the theoretical point of view, instability marks the end of the

easily investigable plastic range where the theory of plasticity can be experimentally verified. Moreover for simple thin shell configurations, experiments can be set up with relative ease. In fact many solutions for simple two-dimensional instability problems can be found in standard texts on plasticity, e.g., Johnson and Mellor [18]. The choice of the bulge test for this investigation lies in the relative ease with which the experiments can be performed. The bulge test is advantageous because

i) There is no uncertain friction effect to be taken into account.

ii) The specimen can be easily cut from sheet metal whose stress-strain properties and the degree of anisotropy can be determined with reasonable accuracy.

iii) The stress and strain at the pole can be easily controlled.

iv) Most important of all, the stress state at the pole is known.

Other methods of realizing biaxial stress systems have been used but the instability strain in the bulge test is greater than most other systems in particular uniaxial tension which is widely used in determining the ductility of the material. Thus if the theory in this case relates well with the experimental results, then it should hold good for most of the processes and stress configurations used in sheet forming, because all of them have instability strains smaller than this case.

Since most of the available experimental data investigating instability in biaxial tension are for materials with an unknown degree of anisotropy; it is really

necessary to include anisotropy in the theoretical models in order to increase the accuracy of the predictions. Also, for isotropic materials most of the problems involving shear and direct stresses can be reduced to those involving the principal direct stresses or only the maximum shear stresses because the principal axes of strain increments always coincide with those of the stresses. For anisotropic materials such a simplification cannot always be effected because the principal axis of stress and strain increment do not coincide except in the principal directions of anisotropy. Thus the inclusion of anisotropy in plasticity equations is likely to become an important factor in explaining the form of the yield function when direct and shear stresses are simultaneously involved.

1.3 Literature Survey

In this section a very brief review of the research papers on the bulge test is given, followed by a review of the findings of Bridgman [7] and Pugh [11, 12] on their work with various metals under hydrostatic pressure.

The Bulge Test

The first attempts to understand the bulge test were experimental. Sachs, Espey and Kasik [13] bulged aluminum diaphragms at room and elevated temperatures up to 500°F. They found that the strain distribution was non uniform along the profile and also, that the limit of uniform straining increased and the maximum pressure decreased with increasing temperature if it was higher that a critical range between 250°F and 400°F.

It was also shown that the bulge is a surface of revolution and is very close to a sphere near the pole. Brown and Thompson [14] used five different types of annealed and hardened low carbon steels. They plotted the stress strain curve for the bulge test and found it to be almost coincident to that of a tension test. They found the strains to be maximum at the pole and that the average radius of curvature of the profile decreases towards the die at small bulge heights, but increased towards the die at more advanced stages.

The theoretical solutions of the bulge test fall into three types: those using total strain theory, those using incremental theory and von Mises yield criterion and those using Tresca yield criterion and the associated flow rule.

The first theoretical solution is due to Gleyzal [15] and thereafter various combinations of different theories have been used by various authors. The theoretical predictions and experimental results have tied in fairly well depending on the type of solution used and also upon the material properties.

In the 1950's Mellor and Loxley bulged diaphragms of eight different types of annealed as well as hardened common sheet materials and concluded that annealed materials exhibit instability while strain hardened ones fracture under increasing pressure, and that the strain distribution, bulge height and curvature depended upon the material properties. They found that Hill's [16] solution for linear strain-hardening materials gave good correlation for strain hardened materials but the agreement between Hill's solution and other experimental values for annealed

materials was poor.

Effects of Hydrostatic Pressure on the Properties of Metals

The effects of pressurization on the properties of metals has long been of interest to scientists, although till today there are but a few theories which allow quantitative predictions to be made to this effect. Although studies on the plastic behaviour of metals under hydrostatic pressure were first conducted by Ross and Eichinger (1929), the most extensive investigations were made during world war II by Bridgman [7], and his work has served as a model for most of the subsequent investigations in this direction.

As a result of studies on a wide variety of metals by several workers, it has been found that in general the ductility (ability to deform without fracture) increased with hydrostatic pressure. Bridgman found that for all but two steels he tested, the ductility was linear with pressure*. These results have been confirmed by other workers. Pugh [11, 12] et al. studied the behaviour of both brittle and ductile materials under pressure and confirmed an increase in ductility with pressure for all metals tested, and a linear increase in the case of steel.

---

* The pressures have not been mentioned because of the generality of the literature survey, but they vary in the range of 20,000 - 200,000 psi. Also some names have been mentioned without any reference in the reference section. This being due to the unavailability of the relevant papers.

For zinc and mazak, Pugh demonstrated for the first time the existence of a sudden pressure induced transition from brittle to ductile behaviour. The metal initially showed little or no change in ductility up to a certain pressure, but above this critical pressure they showed a sudden increase in ductility, and behaved like perfectly ductile materials. Pugh suggested that this sudden transition could be expected in hexagonal metals whose slip systems are normally confined to the basal plane by the operation of new slip systems above a critical pressure. Later Pugh and Green explained this sudden transition in zinc and mazak. It was assumed that the stress-strain relationship is a basic property of the material, but that fracture was measured by some absolute value of the tensile stress. Thus in a tensile test under hydrostatic pressure, a large tensile stress is required for fracture in order to offset the compressive stress due to the pressure so that the not tensile stress achieves the critical value for fracture. Thus a material with a stress-strain curve as shown in Fig. 1.2a will fracture at A when tested in tension at atmospheric pressure, as the critical value of maximum tensile stress is satisfied at this point. In a tensile test under hydrostatic pressure, compressive stresses are induced in the specimen upon which a large tensile stress (point B) has to be superimposed to satisfy the fracture criterion. At a higher pressure the fracture is delayed further to point C. In a material with a flat topped stress-strain curve [Fig. 1.2b] only a small change in hydrostatic pressure is required to increase the

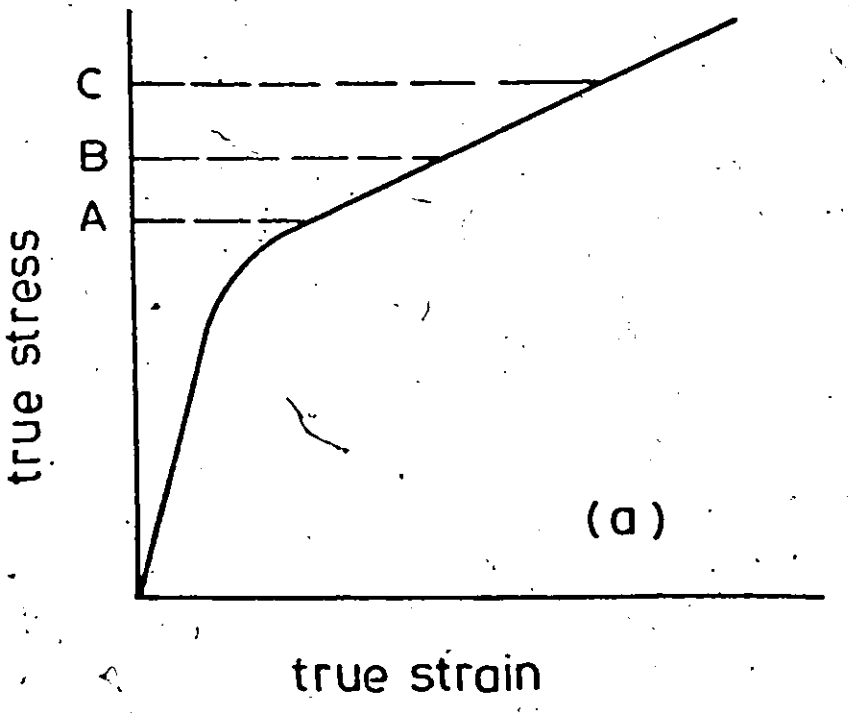

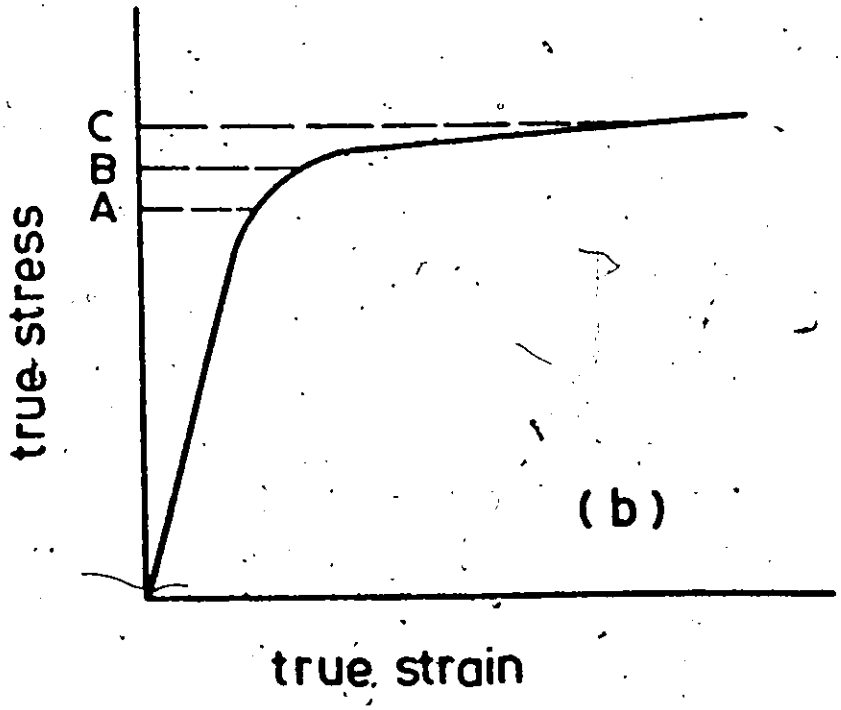

FIG. 1.2 STRESS-STRAIN CURVE AFTER PUGH & GREEN

fracture stress from B to C, producing a large change in strain and thus a sharp transition from brittle to ductile behaviour. This explanation which suggests a direct connection between the abruptness of the brittle to ductile transition and the rate of work hardening was later confirmed when the stress-strain curve for zinc was found to be flat topped.

Some workers have studied the effects of hydrostatic pressure on the yield stress of metals and the results have been very contradictory. The ultimate conclusion drawn was that hydrostatic pressure had no significant effect on yield or flow stress of metals, at least in the pressure range investigated.

Bridgman's inital studies led him to conclude that hydrostatic pressure caused a linear increase in tensile strength. He also found that the strain at maximum load was independent of pressure for some metals implying that the stress-strain curve changed with hydrostatic pressure. Other workers have also found that the tensile strength for all metals tested increased with pressure and at times the increases measured were quite large and these were also contrary to Bridgman's results. It was thought that maybe the results were not accurate as the loads were measured outside the high pressure container. Later Pugh performed tensile tests on zinc, copper, etc. Repeated tests under the same conditions showed good reproducibility and showed that static pressure had no effect on the tensile strength nor had it an effect on the strain corresponding to the maximum load.

As a result of these experimental findings Pugh questioned the validity of the widely accepted solution of an associated problem, namely "that a transverse hydrostatic pressure superimposed on a tensile specimen delayed the onset of necking and resulted in an increased uniform elongation." In 1963 Pugh showed that the mathematical analysis on which many workers for several years had based their results was in error, and it was subsequently conceded that Pugh's analysis was correct. This analysis is basically as follows.

Suppose a tensile specimen is subjected to a tensile stress σ_T and a transverse hydrostatic pressure p (p is negative for a hydrostatic pressure). Now the representative stress for yielding or flow in this combined stress system depends on $(\sigma_T - p)$ whether the Tresca or Huber-Mises-Hencky criterion is used. Thus the origin of the curve of σ_T vs engineering strain e is at $e = 0$ and $(\sigma_T - p) = 0$ or $\sigma_T = p$. The effective load L on the specimen is therefore $(\sigma_T - p)\,A$, where A is its cross-sectional area. Necking starts when the load reaches a maximum value, and so at instability

$$dL = 0 = (\sigma_T - p)dA + A\,d(\sigma_T - p)$$

or

$$\frac{d(\sigma_T - p)}{(\sigma_T - p)} = -\frac{dA}{A} = \frac{de}{1+e}$$

or

$$\frac{d(\sigma_T - p)}{de} = \frac{d\sigma_T}{de} = \frac{(\sigma_T - p)}{1+e}$$

for a test at constant pressure. Thus the necking point is a

point of tangency to the (σ_T, e) curve from the point (-1, p). For the normal tensile test, p = 0, so the tangent is drawn from the point (-1, 0) to the stress-strain curve whose origin is at the point e = 0, σ_T = 0. Thus for the tensile test under a transverse hydrostatic pressure p, both the point and the curve have been displaced by p along the stress axis. Hence both strain and representative stress (σ_T - p) at the maximum load point are unaffected by the transverse hydrostatic pressure.

Bridgman obtained true stress-strain curves for the materials he tested. As a result of numerous tension tests, particularly on steel, it was concluded that to a first approximation, the stress-strain curve is independent of pressure. Again some other workers concluded that hydrostatic pressure did raise the stress-strain curve for certain materials. Therefore, although in a few cases, some of which are open to criticism, contradictory results have been obtained, the results to date show that for materials tested, pressure has little or no effect on the stress-strain curves of metals.

Conclusions

Studies of mechanical properties of metals and alloys under combined stress conditions have produced only a partial explanation of some interesting problems of flow and fracture of materials. The results of different workers have often been contradictory, making it imperative to further improve the research methods and techniques, particularly those concerned with the accuracy of stress measurement.

Tension and torsion tests have shown an increase in the strain to fracture with pressure. The increase in ductility varied for different metals. Materials brittle under atmospheric pressure have shown an abrupt increase in ductility above a certain transition pressure. The tensile strength is not or only slightly affected by pressure.

There is a need for more systematic investigation of mechanical tests as the random nature of previous tests on different materials and the use of different testing methods makes the comparison and analysis of results difficult.

1.4. Applications of Hydrostatic Pressure

Progress in many branches of technology has led to a demand for and the development of new materials. However, materials with the desired properties are of limited value if they cannot be economically formed into the required shapes. It is frequently true that materials, particularly the newer materials with the desired properties are difficult to form either on account of their inherent strength or because of their lack of ductility, or both. The increasing demand for these difficult-to-form metals has been one of the most important factors in the development of new methods of forming in recent years.

Two developments, viz., hydrostatic extrusion, and the application of hydrostatic pressures to the forming of metals, represent new and revolutionary approaches to the field of cold forming. A brief description of the various aspects of hydrostatic pressure in the forming of metals follows.

ydrostatic Extrusion

Hydrostatic extrusion, which was first so named by ugh et al., is essentially a method of extruding a billet hrough a die using a pressurized fluid instead of the ram used n conventional processes with the pressurised fluid acting on he sides of the billet as well as on its back face.

At high extrusion ratios high pressures of up to 450,000 psi may be necessary, which in turn, require that the problem of container design must be overcome if the process is to be acceptable to industry.

The slight change in principle involved in hydrostatic extrusion results in significant technical advantages over the conventional process. Some of the more obvious advantages and features follow from the consideration of a process (Fig. 1.3). It is obvious from Fig. 1,3 that the friction at the billet-container interface is eliminated in hydrostatic extrusion, consequently the extrusion pressure does not increase with length of billet. Further since the pressurised fluid surrounds and gives lateral support to the billet, the stress system in the part of the billet outside the deformation zone in the die is hydrostatic, and equal in magnitude to the pressure in the liquid. Consequently, whatever its length, it is impossible to buckle the billet under the end load which is forcing the billet to extrude through the die. Thus, extremely long billets can be extruded in this way.

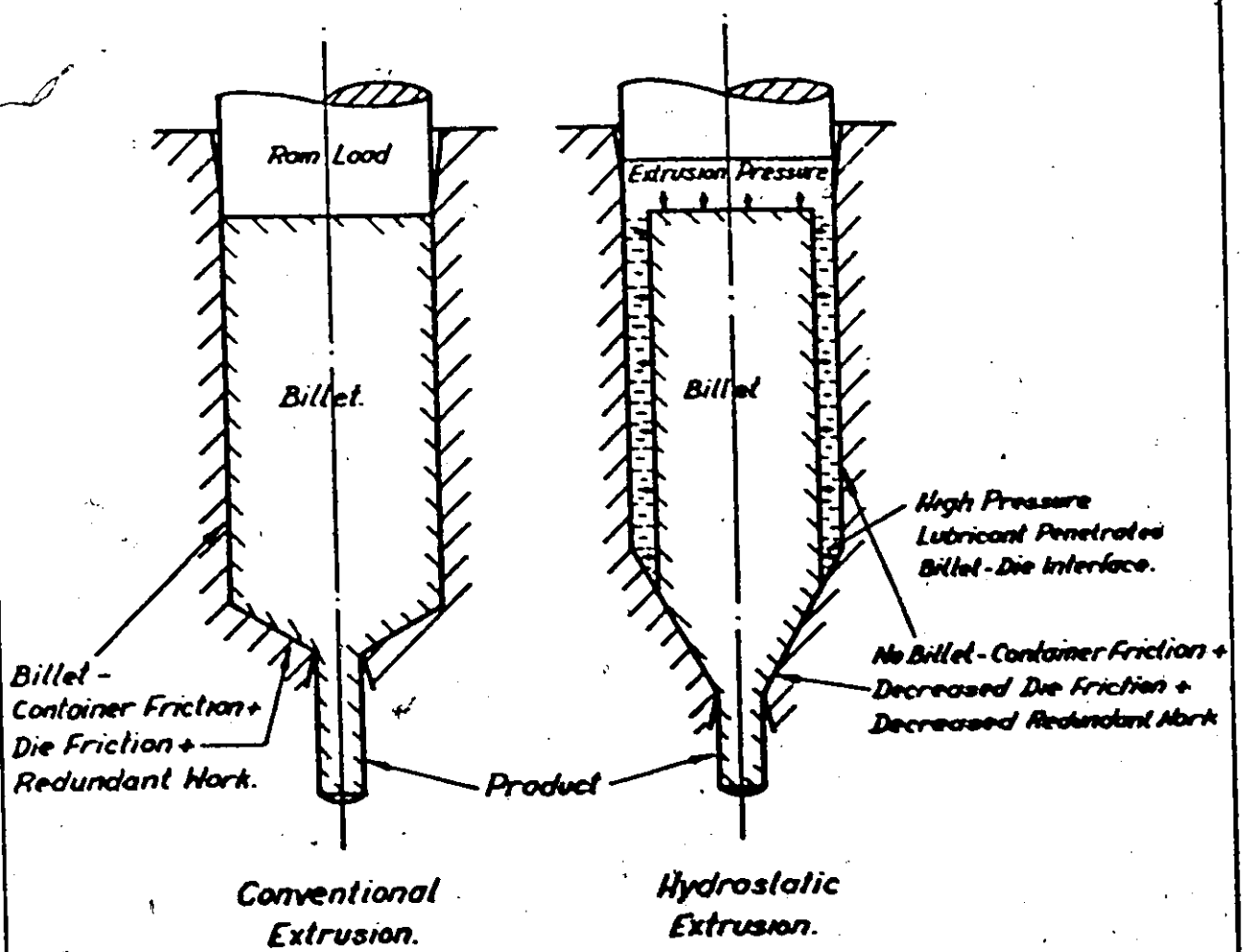

FIG. 1.3 COMPARISON OF CONVENTIONAL & HYDROSTATIC EXTRUSION

The only friction which occurs in hydrostatic extrusion is that between the billet and the die, but even this is low since the high pressure fluid is dragged along the billet-die interface during the extrusion. The extrusion pressure obtained under practical conditions by various workers showed that the pressure for hydrostatic extrusion is frequently 50% or more lower than for conventional extrusion. Other advantages being that billets of any shape and section can be extruded, and close tolerances are not necessary. Furthermore, the billets need not be of constant section along its length.

Disadvantages of the process are that, the billet has to be shaped at one end and held against the die to effect initial sealing. The use of liquid makes loading and unloading of billets in the container more complicated, and the repeated pressurisation and depressurisation requires particular attention to be paid to the design and material of the containers.

Conventional Extrusion against a Back Pressure

The application of hydrostatic pressure to the extrusion process described here involves principles concerned primarily with the modification to the work material rather than to the mechanics of the process. Bridgman in the results of his many investigations showed that the ductility of metals increased with pressure. Pugh et al., suggested that this increase in ductility with pressure explained the surprisingly large reduction of area that can be achieved without fracture in the conventional

extrusion process as compared with the relatively small strains obtained in conventional tensile tests. It also explains the success of many other forming processes in shaping metals without cracking.

Now consider the conventional extrusion of a brittle material, in which the product emerged in a cracked form. Pugh et al. suggested that this was due to the fact that the hydrostatic compressive stresses set up by the extrusion tooling were insufficient to inhibit cracking and that if these stresses could be augmented, for example by immersing the whole extrusion apparatus in a pressurised fluid, a sound uncracked product could be obtained. To test the validity of this hypothesis Pugh and Green carried out a series of experiments, both with the apparatus in an environment of atmospheric pressure and in a pressurised liquid, and confirmed the essential validity of the hypothesis. Experiments have been reported by other workers on the effect of back pressure on the high speed extrusion of zinc, mazak, magnesium, etc. and it was shown that, for extrusions without back pressure and at low speeds satisfactory products were got, but all products were broken or cracked at high speeds. The same materials when extruded at high speed, the use of back pressure resulted in a considerable improvement in the quality.

Differential Pressure (Fluid to Fluid) Extrusion

Differential pressure or fluid to fluid extrusion is a process combining the advantages of back pressure with those of hydrostatic extrusion. This method of extrusion is one of the few

known methods capable of cold forming brittle high strength materials such as alloys of the refractory metals, titanium, tungsten, etc. The equipment for differential pressure extrusion is basically the same as for hydrostatic extrusion except that the volume below the die is filled with a pressurised liquid whose value can be controlled in some convenient manner. The differential in pressure above and below the die must of course equal the extrusion pressure, which is determined by the extrusion conditions. Back pressure in the range of 10,000 - 300,000 psi have been used under varying conditions of tool geometry and metals.

Forging and Related Processes

Under this title, a brief look is taken into the application of hydrostatic pressure, on metal deforming processes in which the stress system is predominantely compressive, such as forging, flanging, bending, shearing, etc.

Bridgman reported work on the effect of prestraining under pressure on the residual atmospheric ductility. In his work using tempered steel, he found that every specimen pulled under pressure, always showed residual ductility when subsequently pulled in tension at atmospheric pressure. Pugh investigated the effects of compressive prestrain under pressure on the residual atmospheric compressive ductility of an aluminum alloy. Cylindrical specimens were compressed in castor oil that had been pressurised to 160,000 psi. After a given prestrain, the compression test was continued at atmospheric pressure until

fracture became apparent, and the results confirmed Bridgman's findings. The results of these experiments suggest that fracture is a consequence of some form of cumulative damage. If the cause of fracture is the opening up of cavaties, then the voids would not be formed so readily under the high hydrostatic pressure, thus yielding a product with less damage and improved properties, particularly of ductility.

Industrial developments on the forging, rolling, etc. of brittle metals have shown, that, by jacketing the metal with a strong ductile metal, successful forgings can be produced owihg to the constraints imposed by the jacket on the brittle metal. Thus steel has been used to jacket beryllium, refractory metals and superalloys for successful forging. Various techniques have been reported for applying restraining pressure in the working of beryllium. One technique for the closed die cold forging was to use a spring loaded annular punch, which applied pressure to the outer annulus of the beryllium while it was being deformed. As the forging punch was driven into the billet, the spring was further compressed, increasing the back pressure during the deformation. This spring loading due to size limitations can be replaced by hydraulic loading on the back pressure punch and the operation carried out in a hydraulic press with concentric rams.

Similarly research workers have shown application of hydrostatic pressure for the process of upsetting, bending, shearing, etc. of metals.

Drawing and Related Processes

Under this title a brief look is taken into the application of hydrostatic pressure on metal deforming processes which involve significant tensile stresses such as drawing processes.

It must be remembered that some metal working processes are limited by factors other than fracture and that such factors may not be affected to the same extent by hydrostatic pressure. It is known that the reduction of area in wire drawing and the draw ratio in deep drawing are limited to necking, and Pugh, both experimentally and theoretically also showed that the initiation of necking in a material under tension is quite unaffected by the pressure of a hydrostatic stress system. Hence to obtain the advantages associated with the application of hydrostatic pressure, it is necessary to remove the limitation imposed by necking. Thus attention has been directed to modification or inversion of those processes that are limited by necking, in such a way that although the starting billet and final product are still the same, no dominant tensile stresses can arise thereby eliminating conditions leading to necking.

In the conventional wire drawing process, the marked increase in strength produced by work hardening in the wire is accompanied by a reduction in ductility and the wire eventually becomes too hard and brittle for further drawing, thus setting a limit to the hardening that can be imparted by this process. Bridgman was the first to carry out wire drawing in a pressurised fluid. In contrast to the hydrostatic extrusion process, the pressure in the fluid above and below the die was the same. The

lower end of the billet after proper shaping was connected to a pull rod and the billet was drawn through the die. Piano wire .076 inches in diameter was drawn down under hydrostatic pressure of 168,000 psi to .026 inches in diameter in 6 passes without interstage annealing. At atmospheric pressure 15 passes were required without interstage annealing for the same reduction. The wire at this stage lost all capacity for further reduction and broke with no preliminary yield. It was also shown that up to a given strain, the flow stress was independent of pressure. However at greater strains, the flow stress of the specimen deformed at atmospheric pressure fell below that pulled under pressure. Thus showing that the application of hydrostatic pressure results in less damage and consequently improved residual properties in the material. Similar results were obtained by Pugh from tests on copper and steel.

The deep drawing of sheet in the presence of a pressurised liquid has received little attention. Some unpublished work by Pugh supported the conclusion that pressurisation did not increase draw ratio except for brittle metals which fractured before necking. Some work was done by Fuchs in this direction. Although the tooling for deep drawing under pressure was basically the same as for conventional drawing, the use of the surrounded high pressure liquid inverted the process and eliminated the unusual tensile stresses. The presence of a pressurised liquid above and below the annular surface of the blank eliminated friction between the blank and the hold down block and die. After the hold down block had been forced down on the blank, the pressurised liquid acting on

the perimeter forced the blank inward, and with the aid of the downward movement of the punch, which sized the bore, caused the blank to extrude between the punch and the die. As only a small force was exerted on the punch, the tensile stresses were considerably reduced. The pressure for this deep drawing operation was about 100,000 psi.

In their recent work on annealed 70/30 Brass and using a hydrostatic pressure of 300 atmospheres El-Sebale and Mellor [17] achieved a drawing ratio of 3.21 as compared to 2.81 at atmospheric pressure, further, with improved lubrication over the flange a drawing ratio of 3.447 was achieved.

Conclusions

The application of hydrostatic pressure to metal working processes has resulted in a variety of modifications that are of considerable importance, and in many cases have led to the development of new metal working processes that have considerable potential either as additions to or as superseding some of the existing methods. It may also be noticed that many features and advantages on the application of hydrostatic pressures to the various metal working processes were similar in nature.

CHAPTER 2

THE TENSILE TEST

2.1. Introduction

In this chapter the stress-strain properties and anisotropic parameters of the materials used in the experiments are determined with the help of simple tension tests.

The consideration regarding the choice of the materials and the working pressures are discussed in section 2.2.

Starting from a three-dimensional stress system, a brief discussion along with the formulations leading to representative stress and representative strain are carried out in section 2.3 (the formulations shown can be found in any text book on plasticity, e.g., Johnson and Mellor [18], Hill [19], etc.)

The theory of simple tension tests for isotropic and anisotropic sheets is given in section 2.4.

The experimental procedure for the tension tests is described in section 2.5.

The results of the tension tests are given in section 2.6.

2.2. Choice of Material and Working Pressure

Since the main objective of this project was to investigate the effect of pressure on the instability strain (stress-strain characteristics) in the bulge test, it was important to

choose the proper working pressure and materials. Our theoretical consideration (Equation (3.16)) indicated that pressure had no effect, where as Equation (3.18) formulated by Hillier [10] based on the thin membrane theory, indicated that this effect increases linearly with the ratio $\bar{p}/\bar{\sigma}$, where $\bar{p}$ is the average of the pressures inside and outside the bulge and $\bar{\sigma}$ is the representative stress in the material at instability. Because of the availability of an existing set up (for the bulge test with back pressure up to 10,000 psi) from the University of Waterloo it was decided to keep the investigation within the existing pressure range of the equipment.

For a given $\bar{p}$, to have a large value of the pressure effect it is necessary to maximize the ratio $\bar{p}/\bar{\sigma}$ (Equation (3.18)). Pugh in his work with metals under pressure had come up with a rather interesting finding. He demonstrated a sudden pressure induced transition from brittle to ductile behaviour in zinc and later, suggested that this transition could be expected in hexagonal metals. It was this interesting result of Pugh, combined with a low value of the constants A and n (zinc and zinc alloys) on which $\bar{\sigma}$ depends which prompted an investigation on these metals, namely, zinc, a heat treated and non-heat treated zinc alloy. It was decided to test these three metals and compare their behaviour under pressure.

The metals were supplied in sheet form by Matthiessen and Hegeler Zinc Company of La Salle, Illinois. The zinc sheet was sold under the trade number as LS-6 and the other two were called Titanaloy (heat-treated and non-heat treated). All the

three sheets were to be supplied .017" x 36" x 84", but on receiving the material it was realized that the sheets came as follows:

LS-6	-	.018"x 36" x 84"
Titanaloy (non-heat treated)	-	.020"x 36" x 84"
Titanaloy (Heat treated)	-	.021"x 36" x 84"

Furthermore it was realized that there was a considerable variation in thickness within a specific sheet. Due to the time factor involved in obtaining the sheets, it was decided to test them the way they were received.

On preliminary testing it was further realized that the zinc sheet (LS-6) had rolling defects and fractured prematurely, hence it was decided to abandon the testing of the zinc sheet and only test the remaining two sheets which have been referred to as the heat treated and non-heat treated material. In the Appendix a brief note about the suppliers comments as regards the material and the microstructure is looked into.

2.3. Representative Stress-Representative Strain Suffix Notation

A brief description on the suffix notation used for the stress and strain components related to an orthogonal co-ordinate system (say x, y, z or 1, 2, 3, etc.) in the chapters and sub-sections to follow is given below.

Direct stresses being defined as σ_{xx}, σ_{yy}, σ_{zz} or σ_{11}, σ_{22}, σ_{33} (often σ_{11} is simply written as σ_1, σ_{22} as σ_2 etc.)

Shear stress being defined as σ_{xy}, σ_{xz}, etc.

The double suffix notation is employed to define the direction of each of the stresses. σ_{xy} means the stress on a plane perpendicular to Ox and parallel to axis Oy. The first suffix gives the direction of the normal to the plane on which the stress acts, and the second one its direction with respect to that plane. Similar suffix notations are used for the strain components.

Determination of Principal Stresses in Three-Dimension

The six components of stress at a point are given in magnitude and direction as shown in Fig. 2.1. Suppose it is desired to evaluate the principal stresses and their directions at a point. (Principal stresses are stresses acting normal to a plane across which there is no shear stress.) Triangle ABC represents the oblique plane. N is a point in the plane ABC and ON is the normal to this plane. α, β and γ are the angles ON makes with the x, y and z axes respectively, and p is the principal stress. ON has directions cosines as follows:

$$\cos \alpha = \ell$$

$$\cos \beta = m$$

$$\cos \gamma = n$$

The stress p is related as follows:

$$\begin{aligned} s_x &= p.\ell \\ s_y &= p.m \\ s_z &= p.n \end{aligned} \qquad (2.1)$$

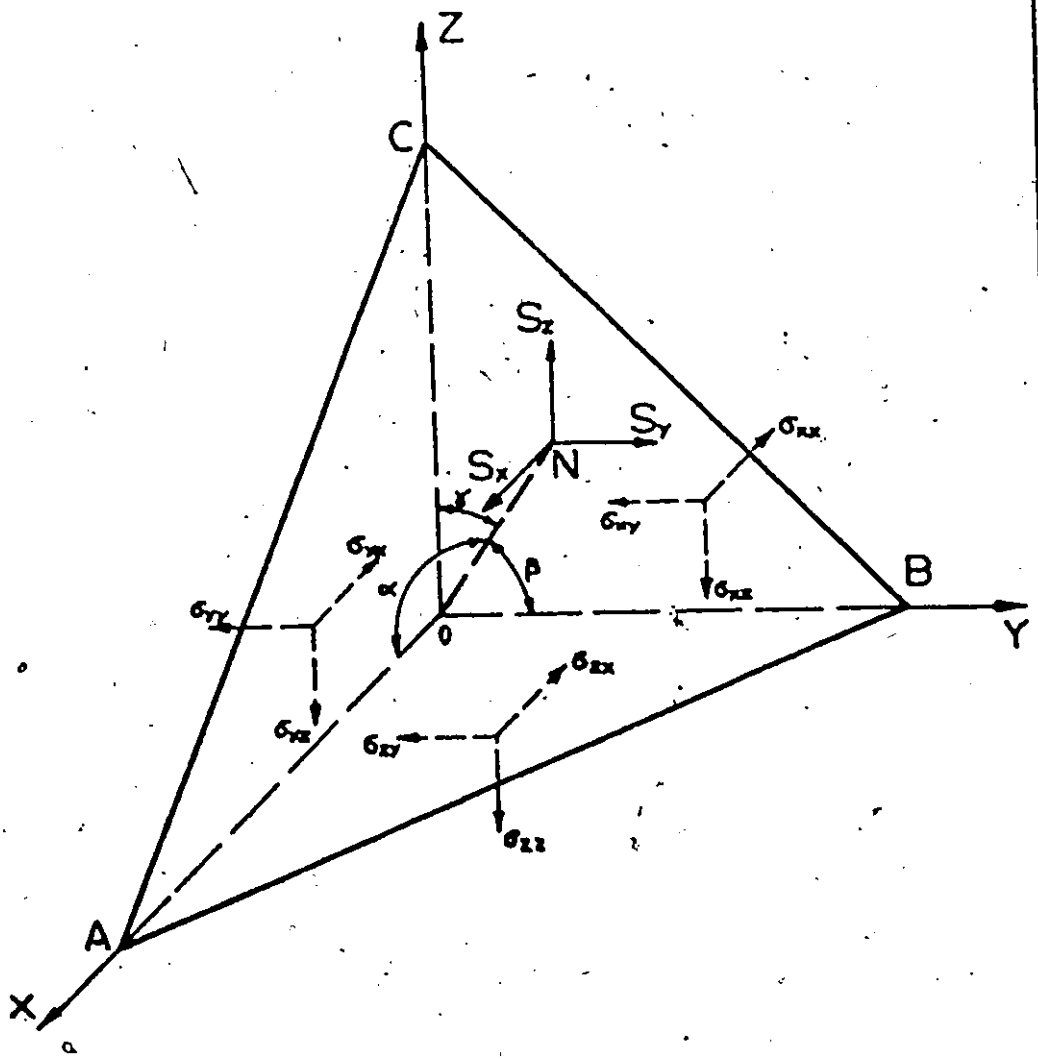

FIG. 2.1 STRESSES ON A DOUBLY OBLIQUE PLANE

he equilibrium of forces in the direction Ox.

$$\text{Area (ABC)} = \sigma_{xx} \cdot \text{Area (OBC)} + \sigma_{yx} \cdot \text{Area (OAC)} + \sigma_{zx} \cdot \text{Area (AOB)}$$

$$\therefore \quad s_x = \sigma_{xx} \cdot l + \sigma_{yx} \cdot m + \sigma_{zx} \cdot n$$

Similarly

$$s_y = \sigma_{yy} \cdot m + \sigma_{xy} \cdot l + \sigma_{zy} \cdot n \qquad (2.2)$$

$$s_z = \sigma_{zz} \cdot n + \sigma_{xz} \cdot l + \sigma_{yz} \cdot m$$

Hence from Equations (2.1) and (2.2) we get

$$(\sigma_{xx}-p)\, l + \sigma_{yx} \cdot m + \sigma_{zx} \cdot n = 0$$

$$(\sigma_{yy}-p)\, m + \sigma_{xy} \cdot l + \sigma_{zy} \cdot n = 0 \qquad (2.3)$$

$$(\sigma_{zz}-p) n + \sigma_{xz} \cdot l + \sigma_{yz} \cdot m = 0$$

Eliminating l, m and n from Equation (2.3) we get a cubic expression for p.

$$p^3-(\sigma_{xx}+\sigma_{yy}+\sigma_{zz})\, p^2-(\sigma_{xy}^2+ \sigma_{yz}^2+\sigma_{zx}^2-\sigma_{xx}\, \sigma_{yy}$$

$$-\sigma_{yy}\sigma_{zz}-\sigma_{zz}\sigma_{xx})\, p -(\sigma_{xx}\sigma_{yy}\sigma_{zz}+2\sigma_{xy}\sigma_{yz}\sigma_{zx} \qquad (2.4)$$

$$-\sigma_{xx}\sigma_{yz}^2-\sigma_{yy}\sigma_{zx}^2-\sigma_{zz}\sigma_{xy}^2) = 0$$

For simplicity Equation (2.4) is often expressed as

$$p^3 - I_1 p^2 - I_2 p - I_3 = 0 \qquad (2.5)$$

where

$$I_1 = \sigma_{xx} + \sigma_{yy} + \sigma_{zz} \tag{2.6}$$

$$I_2 = \sigma_{xy}^2 + \sigma_{yz}^2 + \sigma_{zx}^2 - \sigma_{xx}\sigma_{yy} - \sigma_{yy}\sigma_{zz} - \sigma_{zz}\sigma_{xx}$$

$$I_3 = \sigma_{xx}\sigma_{yy}\sigma_{zz} + 2\sigma_{xy}\sigma_{yz}\sigma_{zx} - \sigma_{xx}\sigma_{yz}^2 - \sigma_{yy}\sigma_{zx}^2 - \sigma_{zz}\sigma_{xy}^2$$

I_1, I_2 and I_3 are known as the first, second and third invariants of the stress tensor. [The word invariant is used simply because, if we selected another orthogonal co-ordinate system x_1, y_1, z_1 (instead of x, y z) then we would arrive at an expression similar to Equation (2.4), but σ_{xx} would be replaced by $\sigma_{x_1x_1}$, σ_{xy} by $\sigma_{x_1y_1}$ etc.] Since the values of p remain unchanged, then the values of I_1, I_2 and I_3 must remain unchanged. Also the cubic equation (2.5) in a real physical situation has three real solutions which are the principal stresses σ_1, σ_2 and σ_3 of this particular system and the values of I_1, I_2 and I_3 in terms of the principal stresses are

$$I_1 = \sigma_1 + \sigma_2 + \sigma_3$$

$$I_2 = -(\sigma_1\sigma_2 + \sigma_2\sigma_3 + \sigma_3\sigma_1) \tag{2.7}$$

$$I_3 = \sigma_1\sigma_2\sigma_3$$

Since plastic yielding can then depend only on the magnitude of the three principal applied stresses and not on their direction, any yield criterion should be a function of the three invariants as given by Equation (2.6) and the precise combination would depend

upon the material.

For many metals it is an experimental fact that yielding is unaffected by a moderate hydrostatic pressure, [defined as $\sigma_m = \frac{\sigma_{xx} + \sigma_{yy} + \sigma_{zz}}{3} = \frac{I_1}{3}$] either applied alone or superposed on some state of combined stresses. This leads to working in terms of reduced or deviatoric stresses defined as

$$\sigma'_{xx} = \sigma_{xx} - \sigma_m \quad \text{etc.} \tag{2.8}$$

The yield criterion now reduces to the form

$$p'^3 - J_2 p' - J_3 = 0 \tag{2.9}$$

where J_2 and J_3 replace I_2 and I_3 in Equations (2.5) and (2.6) simply by writing σ'_{xx} for σ_{xx} etc., and $J_1 = 0$, i.e., $\sigma'_{xx} + \sigma'_{yy} + \sigma'_{zz} = 0$.

Hence the yield criterion is now a function of J_2 and J_3, and these two invariants of the reduced stresses have special importance when considering the yielding of metals.

Tresca and von Mises Yield Criterion

The foregoing has demonstrated from a mathematical point of view that any yield function should be described by some combination of I_1, I_2 and I_3. The experimental fact that the hydrostatic pressure $\sigma_m = I_1/3$ does not influence the yielding of most common engineering materials leads to the conclusion that a yield criterion should be a function of J_2 and J_3. The

question remains what function?

The two yield criterion that have proved to be the most satisfactory for the yielding of isotropic materials are those ascribed to Tresca and von Mises.

The yield criterion of Tresca is expressed in its simplest form when written in terms of the principal stresses, namely.

$$|\sigma_{max} - \sigma_{min}| = \text{constant} \tag{2.10}$$

where σ_{max} and σ_{min} are the maximum and minimum of $(\sigma_1, \sigma_2, \sigma_3)$.

The Tresca criterion is often interpreted as: "yielding occurs when the maximum shear stress in the material reaches a critical value". The right hand side of Equation (2.10) is usually written as

$$|\sigma_{max} - \sigma_{min}| = 2k = y \tag{2.11}$$

where k is the yield shear stress and y is the yield stress in uniaxial tension. The Tresca criterion can also be expressed in terms of J_2 and J_3, but this tends to be too involved for general usage.

The von Mises criterion on the other hand can be shown to be equal to 6 J_2 and this is often expressed in principal stress components as

$$(\sigma_1-\sigma_2)^2 + (\sigma_2-\sigma_3)^2 + (\sigma_3-\sigma_1)^2 = 2\,y^2 = 6\,k^2 \tag{2.12}$$

or in terms of general components

$$(\sigma_{xx}-\sigma_{yy})^2 + (\sigma_{yy}-\sigma_{zz})^2 + (\sigma_{zz}-\sigma_{xx})^2 + 6(\sigma_{xy}^2+\sigma_{yz}^2+\sigma_{zx}^2)$$
$$= 2\,y^2 = 6\,k^2 \qquad (2.13)$$

k and y in Equations (2.12) and (2.13) have the same meaning as defined in Equation (2.11). When plotted in principal stress space Equation (2.12) provides a right circular cylinder whose axis is equally inclined to the principal stress axis. While Equation (2.11) describes a right hexagonal prism which is incribed inside the von Mises cylinder.

In this present work the von Mises criterion will be employed since this function avoids the singularities existing on the yield surface of the Tresca hexagon. It has already been stated that the hydrostatic stress does not cause yielding. From a geometrical point of view a hydrostatic stress state plots as a point on the axis of the cylinder. The radius of the cylinder dictates the current yield stress and this can be shown to be expressible in terms of the deviatoric stresses.

It is also conventional to replace the uniaxial yield stress y in Equation (2.12) by the symbol $\bar{\sigma}$ which is termed the representative stress. $\bar{\sigma}$ is really a measure of the current yield stress of the material and the simplest work hardening hypothesis is that the cylinder merely increases in diameter. Equation (2.13) can be rewritten as

$$\bar{\sigma} = \sqrt{\frac{1}{2}}\,[(\sigma_1-\sigma_2)^2 + (\sigma_2-\sigma_3)^2 + (\sigma_3-\sigma_1)^2]^{1/2} \qquad (2.14)$$

or in terms of deviatoric stresses as

$$\bar{\sigma} = \sqrt{\frac{3}{2}}\,[\sigma_1'^2 + \sigma_2'^2 + \sigma_3'^2]^{1/2} \qquad (2.15)$$

Similarly the representative strain ($\bar{\varepsilon}$) or representative strain increment ($d\bar{\varepsilon}$) is defined apart from the numerical factor, as a similar combination of the strain components and is given as

$$d\bar{\varepsilon} = \sqrt{\frac{2}{9}}\,[(d\varepsilon_1-d\varepsilon_2)^2 + (d\varepsilon_2-d\varepsilon_3)^2 + (d\varepsilon_3-d\varepsilon_1)^2]^{1/2} \qquad (2.16)$$

The factor $\frac{2}{9}$ being so chosen that $d\bar{\varepsilon} = d\varepsilon_1$ in a tensile test.

When a material is deformed plastically, it "work hardens". That is, as the material deforms, its resistance to further deformation increases. Our hypothesis is that the degree of hardening is a function only of the total plastic work and is otherwise independent of the strain path. Therefore

$$\bar{\sigma} = F \int dw = F \int \bar{\sigma}\, d\bar{\varepsilon}$$

and it follows that $\bar{\sigma}$ is a function only of $d\bar{\varepsilon}$ where the integral is taken over the strain path. Therefore

$$\bar{\sigma} = H \int d\bar{\varepsilon} \qquad (2.17)$$

where H is a certain function depending on the metal concerned.

The form of the relationship given by Equation (2.17) has led to the proposal of several empirical relationships between $\bar{\sigma}$ and $\bar{\varepsilon}$ and one of the most common being

$$\bar{\sigma} = A\,\bar{\varepsilon}^{n} \tag{2.18}$$

where A and n are constants and are usually determined experimentally for a given material from say, tensile tests, bulge tests, etc. and then plotting $\bar{\sigma}$ vs $\bar{\varepsilon}$ on a log-log graph paper.

The incremental strain components and the deviatoric stress component relationship is provided by the Levy-Mises equation

$$\frac{d\varepsilon_{xx}}{\sigma'_{xx}} = \frac{d\varepsilon_{yy}}{\sigma'_{yy}} = \frac{d\varepsilon_{zz}}{\sigma'_{zz}} = \frac{d\varepsilon_{xy}}{\sigma_{xy}} = \frac{d\varepsilon_{yz}}{\sigma_{yz}} = \frac{d\varepsilon_{zx}}{\sigma_{zx}} = d\lambda \tag{2.19}$$

where $d\lambda$ is a ratio of proportionality which can vary throughout the straining programme.

2.4. Theory of Simple Tension Tests

This section is divided into two parts.

a) Isotropic sheet

b) Anisotropic sheet

It is assumed that the principal axes of anisotropy are along (x_1) and transverse (x_2) to the direction of rolling and normal to the plane of the sheet (x_3). For a specimen of uniform cross section area A, subjected to a tensile force P, the applied stress

$$\bar{\sigma}_1 = P/A = P/(w.t) = P.\ell/(\ell_o.w_o.t_o) \tag{2.20}$$

where ℓ_o, w_o, t_o are the original length, width and thickness and ℓ, w, t are the current length, width and thickness of the specimen respectively. For constant volume $\ell_o w_o t_o = \ell.w.t.$

For large deformations, lograthmic strain is a better indication of strain than the engineering strain, and the strains therefore are

$$\bar{\varepsilon}_1 = \ln (l/l_o)$$

$$\bar{\varepsilon}_2 = \ln (w/w_o) \qquad (2.21)$$

$$\bar{\varepsilon}_3 = \ln (t/t_o)$$

a) Isotropic Sheet

To take into account the various stress and strain systems we make use of the representative stress and representative strain increment Equations (2.14) and (2.16) These equations are rewritten here for convenience

$$\bar{\sigma} = \sqrt{\frac{1}{2}} \left[(\sigma_1-\sigma_2)^2 + (\sigma_2-\sigma_3)^2 + (\sigma_3-\sigma_1)^2\right]^{1/2} \qquad (2.14)$$

$$d\bar{\varepsilon} = \sqrt{\frac{2}{9}} \left[(d\varepsilon_1-d\varepsilon_2)^2 + (d\varepsilon_2-d\varepsilon_3)^2 + (d\varepsilon_3-d\varepsilon_1)^2\right]^{1/2} \qquad (2.16)$$

where

σ_1, σ_2, σ_3 are the principal stresses

$d\varepsilon_1$, $d\varepsilon_2$, $d\varepsilon_3$ are the principal strain increments.

Since for uniaxial tension

$$\sigma_2 = \sigma_3 = 0$$

$$\epsilon_1 = -\frac{1}{2}\epsilon_2 = -\frac{1}{2}\epsilon_3$$

Then from Equations (2.14) and (2.16) we get

$$\bar{\sigma} = \sigma_1 \tag{2.22}$$

$$\bar{\epsilon} = \epsilon_1 \tag{2.23}$$

b) Anisotropic Sheets

As with the isotropic case, for a simple tension test under consideration, the representative stress $\bar{\sigma}$ as defined by Hill becomes

$$\bar{\sigma} = \sqrt{\frac{3}{2I}}\left[F(\sigma_2-\sigma_3)^2 + G(\sigma_3-\sigma_1)^2 + H(\sigma_1-\sigma_2)^2\right]^{1/2} \tag{2.24}$$

where

$$I = F + G + H$$

The representative strain increment as defined by Hill becomes

$$d\bar{\epsilon} = \sqrt{\frac{2}{3}\frac{I}{Q^2}}\left[F(Gd\epsilon_2-Hd\epsilon_3)^2 + G(Hd\epsilon_3-Fd\epsilon_1)^2 + H(Fd\epsilon_1-Gd\epsilon_2)\right]^{1/2} \tag{2.25}$$

where

$$Q = FG + GH + HF$$

thus we see that when F = G = H, Equations (2.24) and (2.25) reduce to the isotropic expression as given by Equations (2.14) and (2.16).

In Fig. (2.2) the axes $\bar{x}_1$ and $\bar{x}_2$ are along the longitudinal and transverse axes of the specimen which is cut at an angle α (positive counter-clockwise to the direction of rolling.

The stresses when referred to the principal axes of anisotropy x_1 and x_2 are

$$\begin{aligned} \sigma_{11} &= \bar{\sigma}_1 \cos^2 \alpha \\ \sigma_{22} &= \bar{\sigma}_1 \sin^2 \alpha \\ \sigma_{12} &= \bar{\sigma}_1 \sin \alpha \cos \alpha \end{aligned} \tag{2.26}$$

If the material obeys Hill's theory of anisotropy, strain increments will be

$$\begin{aligned} d\varepsilon_{11} &= [(G+H) \cos^2 \alpha - H \sin^2 \alpha] \bar{\sigma}_1 \cdot d\lambda \\ d\varepsilon_{22} &= [(F+H) \sin^2 \alpha - H \cos^2 \alpha] \bar{\sigma}_1 \cdot d\lambda \\ d\varepsilon_{33} &= -[F \sin^2 \alpha + G \cos^2 \alpha] \bar{\sigma}_1 \cdot d\lambda \\ d\varepsilon_{12} &= (N \sin \alpha \cos \alpha) \bar{\sigma}_1 \cdot d\lambda \end{aligned} \tag{2.27}$$

where F, G, H and N are the anisotropic parameters and $d\lambda$ is a proportionality ratio. On transforming these strain increments to the axes $\bar{x}_1$ and $\bar{x}_2$ in the specimen, we get

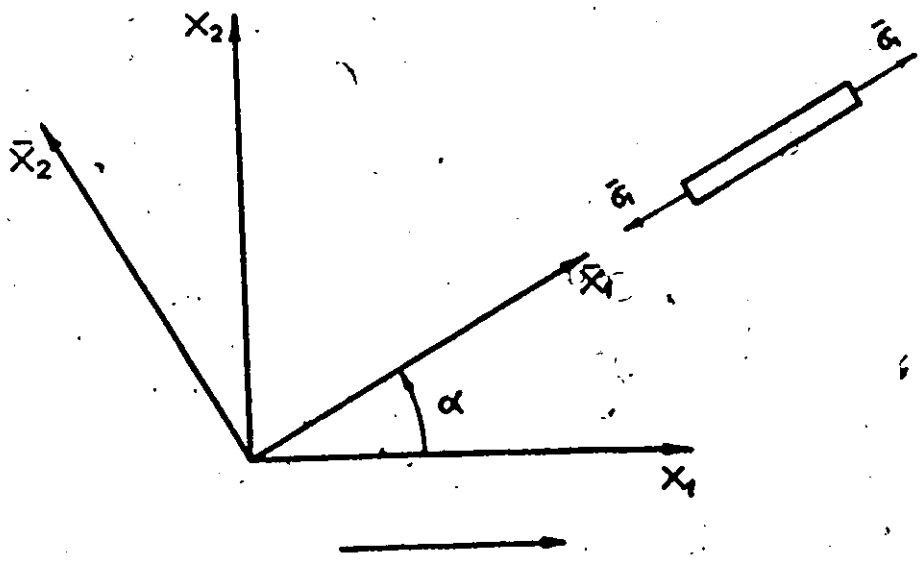
X_2
$\bar{X}_2$
$\bar{\sigma}$
$\bar{\sigma}$
$\bar{X}_1$
α
X_1
direction of rolling

FIG. 2.2

$$d\bar{\varepsilon}_1 = d\varepsilon_{11} \cos^2 \alpha + d\varepsilon_{22} \sin^2 \alpha + 2d\varepsilon_{12} \sin \alpha \cos \alpha$$

$$d\bar{\varepsilon}_2 = d\varepsilon_{11} \sin^2 \alpha + d\varepsilon_{22} \cos^2 \alpha - 2d\varepsilon_{12} \sin \alpha \cos \alpha \qquad (2.28)$$

$$d\bar{\varepsilon}_3 = d\varepsilon_{33}$$

Substituting from Equations (2.27) into (2.28) and simplifying we get

$$d\bar{\varepsilon}_1 = [(F+H) \sin^2 \alpha + (G+H) \cos^2 \alpha + (2N-F-G-4H) \cos^2 \alpha \cdot \sin^2 \alpha]$$

$$d\bar{\varepsilon}_2 = [(F+G+4H-2N) \sin^2 \alpha \cos^2 \alpha - H] \bar{\sigma}_1 \cdot d\lambda \qquad (2.29)$$

$$d\bar{\varepsilon}_3 = d\varepsilon_{33} = - [F \sin^2 \alpha + G \cos^2 \alpha] \bar{\sigma}_1 \, d\lambda .$$

The ratio of the transverse to the through thickness strain can be calculated from Equations (2.29)

$$R_\alpha = \frac{d\bar{\varepsilon}_2}{d\bar{\varepsilon}_3} = \frac{[(F+G+4H-2N) \sin^2 \alpha \cos^2 \alpha - H]}{- [F \sin^2 \alpha + G \cos^2 \alpha]} \qquad (2.30)$$

Hence

$$R_0 = \frac{H}{G}$$

$$R_{90} = \frac{H}{F} \qquad (2.31)$$

$$R_{45} = \frac{2N-(G+F)}{2(G+F)}$$

where R_0, R_{90} and R_{45} are the 'R' values at 0^0, 90^0 and 45^0 to the direction of rolling respectively.

If by performing experiments on the sheet it is found that the measured 'R' value is unchanged with orientation, the sheet is said to have planar isotropy, and if R = 1 then the sheet is isotropic. The R-value of any angle α (measured anticlockwise from the rolling direction) is given by Equations (2.30). Thus according to this theory, we see that planar isotropy occurs when N = F + 2H = G + 2H in which case R_α always equals H/F or H/G.

A technological definition for planar isotropy is sometimes employed and this is defined as:

$$\Delta R = \frac{R_0 + R_{90} - R_{45}}{2} \qquad (2.32)$$

Equation (2.32) is not a mathematically rigorous definition of anisotropy, but has found uses in the press shop. Certainly for sheet steel it has been found that ΔR can give a useful indication of earing in the deep drawing test.

It has already been mentioned that a constant R-value, independent of rotation, implies planar isotropy. However, for $R \neq 1$ the material is still anisotropic. A high R-value ($R > 1$) implies that the material has a high resistance to thinning, and the reverse is true for $R < 1$. Consequently the R-values (for a sheet with planar isotropy) is regarded as a measure of the Normal Isotropy and is often given as

$$\bar{R} = \frac{R_0 + 2R_{45} + R_{90}}{4} \qquad (2.33)$$

or in more general terms. If R_α is determined for m directions, the average R may be calculated as

$$\bar{R} = \frac{1}{2(m-1)} [R_{\alpha 1} + 2R_{\alpha 2} + ... 2R_{\alpha}(m-1) + R_{\alpha}] \qquad (2.34)$$

Here again Equations (2.33) and (2.34) are technological definitions which have found their uses in press shop.

The recognition of the role that the R-value can play in certain metal forming processes has lead to an increased activity in the role of 'Texture-Hardening'. The problem lies in first identifying the role 'R' might play and then suitably processing the sheet to produce the desired texture. e.g., an increased R-value tends to increase the deep drawing capabilities of sheet. All evidence up to now would suggest a similar trend for stretch forming operations.

2.5. Experimental Procedure for Tension Tests

The variation of the strain ratio, the anisotropic constants, and the generalized stress-strain characteristics for the two materials were determined from the tension tests. The procedure was as follows:

1. A group of three blanks each for the two different materials were randomly chosen from the available set. From these blanks pieces were cut along $\alpha = 0^0$, 45^0 and 90^0 to the direction of rolling as shown in Fig. (2.3). After machining these pieces to the proper ASTM specifications for tensile testing of sheet metal, the

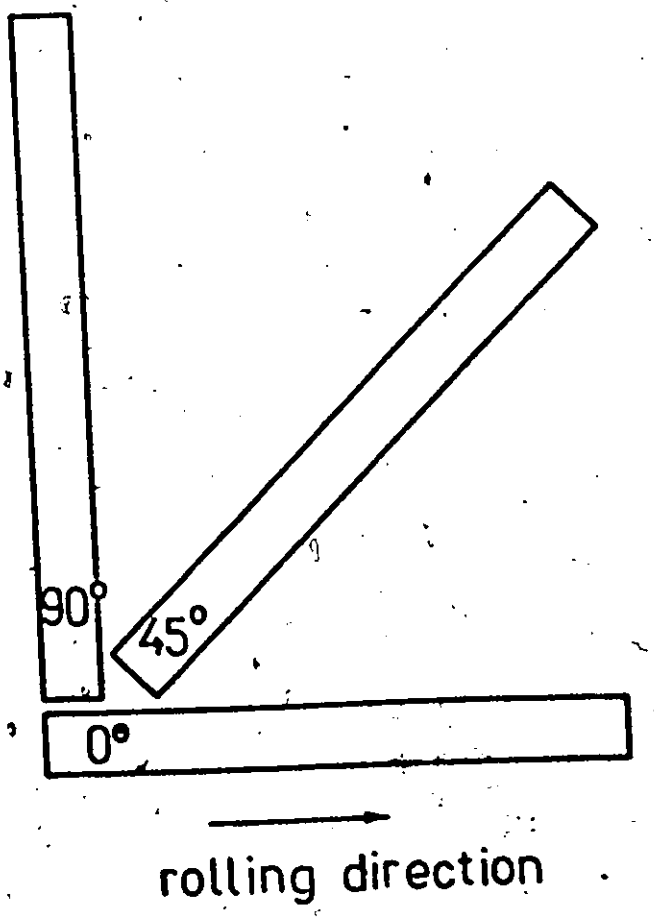

FIG. 2.3 Tensile specimens in three different directions with respect to the rolling direction.

finished specimens were carefully marked to indicate the material, the direction of rolling, and the specimen number. Since the direction of rolling was clearly visible on the blank sheets, no elaborate procedure was used to confirm this.

2. A load cell range of 50 lbs. to the inch, cross-head speed of .2"/min and a 50% extensiometer calibrated to give a 1" chart length for every 2.5% extensions of the specimen was used for all the experiments. This gave a chart length of reasonable size for each test.

3. Because of the multiple necking of the material on a microscope level at low percentage elongations, and which became very visible at higher percentage elongations two different procedures were used as follows:

   a) Determining of the stress-strain curve with the help of an extensiometer.

   b) Determining the variation of the strain ratio and the anisotropic constants with the help of grids for a specific percentage elongation of the material.

4. To perform part (a) of the tension test two specimens for each direction (i.e., $\alpha = 0^{o}$, 45^{o} and 90^{o}) and for each material were chosen at random from the machined lot. A specimen was carefully held between the jaws of the Instron testing machine, taking care to avoid eccentricity and any initial loading. The initial width and thickness were measured at three cross sections evenly distributed

over the range of the extensiometer knife edges, (with a vernier micrometer having a least count equal to .0001 inches) and the extensiometer carefully attached, avoiding any slack or overloading of the extensiometer. The graph calibrations were then carefully adjusted and the load applied to about 25-30% elongation or fracture, depending upon whichever occurred first. From the load-elongation curve, the true stress-strain curves were computed, and the procedure repeated for the other remaining specimens.

To perform part (b) of the experiment the tensile specimens were grided. The griding procedure used was identical to the one described later in the bulge test section, with the exception of rectangular grids being used in place of circular grids. In this case four specimens for each direction and for each material were chosen at random. The length and width of the three different marked grids placed along the centre line of the specimen, evenly distributed over the range of the extensiometer knife edge was measured with a tool makers microscope having a least count of .0001 inches. The specimen was set up in the Instron testing machine in exactly the same manner as in part(a). Two specimens of each type were loaded individually to 6% elongation as read from the graph and the remaining two in a similar manner to 10% elongation. The specimen was then unloaded,

the length and width of the marked grids were measured again and the R-values calculated from which the anisotropic parameters were determined.

5. Zero errors were noted in all cases, and appropriate corrections were applied wherever necessary. Care was taken to avoid backlash in instruments wherever necessary.

2.6. Results of Tension Tests

a) Strain Ratios

Although the three strains ε_1, ε_2 and ε_3 were measured independently, because of the greater probable error in ε_3, only ε_1 and ε_2 were used for calculating the strain ratios and the anisotropic parameters. Due to the multiple necking of the material, it was noted that there was a large scatter in the R-value for any one specimen at the three points under consideration at ten percent elongation. Hence the results for these tests have not been reported. On the remainder of the specimens at six percent elongation, the scatter in the measured R-values still existed, but this scatter was within reasonable limits resulting in fairly consistent averaged R-values. These values along the various directions of rolling along with the average normal anisotropy as obtained from Equation (2.31) are as reported in Table (2.1).

The R-values reported in Table (2.1) were used for calculating the anisotropic parameters with the help of Equations (2.29) and are as reported in Table (2.2).

TABLE 2.1

R-Values for $\epsilon = 6\%$

1. Non Heat Treated Material

Test No.	R_o	R_{45}	R_{90}	$\bar{R}_{AVE}$
1	.341	.453	.655	.475
2	.356	.462	.658	.484
Average	.348	.457	.656	.479

2. Heat Treated Material

Test No.	R_o	R_{45}	R_{90}	$\bar{R}_{AVE}$
1	.22	.194	.429	.259
2	.214	.207	.438	.266
Average	.217	.200	.433	.262

TABLE 2.2

Anisotropic Parameters for $\varepsilon = 6\%$

1. Non Heat Treated Material

Test No.	F	G	H	N	F + 2H	G + 2H
1	1	1.92	.655	2.783	2.31	3.23
2	1	1.848	.658	2.740	2.316	3.164
Average	1	1.884	.656	2.761	2.313	3.197

2. Heat Treated Material

Test No.	F	G	H	N	F + 2H	G + 2H
1	1	1.95	.429	2.047	1.858	2.808
2	1	2.046	.438	2.153	1.876	2.922
Average	1	1.998	.433	2.100	1.867	2.865

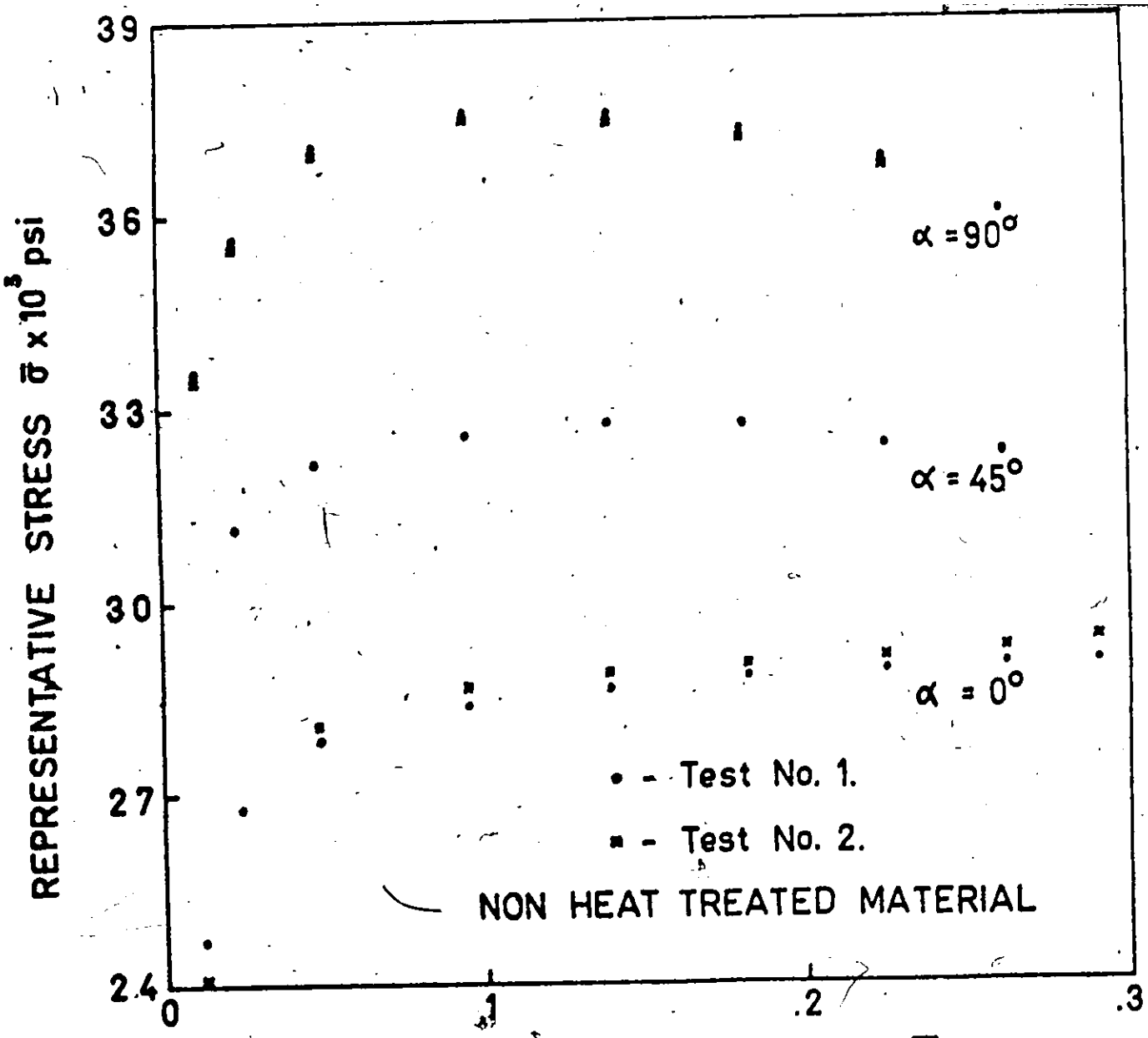

FIG. 2.4 REPRESENTATIVE STRAIN $\bar{\epsilon}$

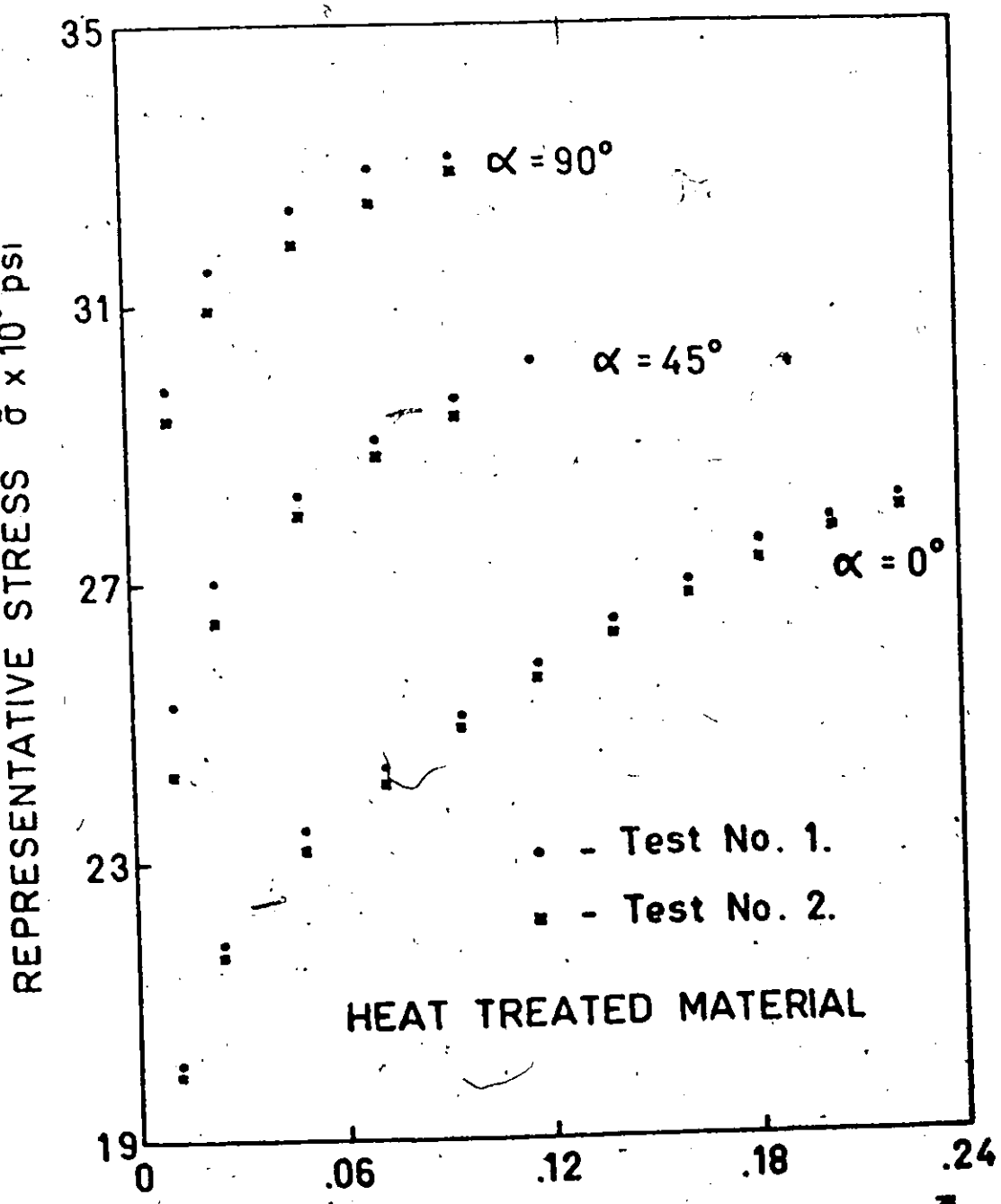
35
31
27
23
19
0
.06
.12
.18
.24
REPRESENTATIVE STRESS $\bar{\sigma} \times 10^3$ psi
REPRESENTATIVE STRAIN $\bar{\varepsilon}$
$\alpha = 90°$
$\alpha = 45°$
$\alpha = 0°$
• - Test No. 1.
▪ - Test No. 2.
HEAT TREATED MATERIAL

FIG. 2.5

b) Representative Stress-Strain Curve

The representative stress and strain for each tension test were calculated, and the stress-strain curves for the various angles with respect to the rolling direction are as shown in Figs. (2.4) and (2.5). The individual curves were then linearized and a least square curve fitted. The values of the constants A and n so determined are as shown in Tables (2.3) and (2.4).

The results of this section are now summarized and discussed.

i) From Table (2.2) we see that for both the materials since $N \neq F + 2H \neq G + 2H$, the materials do not have planar isotropy.

ii) From Tables (2.3) and (2.4) we see that the constants A and n vary with α. In other words, the $\bar{\sigma} - \bar{\varepsilon}$ curve for a given blank is not unique.

Note

After calculating a few of the representative stresses and strains from a tension test data using the already calculated anisotropic parameters and Equations (2.33) and (2.34) and on comparing these results with the representative stress and strain calculated by Equations (2.15) and (2.16) for the same tension data, it was seen that the variation of the results calculated by the two methods was less than 15%. Hence it was decided for ease of computation to present the results using Equations (2.15) and (2.16) only.

TABLE 2.3

The Constant A in kpsi for

1. Non Heat Treated Material

Angle with the direction of rolling α^{o}

Test No.	0^{o}	45^{o}	90^{o}
1	24.0	28.00	30.6
2	24.3	x	30.45
Average	24.15	28.00	30.525

2. Heat Treated Material

Test No.	0^{o}	45^{o}	90^{o}
1	15.1	21.9	28.1
2	14.75	21.25	27.3
Average	14.925	21.575	27.70

TABLE 2.4

The Constant n for

1. Non Heat Treated Material

Test No.	Angle with the direction of rolling α^0		
	0^0	45^0	90^0
1	.0337	.0314	.0424
2	.0360	x	.0443
Average	.0348	.0314	.0433

2. Heat Treated Material

Test No.	0^0	45^0	90^0
1	.1178	.0685	.0375
2	.1214	.0683	.0403
Average	.1196	.0684	.0389

CHAPTER 3

THE BULGE TEST

3.1. Introduction

In this chapter the bulge test is introduced. The variation of the stress-strain characteristics of the materials under superimposed hydrostatic pressure (the maximum pressure used was 10,000 psi) is checked experimentally by means of the bulge test (circular aperture).

A brief look is taken into the theory of bulging of circular diaphragm under hydrostatic pressure, and some formulations are presented in Section 3.2 under a few different headings.

The hydraulic circuit, the die and the method of preparing the bulge specimens are discussed in Section 3.3.

The experimental procedure for the bulge test for the materials is described in Section 3.4.

The results of the bulge test are given in Section 3.5.

3.2. Theory of the Bulge Test

The ductility of sheet metal under biaxial stress is often examined by means of the so called "bulge test". A uniform plane sheet is placed over a die with a circular or elliptical aperture and is firmly clamped around the perimeter. An increasing

hydrostatic pressure is applied to one side of the diaphragm causing it to bulge through the aperture. From the measured profile and thickness of the plastically deformed diaphragm near the pole, it is possible to calculate the local state of stress in terms of the applied pressure. If, in addition, the state of strain is measured by means of scribed grids, the stress-strain characteristics of the metal under biaxial tension can be obtained. One advantage of this test over the simple tensile test is that a greater range of preinstability strain can be attained. To understand the significance of this test it is desirable to have a theory which explains how the varying shape of the bulge, and the distribution of strain, depends on the properties of the metal.

The assumptions made in predicting the onset of instability in the bulge are outlined.

Assumptions

The material is assumed to obey Hill's yield criterion and associated flow rule for anisotropic materials. The assumptions are as follows:

1. The material is incompressible.
2. Elastic strains are negligible.
3. Bauschinger effect, strain rate and temperature effects are neglected.
4. The state of anisotropy is such that three mutually orthogonal axes of symmetry, called the axis of

anisotropy, exist everywhere. These axes are assumed to be along and transverse to the direction of rolling (x_1 and x_2) and normal to the plane of the sheet.

5. If the principal axes of stress coincide with the axes of anisotropy, so do the principal axes of strain increments. Otherwise, the principal axes of stress and strain increments are not necessarily coincident.

6. The state of anisotropy remains effectively unchanged as the material strain hardens.

7. A unique generalized stress-strain curve $\bar{\sigma} - \bar{\varepsilon}$ exists for the material.

The assumptions regarding the bulge are;

8. The diaphragm is thin as compared with the radius of the clamping die.

9. The edge effects at the clamping die are localized and can be disregarded when considering the condition at the pole.

Calculation of Critical Subtangent Including Back Pressure in the Analysis

If a circular sheet of isotropic material is clamped (Fig. 3.1) around a circle of radius 'a' and subjected on the inside face to a hydraulic pressure p_i and a pressure p_o on the outside face, ($p_i > p_o$). Hill [16] proposed that the bulged

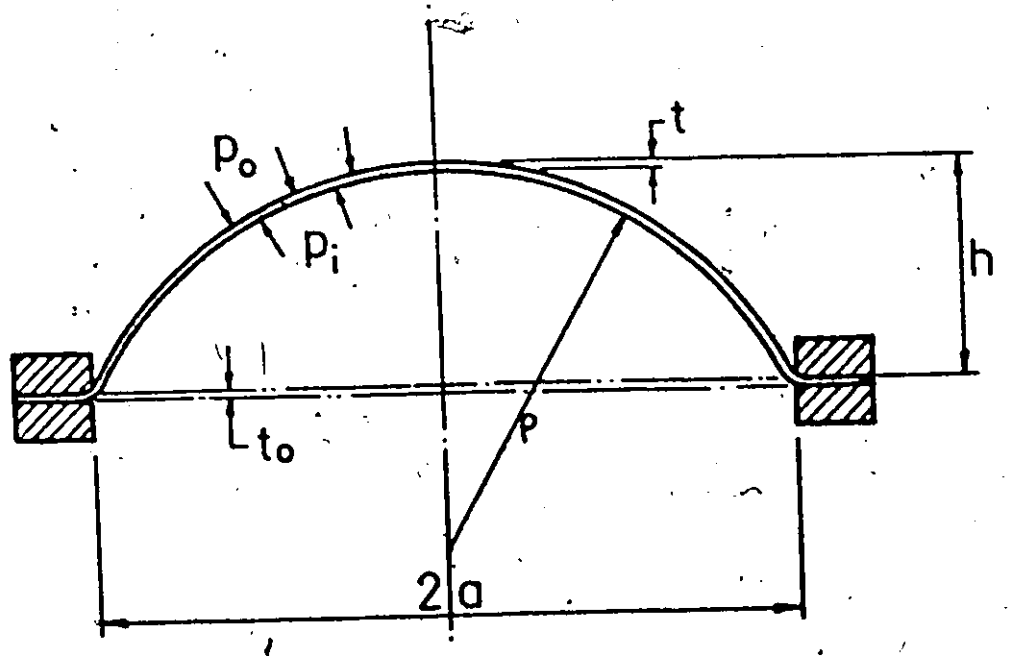

FIG. 3.1 BULGING OF A CIRCULAR DIAPHRAGM

sheet at any instance was a spherical cap except in the region of the clamped edge. The radius of curvature ρ of a meridian cross section is therefore uniform and varies only with the polar height h. Hence from the geometry of the assumed deformation Hill derived the following relationship

$$\rho = \frac{a^2+h^2}{2h} \tag{3.1}$$

and at the pole the principal strains were given by

$$\varepsilon_1 = \varepsilon_2 = \ln\left(1+\frac{h^2}{a^2}\right) = \frac{1}{2}\,|\varepsilon_3| = \frac{\bar{\varepsilon}}{2} = \frac{1}{2}\,\left|\ln\frac{t}{t_o}\right| \tag{3.2}$$

For the equilibrium of a small cap of sphere at the pole of the bulge, we see that

$$\sigma_1 = \sigma_2 = \left(\frac{p_i-p_o}{2t}\right)\rho - \bar{p} \tag{3.3}$$

where

$$\bar{p} = \frac{p_i+p_o}{2}$$

The representative stress $\bar{\sigma}$ is found as

$$\bar{\sigma} = \left(\frac{p_i-p_o}{2t}\right)\rho \tag{3.4}$$

and the deviatoric stresses as

$$\sigma_1' = \sigma_2' = \frac{\bar{\sigma}}{3} \quad \text{and} \quad \sigma_3' = -\frac{2}{3}\,\bar{\sigma} \tag{3.5}$$

The principal strain increments are related as

$$d\varepsilon_1 = d\varepsilon_2 = -\frac{d\varepsilon_3}{2} \tag{3.6}$$

and the representative strain increments are

$$d\bar{\varepsilon} = 2d\varepsilon_1 = -d\varepsilon_3 \tag{3.7}$$

It has been found from experiments that when the pressure reaches its maximum, a secondary bulge begins to form over about the top half of the diaphragm and this continues under a falling pressure. The pressure maximum is regarded as the moment when the process becomes unstable. At the point of instability $dp_i = 0$ and from Equation (3.4) we get

$$\frac{d\bar{\sigma}}{\bar{\sigma}} = \frac{d\rho}{\rho} - \frac{dt}{t} \tag{3.8}$$

Note: In the analysis without back pressure. In Equation (3.4) $p_o = 0$ and we get

$$\bar{\sigma} = \frac{p_i \rho}{2t} \tag{3.9}$$

Again, at the point of instability $dp_i = 0$ and from Equation (3.9) we get Equation (3.8). From Equations (3.1) and (3.2) it is easily verified that

$$\frac{d\rho}{\rho} = -\frac{d\varepsilon_3}{2} + \frac{d\varepsilon_3}{2h}\rho \tag{3.10}$$

Substituting Equations (3.10) into (3.8) and using (3.7) we get

$$\frac{d\bar{\sigma}}{\bar{\sigma}} = \frac{d\bar{\epsilon}}{2} + d\bar{\epsilon} - \frac{\rho}{2h}\, d\bar{\epsilon}$$

$$\frac{1}{\bar{\sigma}} \frac{d\bar{\sigma}}{d\bar{\epsilon}} = \left(\frac{3}{2} - \frac{\rho}{2h}\right) \tag{3.11}$$

Assuming that the material has a representative stress-strain curve fitted by the relation $\bar{\sigma} = A(\bar{\epsilon})^n$. Then

$$\frac{d\bar{\sigma}}{\bar{\sigma}.d\bar{\epsilon}} = \frac{n}{\bar{\epsilon}} = \frac{n}{\epsilon_3} \tag{3.12}$$

where ϵ_3, the through thickness strain is assumed positive. From Equations (3.11) and (3.12) we get

$$\frac{n}{\epsilon_3} = \frac{3}{2} - \frac{\rho}{2h} \tag{3.13}$$

Now $\frac{\rho}{h}$ is a function of ϵ_3 (from Equations (3.1) and (3.2)) and can be expanded in terms of ϵ_3. If this is done the R.H.S. of Equation (3.13) is given (approximately) by

$$\frac{n}{\epsilon_3} = \frac{11}{8} - \frac{1}{2\epsilon_3}$$

$$\therefore \quad \epsilon_3 = \frac{4}{11}(2n + 1) \tag{3.14}$$

Thus we see that the remarkable feature of the balanced biaxial tension test is that no matter how heavily work hardened the material is initially, the strain at fracture is always greater than $\frac{4}{11}$. This fact makes the "bulge test" a very suitable method

of obtaining the stress-strain characteristics in biaxial tension.

Going back to the critical subtangent analysis, substituting Equations (3.1) into (3.11) and rearranging we get

$$\frac{1}{\bar{\sigma}} \frac{d\bar{\sigma}}{d\bar{\varepsilon}} = z^{-1} = \{1 + \frac{1}{4}(1 - \frac{a^2}{h^2})\} \tag{3.15}$$

Thus from the above result we see that the subtangent is independent of the back pressure. Similarly it can be shown that the critical subtangent in the case of an anisotropic sheet can be given by

$$z^{-1} = \frac{1}{\beta}\{1 + \frac{1}{4}(1 - \frac{a^2}{h^2})\} \tag{3.16}$$

where

$$\beta = \{\frac{(F + G + H)(F + G + 4H)}{6(FG + GH + HF)}\}^{1/2} \tag{3.17}$$

It is interesting to note that the thickness of the diaphragm was not neglected in deriving Equation (3.15). Using the conventional thin membrane theory where the thickness is neglected, Hillier [10] investigated the effect of pressure on forming processes for isotropic materials. If the same theory is used in the analysis for anisotropic materials, the expression for the critical subtangent becomes

$$z^{-1} = \frac{1}{\beta^2}\{\beta - \frac{\bar{p}}{\bar{\sigma}}\}\{1 + \frac{1}{4}(1 - \frac{a^2}{h^2})\} \tag{3.18}$$

for isotropic sheets the above expression reduces to

$$z^{-1} = \left(1 - \frac{\bar{p}}{\bar{\sigma}}\right) \left\{1 + \frac{1}{4}\left(1 - \frac{a^2}{h^2}\right)\right\} \qquad (3.19)$$

which is the same as the result derived by Hillier [10].

Equations (3.18) and (3.19) are a consequence of omitting the sheet thickness in the equilibrium equations and predict the strong influence of pressure on the point of instability. It was mentioned earlier that the experimental work of Pugh illustrated that many materials did show a brittle to ductile transition with the application of a hydrostatic pressure. Furthermore the magnitude of the hydrostatic pressure was relatively low for one or two materials with hexagonal packed structures.

It was because of this experimental evidence and the fact that Equation (3.15) was established independent of material properties that motivated this present project.

Representative Stress-Strain for Bulge Test-Anisotropic Sheet

Referring to Fig. 3.1 and taking the axis of anisotropy as x_1, x_2 and x_3 as the reference axis, the principal stresses at the pole are

$$\sigma_{11} = \sigma_1, \sigma_{22} = \sigma_2, \sigma_{33} = -\left(\frac{p_o+p_i}{2}\right) = -\bar{p} \qquad (3.20)$$

Here, the negative sign indicates compression.

The bulge being in the plastic state, the principal stresses σ_j and strain increments $d\varepsilon_j$ $(j = 1,2,3)$ are related to the generalized stress $\bar{\sigma}$ and generalized strain increment $d\bar{\varepsilon}$

by the yield criterion as defined by Hill [19] and given by Equation (2.24) rewritten here as

$$\bar{\sigma} = \sqrt{\frac{3}{2I}} \left[F(\sigma_2+\bar{p})^2 + G(\sigma_1+\bar{p})^2 + H(\sigma_1-\sigma_2)^2\right]^{1/2} \tag{3.21}$$

and the associated flow rule

$$d\varepsilon_j = \frac{3}{2} \left(\frac{d\bar{\varepsilon}}{\bar{\sigma}}\right) B_j \quad (j = 1,2,3) \tag{3.22}$$

where

$$\begin{aligned} I &= F + G + H \\ B_1 &= \frac{1}{I} [G(\sigma_1+\bar{p}) + H(\sigma_1-\sigma_2)] \\ B_2 &= \frac{1}{I}[F(\sigma_2+\bar{p}) + H(\sigma_2-\sigma_1)] \\ B_3 &= -\frac{1}{I} [F(\sigma_2+\bar{p}) + G(\sigma_1+\bar{p})] \end{aligned} \tag{3.23}$$

from the equation of incompressibility and Equations (3.22) and (3.23) we have

$$B_1 + B_2 + B_3 = 0$$

The stress σ_1 and σ_2 at the pole can be calculated in terms of the bulge geometry by considering the equilibrium of forces normal to the bulged surface. Thus for a bulged diaphragm it [illegible]sily verified that

$$\sigma_2 = \left(\frac{p_i-p_o}{t}\right) \rho - 2\bar{p} \tag{3.24}$$

[illegible]ole if we take

$$d\varepsilon_1 = d\varepsilon_2 \text{ or } B_1 = B_2 \tag{3.25}$$

from Equations (3.23), (3.24) and (3.25) we get the stresses as

$$\sigma_1 = \frac{(F+2H)(p_i-p_o)}{(F+G+4H)t}\rho - \bar{p}$$

$$\sigma_2 = \frac{(G+2H)(p_i-p_o)}{(F+G+4H)t}\rho - \bar{p} \qquad (3.26)$$

$$\sigma_3 = -\bar{p}$$

and from Equations (3.21) and (3.26) we get

$$\bar{\sigma} = \left[\frac{3(FG+GH+HF)}{2I(F+G+4H)}\right]^{1/2} \cdot \left(\frac{p_i-p_o}{t}\right)\rho \qquad (3.27)$$

If the three direct strains are measured independently the incompressibility condition

$$\varepsilon_1 + \varepsilon_2 + \varepsilon_3 = 0 \qquad (3.28)$$

may be used to check the accuracy of the measurements. If the strain ratios during the test remain constant, the generalized strain $\bar{\varepsilon}$ may be calculated from Equation (2.25) rewritten here in the generalized strain form as

$$\bar{\varepsilon} = \sqrt{\frac{2}{3}}\,\frac{I}{Q^2}\left[F(G\varepsilon_2-H\varepsilon_3)^2 + G(H\varepsilon_3-F\varepsilon_1)^2 + H(F\varepsilon_1+G\varepsilon_2)^2\right]^{1/2} \qquad (3.29)$$

where $Q = FG + GH + HF$.

However, if only the thickness strain ε_3 or the other two strains are measured, the generalized strain may be calculated from

Equations (3.28) and (3.29) which gives

$$\bar{\varepsilon} = \left[\frac{6(FG+GH+HF)}{(F+G+H)(F+G+4H)}\right]^{-1/2} \varepsilon_3 \qquad (3.30)$$

Thus the generalized stress-strain can be determined from the bulge test data. These values can be linearized and a least square curve fitted to get the values of A and n.

If the material is isotropic and for bulging without back pressure Equations (3.27) and (3.30) reduce to the form

$$\bar{\sigma} = \sigma \qquad (3.31)$$

$$\bar{\varepsilon} = 2\varepsilon \qquad (3.32)$$

where

$$\sigma = \sigma_1 = \sigma_2, \sigma_3 = 0$$

$$\varepsilon = \varepsilon_1 = \varepsilon_2, \quad \varepsilon_3 = \varepsilon_t = \text{thickness strain.}$$

3.3. The Hydraulic Circuit

In this section a general outline of the hydraulic circuit, description of the die and method of preparing the specimens for the bulge test are given.

a) The Hydraulic Circuit

A schematic arrangement of the hydraulic circuit designed for a maximum pressure of 10,500 psi. is as shown in Fig. 3.2. High pressure autoclave fittings were used. This

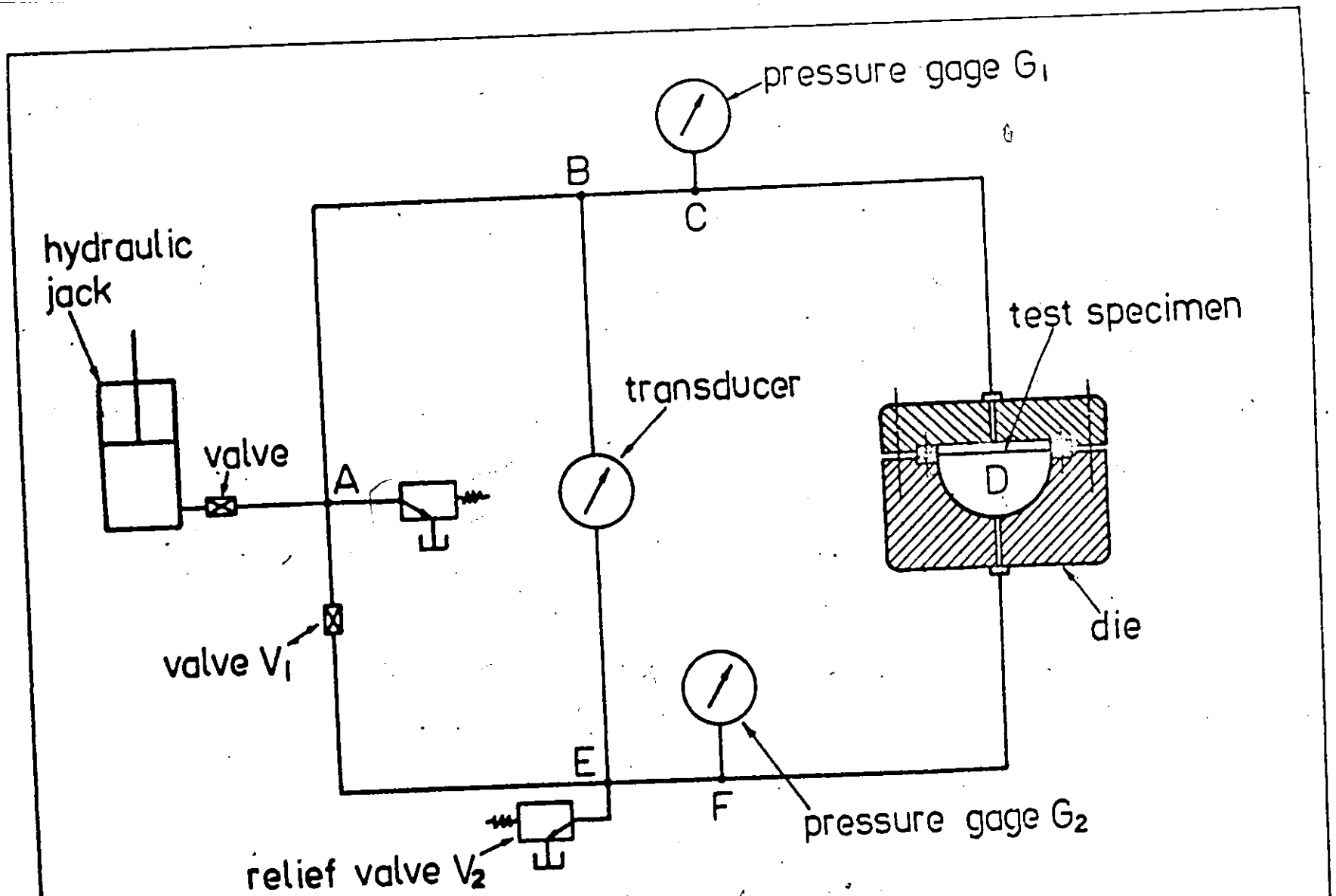

FIG. 3.2 HYDRAULIC CIRCUIT FOR BULGE FORMING.

resulted in a leak free circuit in which parts could be easily connected or disconnected. The pump was connected to point A by a flexible hose. The points C and F were connected by two flexible hoses to the top and bottom outlets of the die respectively.

From the point A, the two sides of the circuit (i.e., the side ABC and the side AEF) were made of equal length, and with the same number of similar fittings. This was done so that a pressure pulse from A travelling along the paths ABC and AEF would reach the specimen at the same instant. For the same reason the transducer (as described later) was located at equal distance from the two lines. To reduce the temperature variation at the transducer diaphragm, the transducer was placed away from the lines, so that there was no flow of oil past its diaphragm.

The oil sold under the trade name Enerpac HF-101, was used as the Hydraulic Fluid. The tubing was designed to keep the oil velocity low, in order to reduce the temperature rise and pressure pulses. There was some unavoidable heating of the oil as it was released through the pressure relief valve V_2 at high pressure. The back pressure p_o was controlled manually with the help of the pressure relief valve V_2, and the pressure differential required to bulge the specimen was created by adjusting the needle valve V_1. The pressure differential was measured by the transducer. The Heise pressure gauge G_1, reading up to a maximum of 650 psi along with a dead weight tester was used for

calibrating the transducer. The back pressure p_o was measured by the Crossby AlH gauge G_2 reading up to 15,000 psi maximum with 50 psi divisions.

b) The Die

The die base and cover were machined out of SPS-245 forged steel. The die is shown in the open position in Fig. 3.3. To prevent drawing in of the specimen, two clamping rings made of hardened and ground steel were used. The specimen, held between the rings by 16 - 5/16 diameter screws, was clamped independently of the cover. The clamping rings were serrated with grooves to prevent slipping of the specimen. In order to prevent fracture of the specimen at the rim, the inner edge of the lower ring was rounded off to a reasonable radius. The concentricity of the centre of the clamping rings with that of the grid photographed on the specimen was achieved with the help of the master locating fixture.

c) The Transducer

The accuracy and reliability of the bulge test results depended largely on the accuracy with which the pressure differential required to burst the diaphragm at various hydrostatic back pressures was measured. Thus making the transducer the most vital part of the bulge test equipment.

A diaphragm type transducer designed by Kular [6] (see Figs. 3.4 and 3.4(a)) was used in the hydraulic circuit.

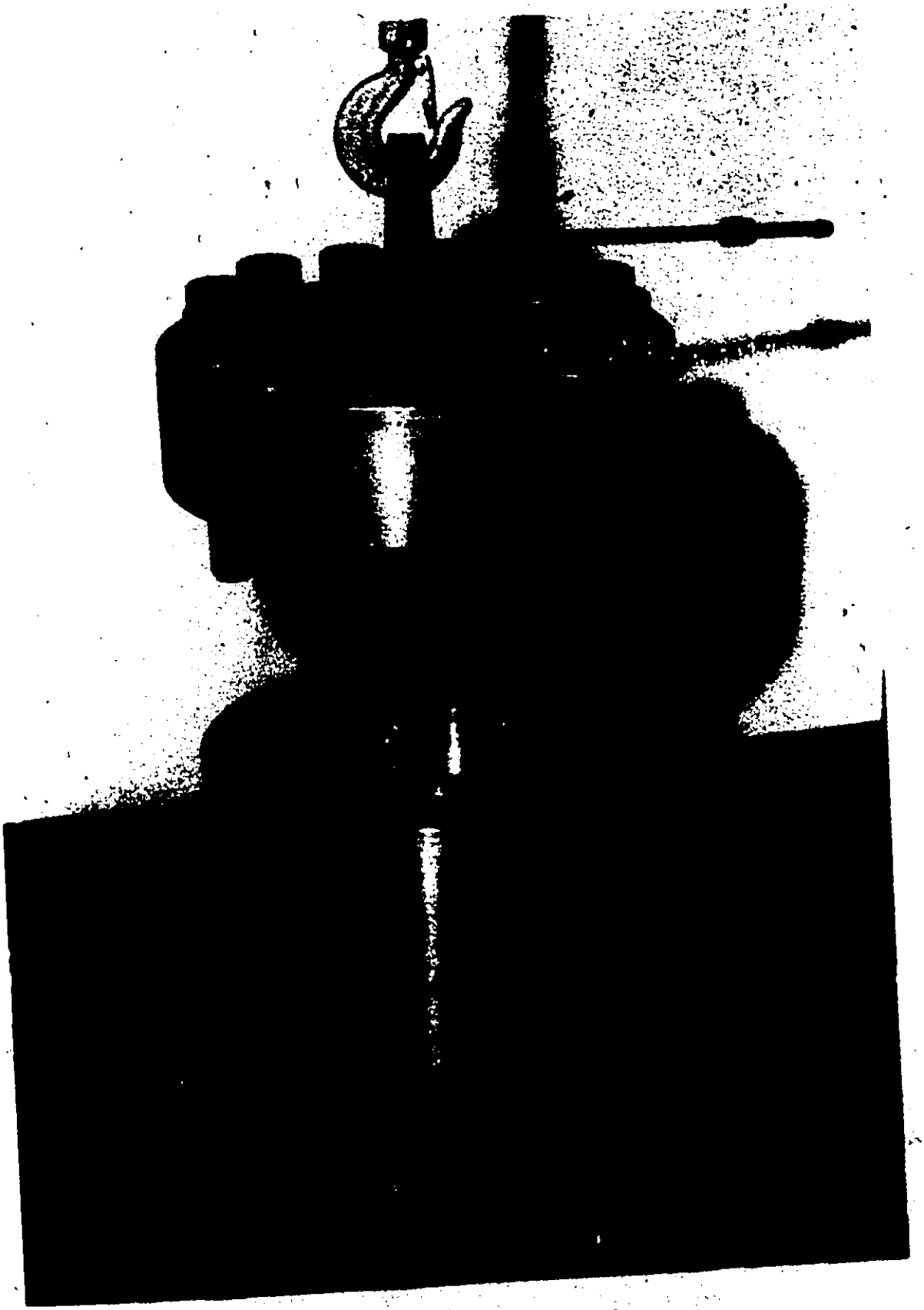

FIG. 3.3. DIE OPEN POSITION.

FIG. 3.4. TRANSDUCER WITH BAH-1.

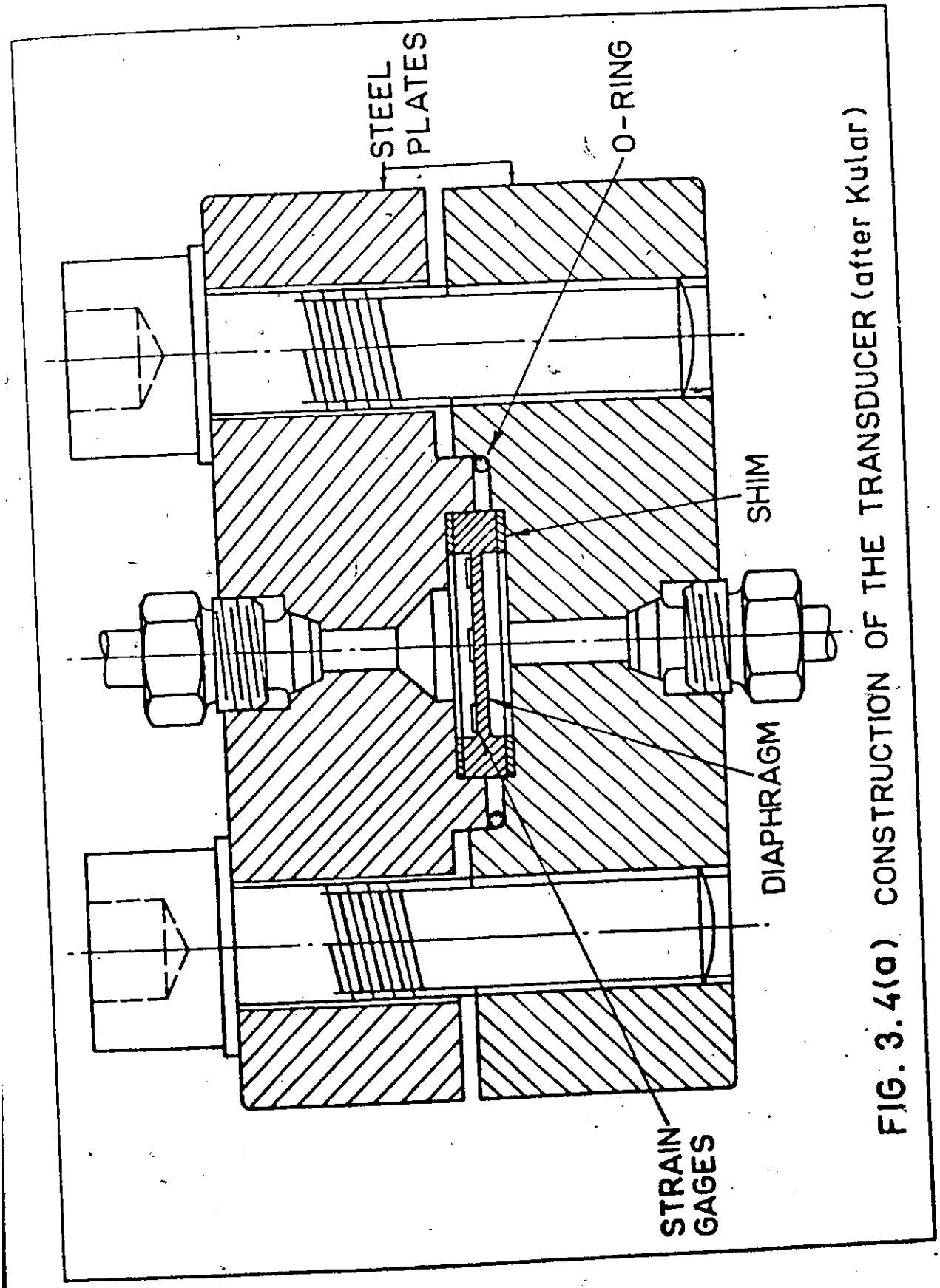

FIG. 3.4(a) CONSTRUCTION OF THE TRANSDUCER (after Kular)

In this transducer the line pressure acts directly on four strain gauges mounted on the same side of a steel diaphragm enclosed in a pressure chamber. The gauges are connected to form a Wheatstone Bridge circuit, such that the temperature and pressure effects are compensated, and the sensitivity is increased 4-5 times that of a transducer using only one gauge at the centre of the diaphragm. The electrical output was measured by an Ellis-Bridge Amplifier and Meter model BAM-1.

Calibration

Before the transducer can be used with confidence the effect of line pressure on its calibration curve should be precisely known and should be repeatable. Ideally the transducer should be calibrated for each line pressure at which it is to be used. A possible error could be due to the change in calibration due to the effect of direct hydrostatic pressure on the gauge factor on the strain gauges. Kular [6] in his experiments on the sensitivity of the transducer, verified that within the pressure range and accuracy for our experiments, the gauge factor is unaffected by hydrostatic pressure. In other words, the calibration curve obtained at zero line pressure is independent of the line pressure, moderate changes of temperature and low frequency changes of pressure differential.

The transducer was calibrated against a Heise pressure gauge, which, in turn, was calibrated against a portable dead weight gauge tester. The sensitivity of the transducer was found

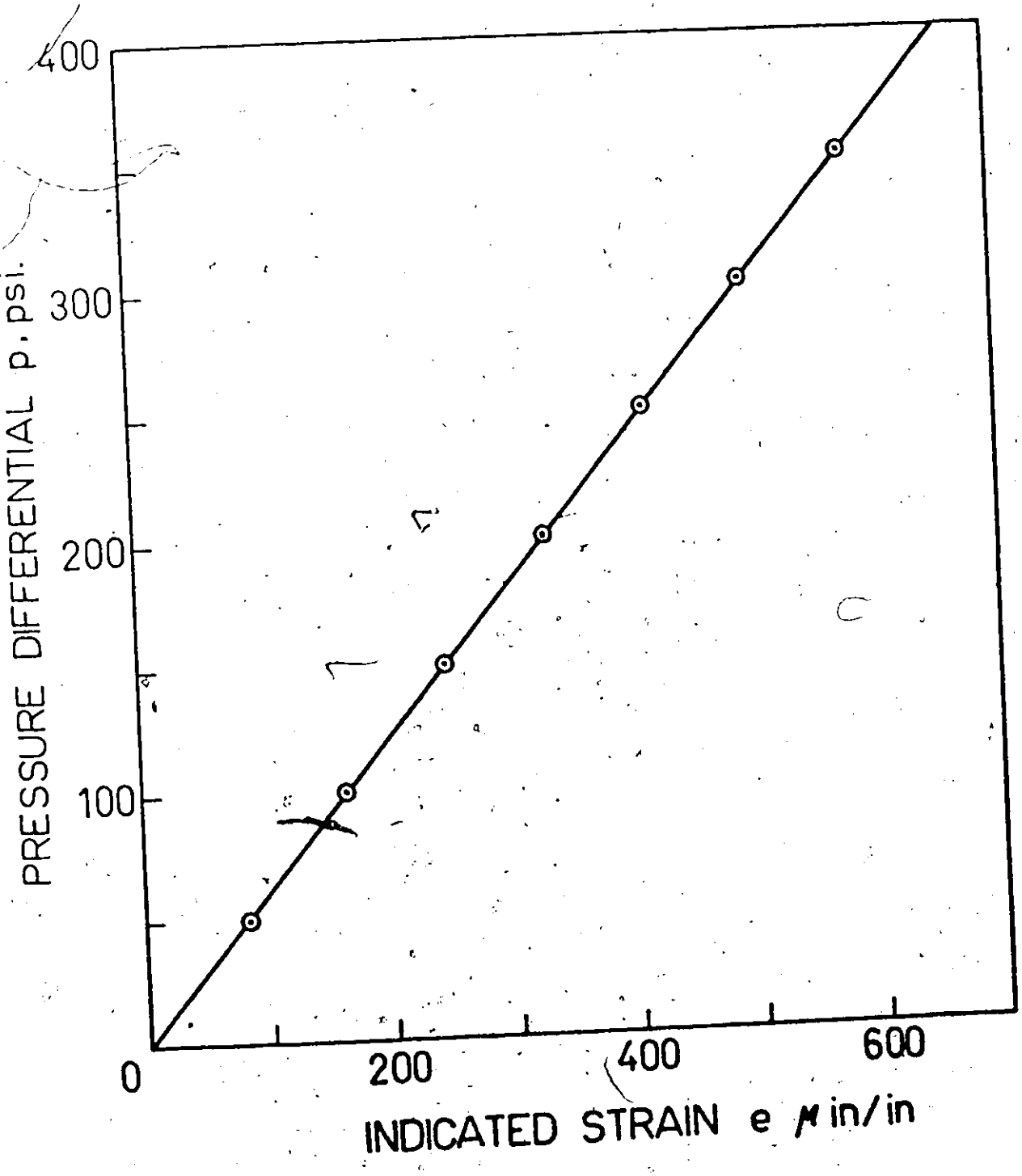

FIG. 3.5 CALLIBRATION CURVE FOR THE TRANSDUCER

to be 1.64 microstrain per psi differential. The calibration curve for our transducer is as shown in Fig. 3.5 and agrees well with the curve obtained by Kular [6].

d) Preparation of Bulge Specimen

For tests on the two materials, the strain distribution and bulge profile were determined using the photogrid method. It was necessary to align and centre the grid properly in preparing the specimen. 8" x 8" blanks were cut from the original sheet and locating holes were drilled along and transverse to the direction of rolling. The holes for clamping screws were drilled next, and finally, the square blanks were turned to 8" diameter blanks ready for photogriding.

The negative for the final photogriding on the specimen, was a contact print of a plexiglass plate with grids consisting of concentric circles 20 to an inch and radial lines at 15^0 intervals. The centre of the grid and the 0^0 - 180^0 (x_1) and 90 - 270^0 (x_2) axes were carefully located with the help of master locating fixtures.

The photogriding of the specimen was carried out by a method described by Baraya et al. [21]. This method consists of applying a light sensitive solution onto a clamped specimen, exposing the specimen under ultra violet light and then developing the exposed specimen in a regular photographic developing procedure.

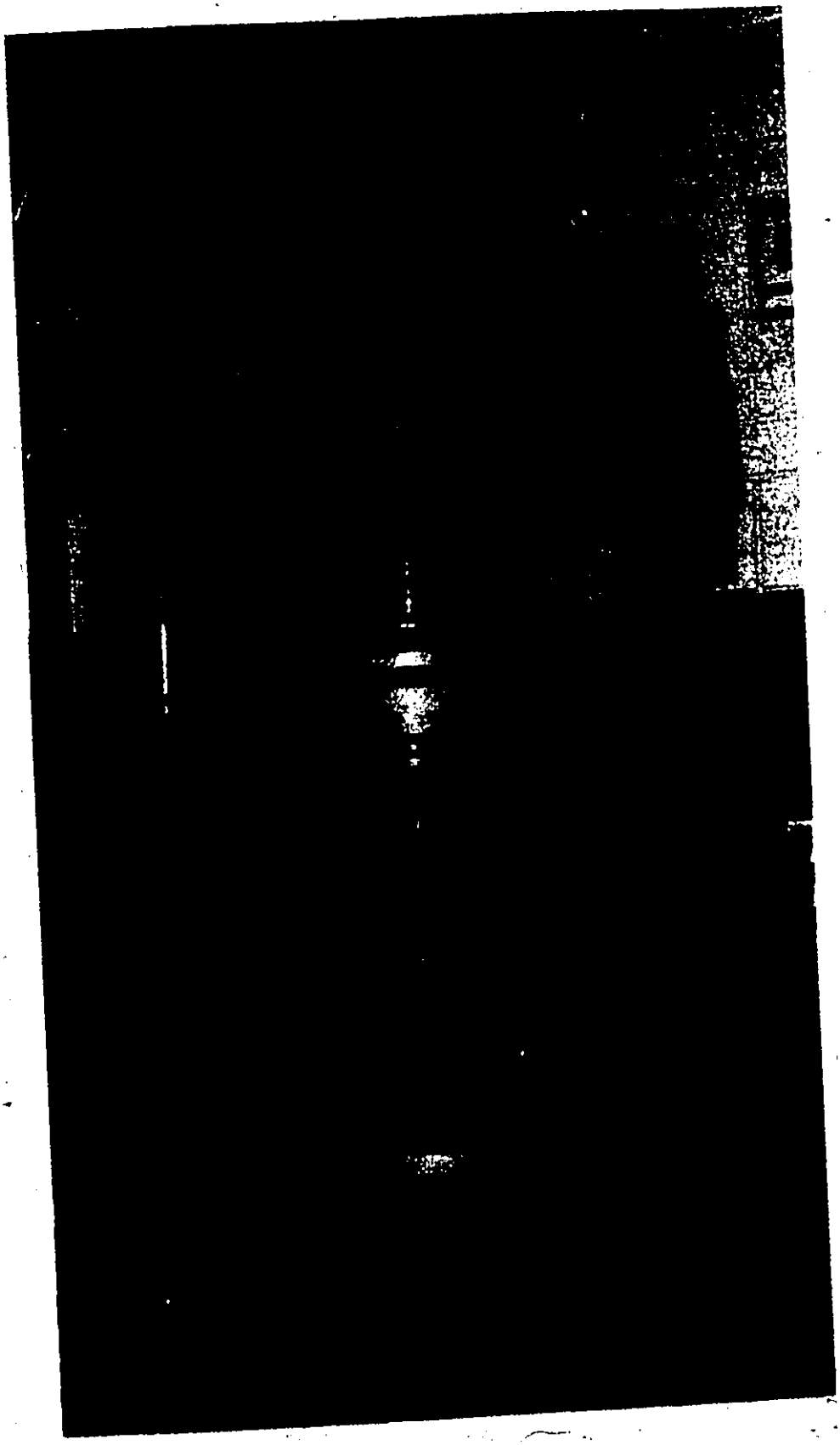

FIG. 3.6. HYDRAULIC JACK UNDER TINIUS OLSEN MACHINE.

3.4 Experimental Procedure for Bulge Test without Back Pressure

The main objective of these experiments was to determine the bulge profile, the radius of curvature and strain distribution along the profile. It was also intended to determine the stress-strain characteristic at atmospheric pressure. The procedure was as follows:

1. A Enerpac hydraulic jack with 10,000 psi maximum working pressure and 10 ton capacity was used as a source of oil pressure. The jack was filled with oil by means of a Enerpac hand pump. The jack was then compressed by means of a 300 k lbs Tinius Olsen Testing machine [see Fig. 3.6]. This machine was maintained at a constant crosshead speed so that a constant non pulsing flow of oil was obtained. The capacity of the hydraulic jack was enough to carry out one test in a single filling.
2. A specimen with grids photographed on it, was placed in position and clamped in the die. Then the space above the specimen was filled to the brim with oil and the die cover lower in position. Some oil always spilled out expelling any air bubbles in the space between the specimen and the die cover. The die cover was tightened using a pneumatic torque wrench.
3. In this set of experiments the needle valve V_1 (Fig. 3.2) was always closed and relief valve V_2 was fully opened to ensure that there was no back pressure. The assembled apparatus is as shown in Fig. 3.7.

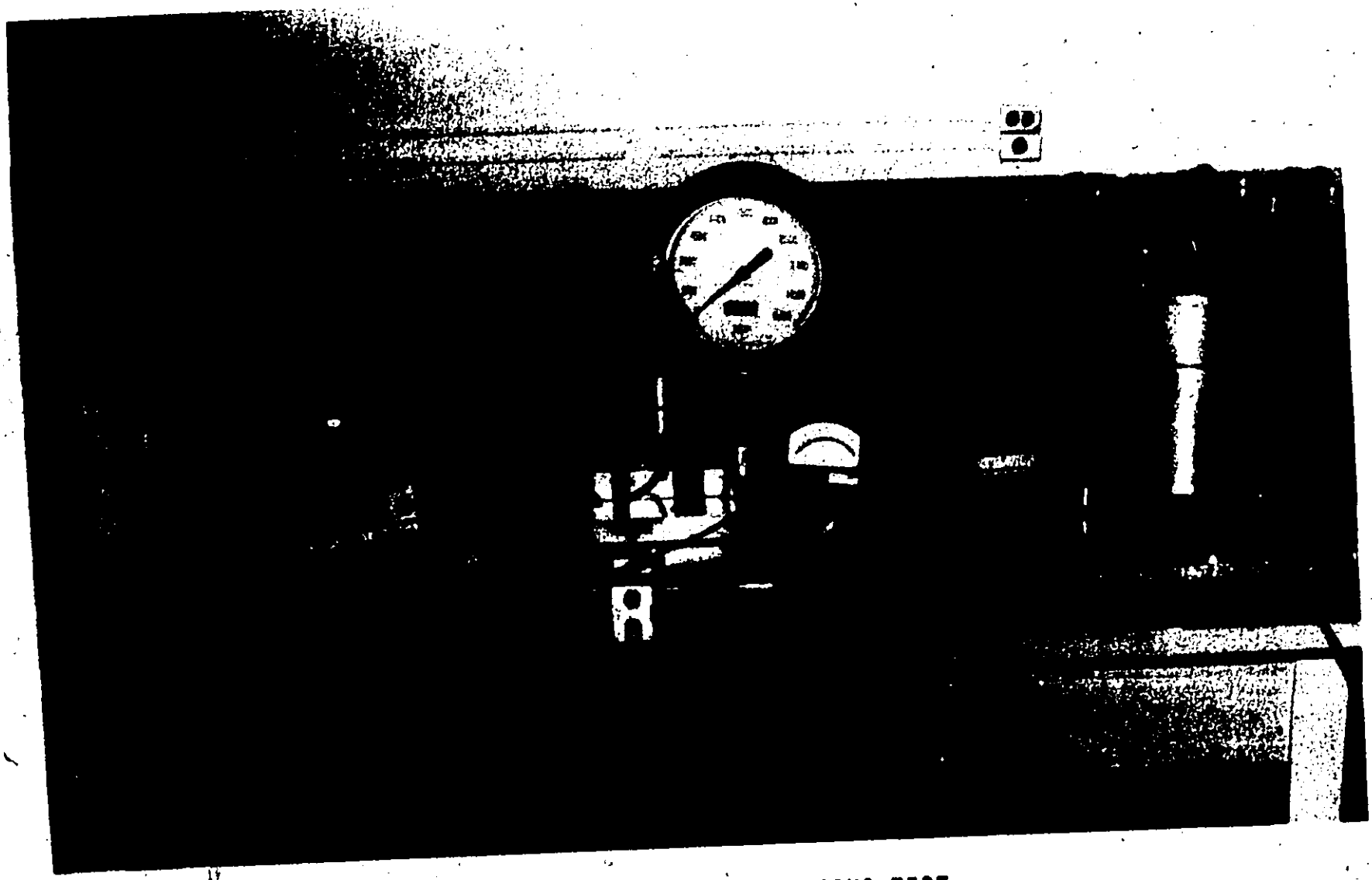

FIG. 3.7. ASSEMBLED APPARATUS FOR BULGING TEST (WITH AND WITHOUT BACK PRESSURE.)

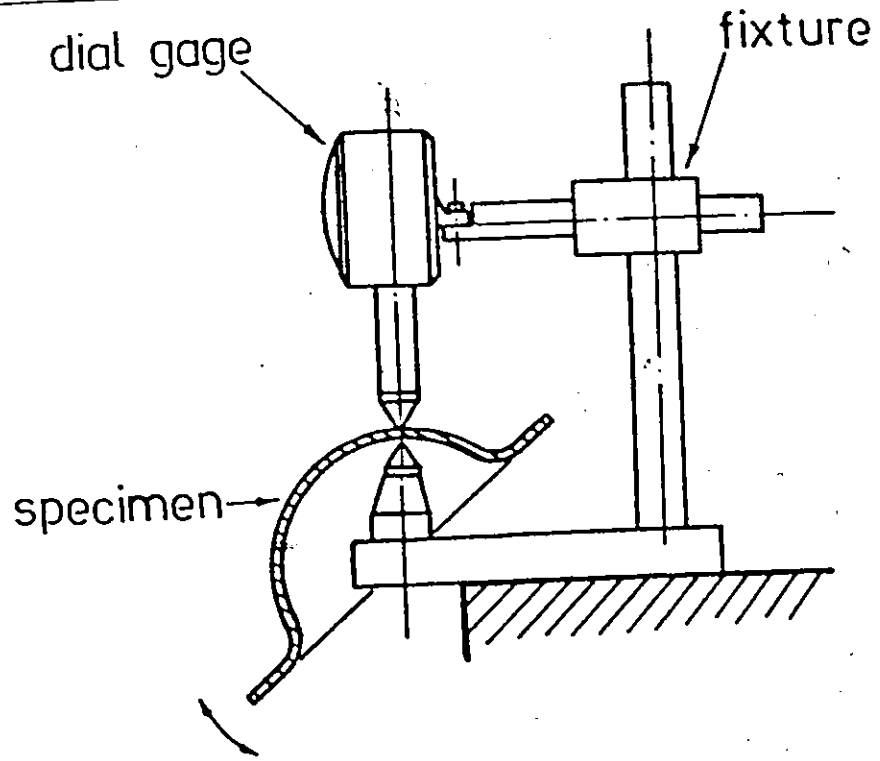
dial gage
fixture
specimen

FIG. 3.8

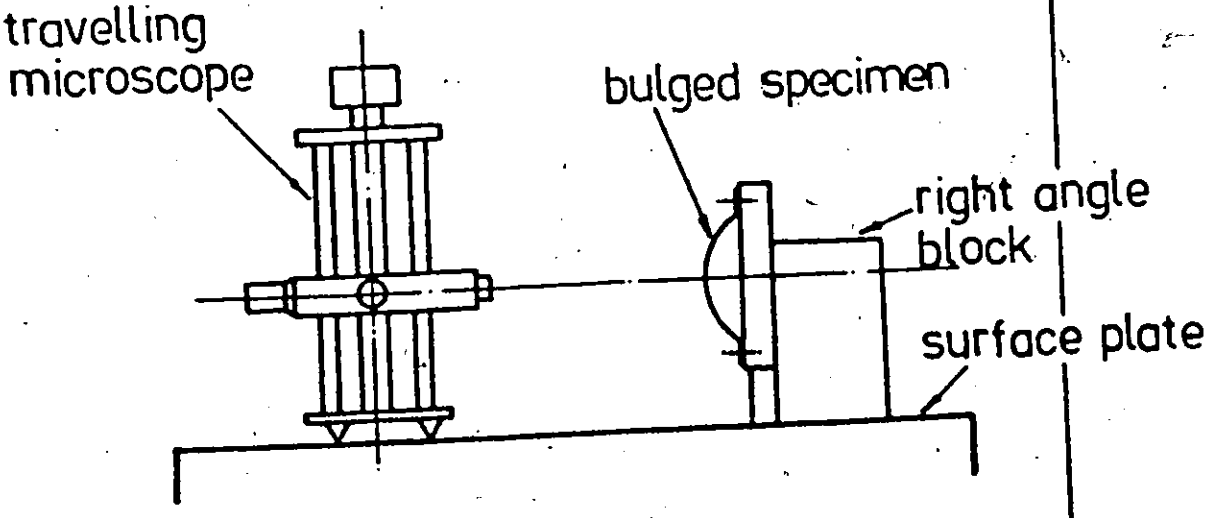
travelling
microscope
bulged specimen
right angle
block
surface plate

FIG. 3.9

After the pressure measured by the Heise Gauge had been raised by an amount estimated to give approximately equal increments of polar strain between steps, the specimen was taken out, and the polar thickness, its height, polar radius of curvature and current diameter of every third circle along x_1 and x_2 ($\theta = 0^o$ and 90^o) direction was measured up to the fifteenth circle.

4. The thickness was measured by means of a dial gauge reading up to 0.0001 inches. The dial gauge was mounted as shown in Fig. 3.8. Special care was taken to ensure aligning of the lower tip of the dial gauge and the tip of the rest arm below the dial gauge. The bulged specimen was inserted between the tips with extreme caution. It was then rocked up and down (as shown by the arrow in Fig. 3.8) while watching the needle on the dial gauge. The minimum reading indicated during the swings was the thickness at the dome. With a little experience, the minimum was quite easily indicated with a minimal of error.

5. The diameter of the circles was measured by means of a travelling microscope reading up to 0.001 centimeters. The specimen was clamped to a rigid angle block (Fig. 3.9) such as to ensure measuring of the circles along the vertical axis ($\theta = 0^o$ and 90^o). The travelling microscope was also placed on the same surface plate at an appropriate distance from the specimen and focused on the lines.

The crosswire was always focussed on the inner edge of the circle. The microscope was always moved from right to left so as to avoid backlash error and care was also taken not to disturb the line of sight while taking readings.

6. The height of the bulge was measured by means of a height gauge reading up to 0.001 inches. A dial gauge reading up to 0.0001 inches was extended from the tip of the height gauge and lowered on to the specimen. The dial gauge showed a deflection as soon as its tip touched the dome of the specimen.
7. The polar radius of curvature along $\theta = 0^{o}$ and 90^{o} was measured with a spherometer.

After all the readings were taken the procedure was repeated so as to give about five reasonably spaced readings for the stress-strain characteristics before the specimen fractured. Two blanks were tested for each material without back pressure and the appropriate curves approximated.

As a matter of cross check to see how the results got by the above procedure fared with those got by the equipment designed by Albertin [20], another set of experiments were carried out. A brief description of the equipment and experimental procedure is as given below. The equipment set up is as shown in Fig. 3.10.

The main components of the equipment are:

a) The bulging die

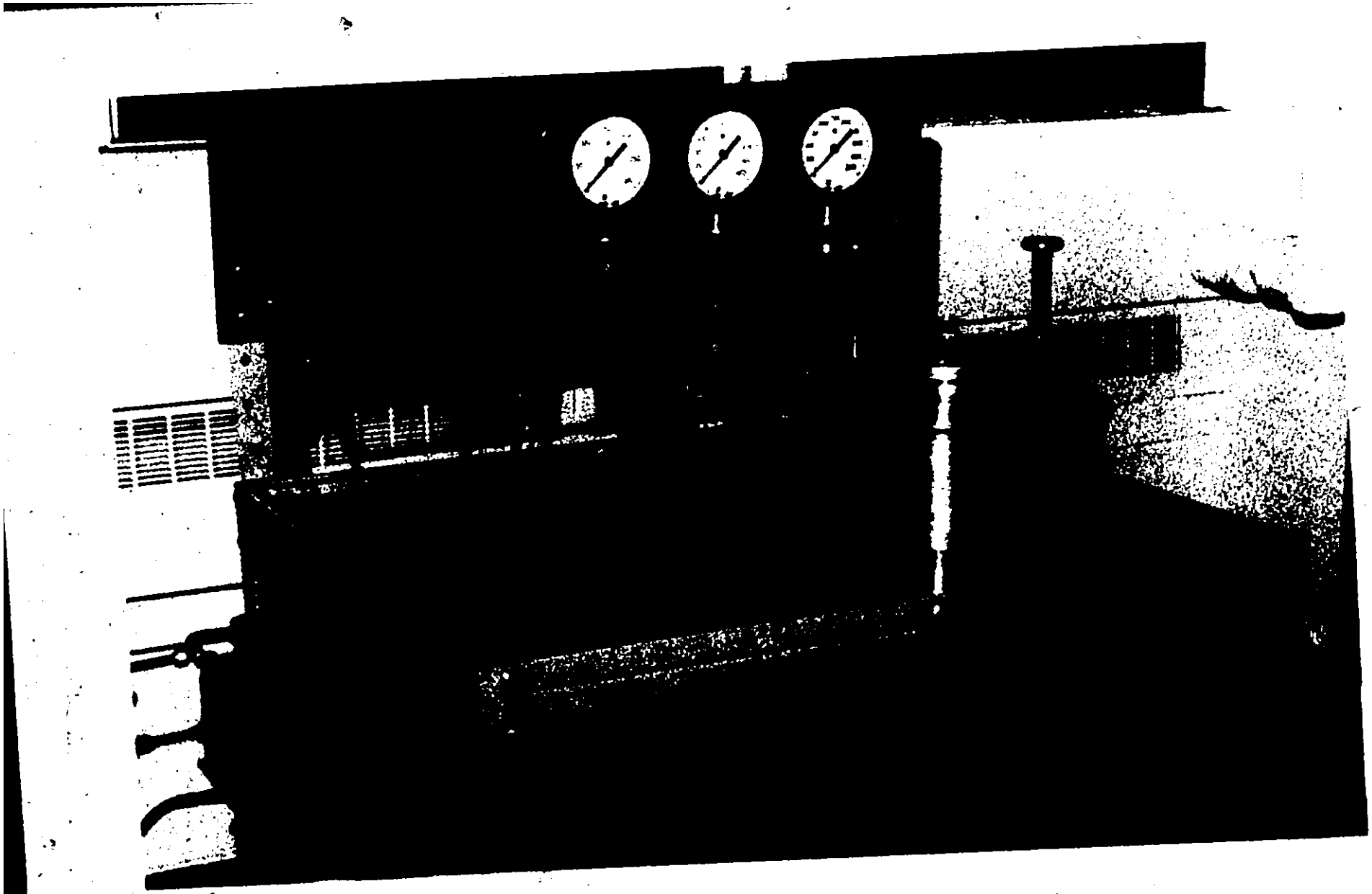

FIG. 3.10. BIAXIAL TEST EQUIPMENT.

b) The biaxial test unit (consisting of the extensometer and spherometer).

In this die for the bulging of spherical diaphragms, the clamping mechanism is an integral part of the die. A specimen is put in place and initially clamped by a die ring screwed into the body of the die on top of the specimen. Further desirable clamping of the specimen is achieved from the underside of the specimen by a clamping ring actuated by hydrostatic pressure.

The biaxial test unit consists of the extensometer and spherometer. Both being combined into one unit working in two mutually perpendicular planes. The extensometer measures the extension and the spherometer measures the curvature at the pole of the bulge. The unit is slipped on the top of the die and the instrument probes rest on the surface of the specimen and follow the path of the bulging specimen. The movement of these probes is registered on the two outside dial gauges and the extension is derived from their sum. The stress-strain curve for the diaphragm material is then computed from the extensometer and spherometer readings. The hydraulic pressure is supplied by means of a hand pump and readings are taken at fixed increments of strain while noting the corresponding hydraulic pressure applied.

The results and conclusions of this test are presented along with those for the previous test and the tests with back pressure.

Procedure for Bulge Test with Back Pressure

This section is subdivided into two parts. In part "a" the scheme of these tests is given and in part "b" the procedure is described.

a) Scheme of Experiments

The initial plan of the experiments was to perform two tests at each back pressure from 0 to 10 kpsi at an interval of 2 kpsi. The rest of the specimens were to be used for initial trial and some were to be kept in case of further experimentation. In order to have a preliminary idea of the results and also to get some feel for the equipment, some tests were carried out at 6 kpsi back pressure (this pressure being chosen because it fell midway within the testing range). At this stage of testing it was realized that the stress-strain characteristics were unaffected by back pressure. This was later confirmed by further tests at 6 kpsi. Thus it was decided to abandon the idea of tests at lower back pressures, and the remaining tests at higher back pressures were carried out.

Since the idea was to compare the stress-strain characteristics of the two materials without back pressure, to those of the material with back pressure, the procedure of testing was exactly the same as that of the tests without back pressure. The bulge test was performed in steps with each back pressure. At each stage of bulging the specimen was taken out of the die and its polar strain, polar radius of curvature, etc. was measured.

In all a total of approximately 35 specimens of the two materials were tested.

b) Procedure

1. The source of high pressure oil was exactly the same as described under the heading "Experimental procedure for bulge test without back pressure".
2. The strain gauge leads from the transducer were connected to the Bridge Amplifier and Meter Model BAM-1. A "Fairchild" digital voltmeter was connected to the bridge amplifier and was used for reading the pressure differential.
3. The cavity in the base of the die was filled with oil and the specimen was placed in position and clamped. Then the space above the specimen was filled to the brim with oil and the die cover lowered and tightened.
4. A view of the whole apparatus is as shown in Fig. 3.7. The valve V_1 [Fig. 3.2] was fully opened and the Tinius Olsen machine started. The desired back pressure p_o was controlled manually with the help of the pressure relief valve V_2.

   At pressures near 10 kpsi, it was not as easy to control p_o as at lower pressures (say 6 kpsi). This was due to the fact that the pressure p_o was dissipated in the relief value V_2. The rise in temperature and the consequent change in viscosity of an oil caused instability in the oil flow, resulting in a sudden change in p_o.

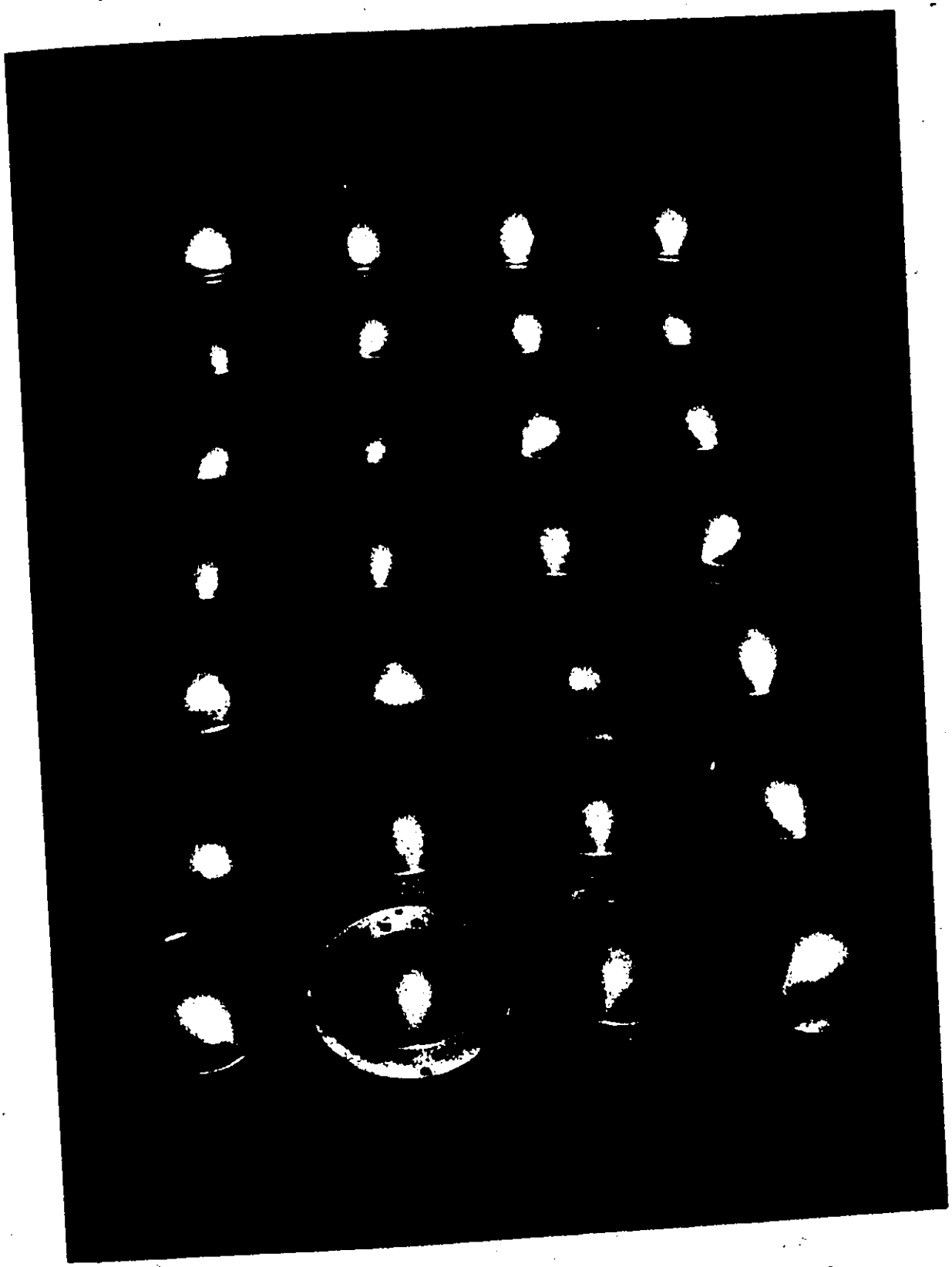

FIG. 3.11. MOST OF THE BULGED SPECIMENS.

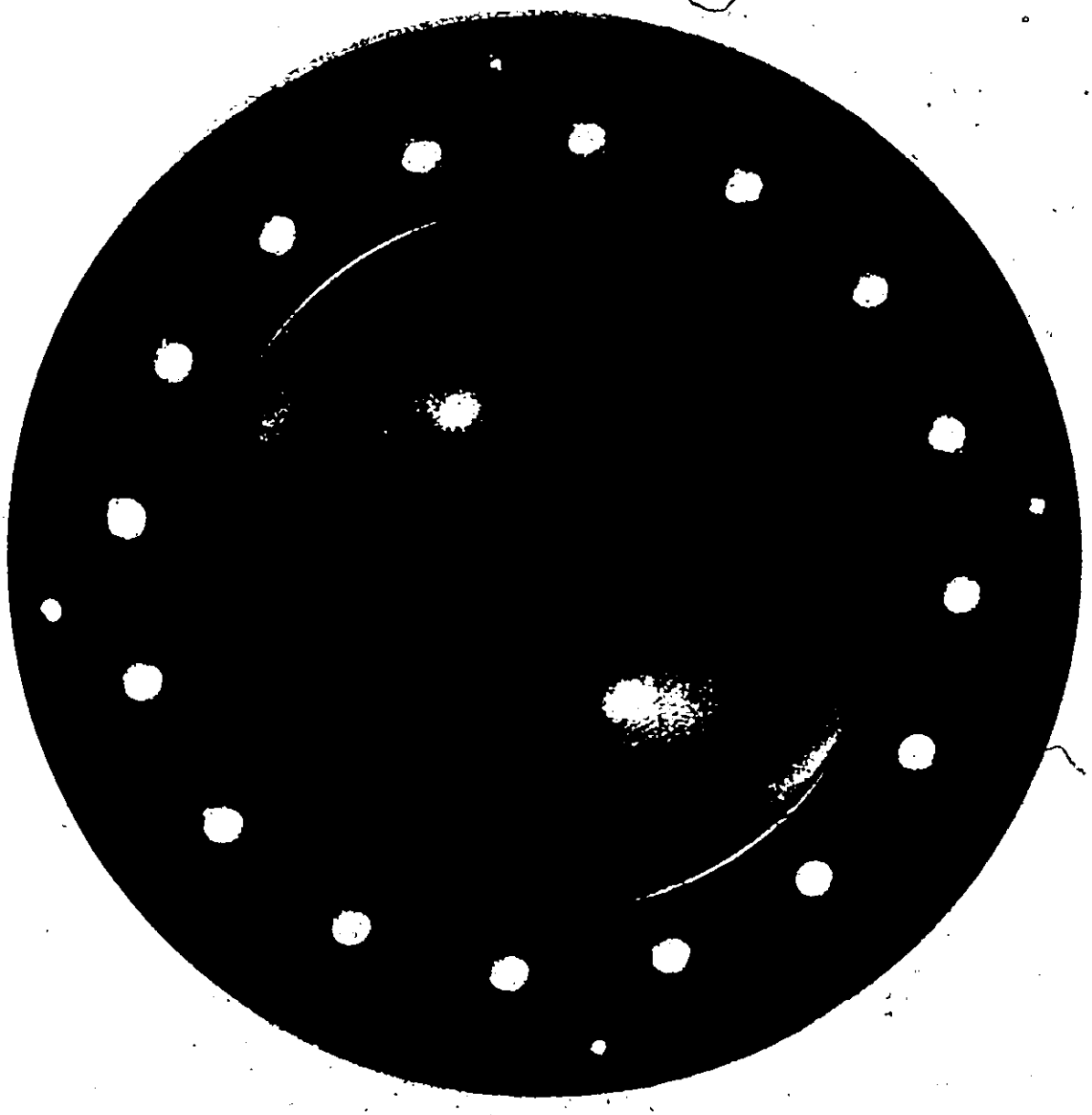

FIG. 3.12. BULGED SPECIMEN WITH GRID.

Another source of pressure pulse was the occasional air bubbles which crept into the system in spite of all the precautions taken to keep them out.

The above problems were overcome to a great extent by letting the valve V_2 cool between every stage of the experiment.

5. When the pressure in the system had been raised to p_o, the valve V_1 was slowly closed keeping p_o constant as far as possible. The pressure differential caused by V_1 was supported by the clamped specimen and was shown by the neon numbers of the digital voltmeter. The increment in pressure differential was so adjusted so as to give 5-6 well spaced points on the stress-strain curve. A picture of most of the bulged specimens is as shown in Fig. 3.11. A picture of one of the specimens near the instability range is as shown in Fig. 3.12.

6. The various readings of the bulged specimen were taken in exactly the same manner as described under the heading "Experimental procedure for bulge test without back pressure".

7. The calibration of the transducer was checked in the beginning, at the end and at various stages of the test series in a similar manner described under "The Transducer" section. The calibration was found to be unchanged, thus indicating proper functioning of the transducer.

3.5. Results of Bulge Tests

The results for the two materials tested are as presented in Figs. 3.13 to 3.25 and the values of the constants A and n of Equation 2.18, as determined from the bulge test are as given in Table 3.1. An average of two tests at each back pressure were used in the plotting of all the results and the results are discussed briefly.

a) Strain Distribution

The circumferential strain along the profile for the two materials up to the fifteenth circle is shown in Figs. 3.13 and 3.20. Both the plots are for the bulge test without back pressure. Plots for tests with various back pressures were similar and thus, have not been reported. It appears that the degree of anisotropy although not very severe is apparent for strains along $\theta = 0^0$ and 90^0. The ratio of strains ε_1 and ε_2 in the plane of the bulge at the pole (measured along the first circle) was found to be very close to unity within accuracy of the measurement.

Plots for polar radius of curvature 'ρ' vs polar thickness strain ($\varepsilon_3 = \varepsilon_t$) for the two materials are as shown in Figs. 3.15 and 3.22 also plots for polar height "h" vs polar thickness strain are as shown in Figs. 3.16 and 3.23. On superposing Fig. 3.15 on 3.22 and also on superposing Fig. 3.17 on 3.23, we see that the similar plots are almost identical within accuracy of the measurements, i.e., no difference in performance was obtained

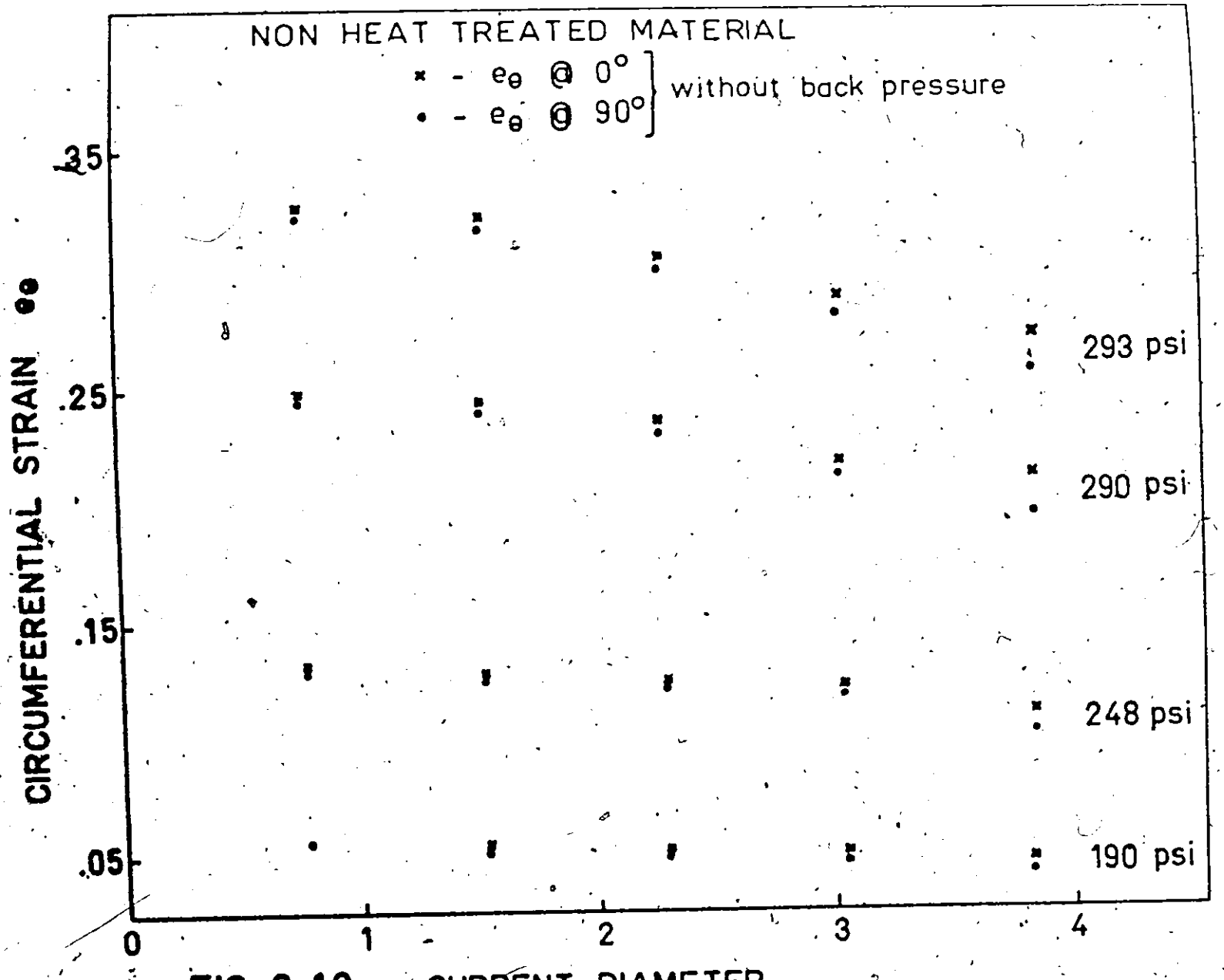
NON HEAT TREATED MATERIAL
× - e_θ @ 0°
• - e_θ @ 90°
without back pressure
293 psi
290 psi
248 psi
190 psi
CIRCUMFERENTIAL STRAIN e_θ
.35
.25
.15
.05
0
1
2
3
4
CURRENT DIAMETER

FIG. 3.13

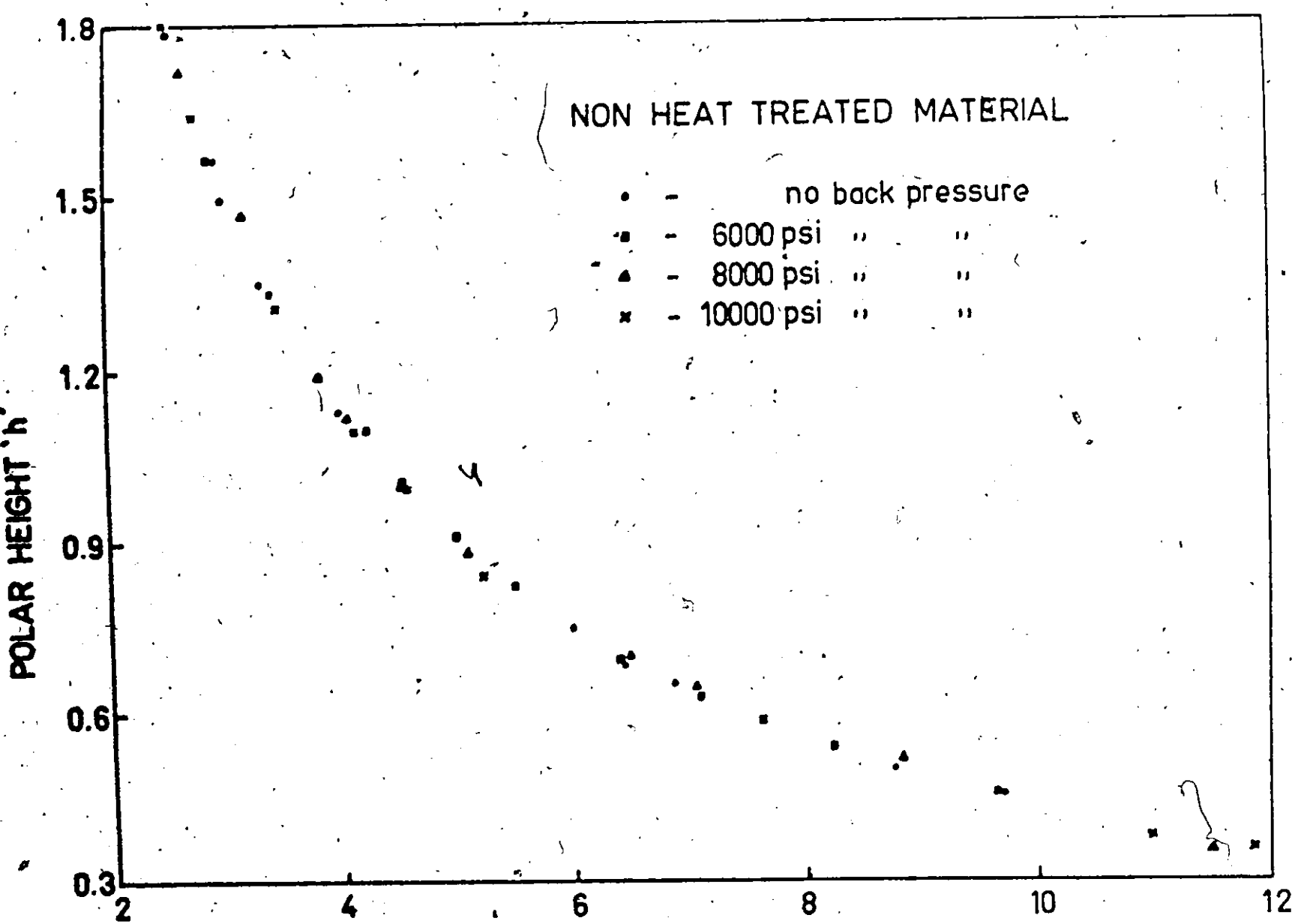

FIG. 3.14 POLAR RADIUS OF CURVATURE 'e'

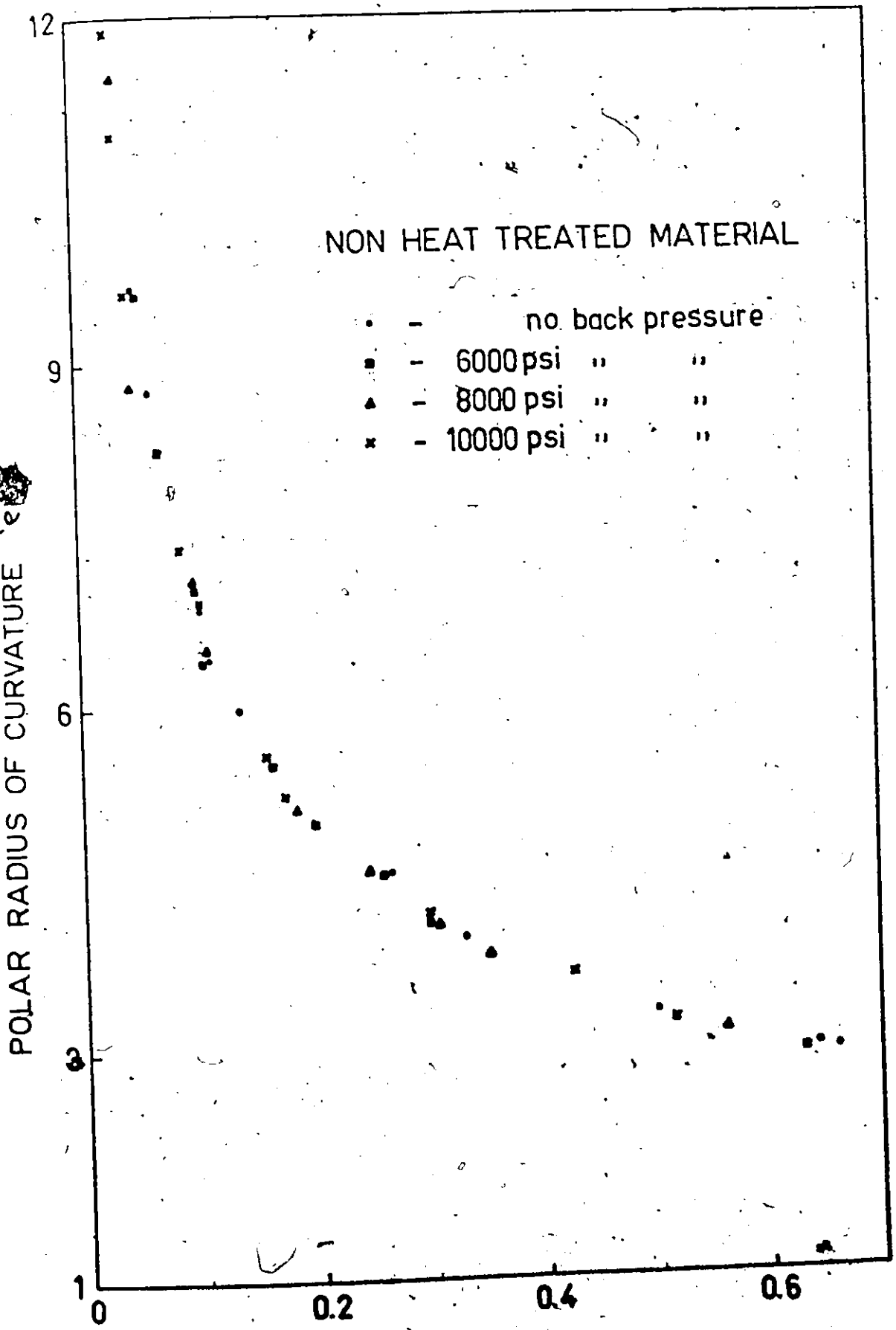

FIG. 3.15 POLAR THICKNESS STRAIN 'ε_t'

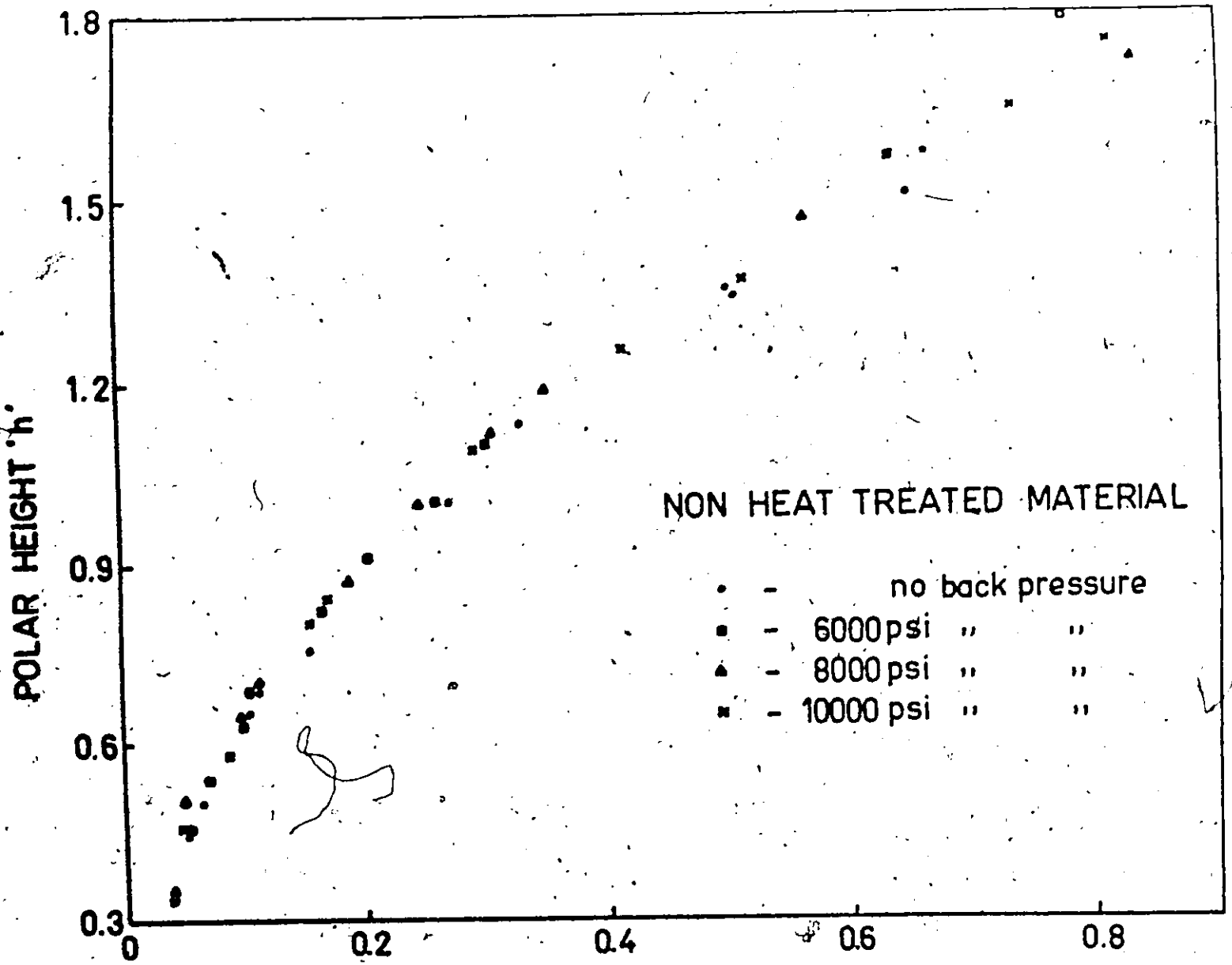

FIG. 3.16 POLAR THICKNESS STRAIN 'ϵ_t'

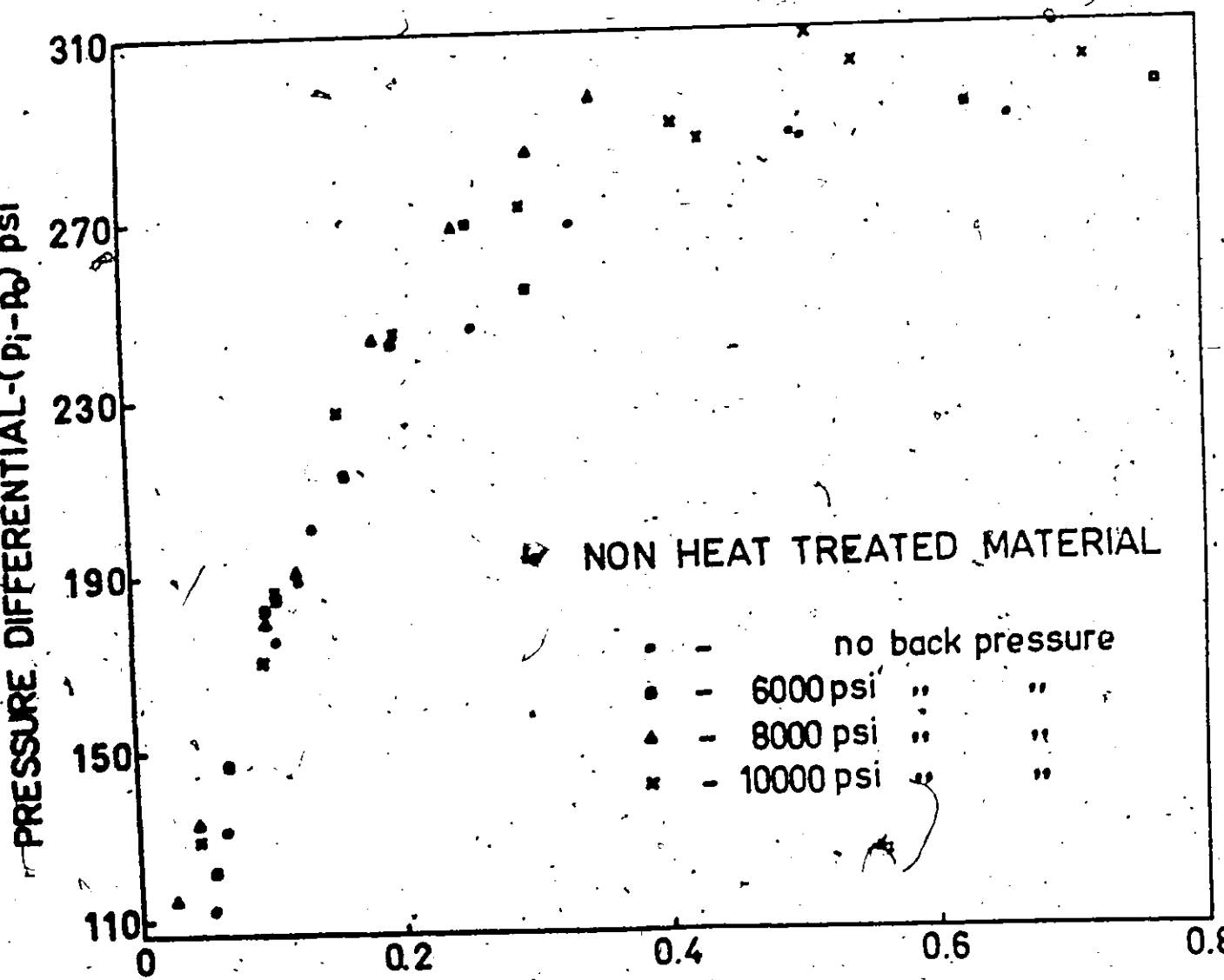

FIG. 3.17 POLAR THICKNESS STRAIN 'ε_t'

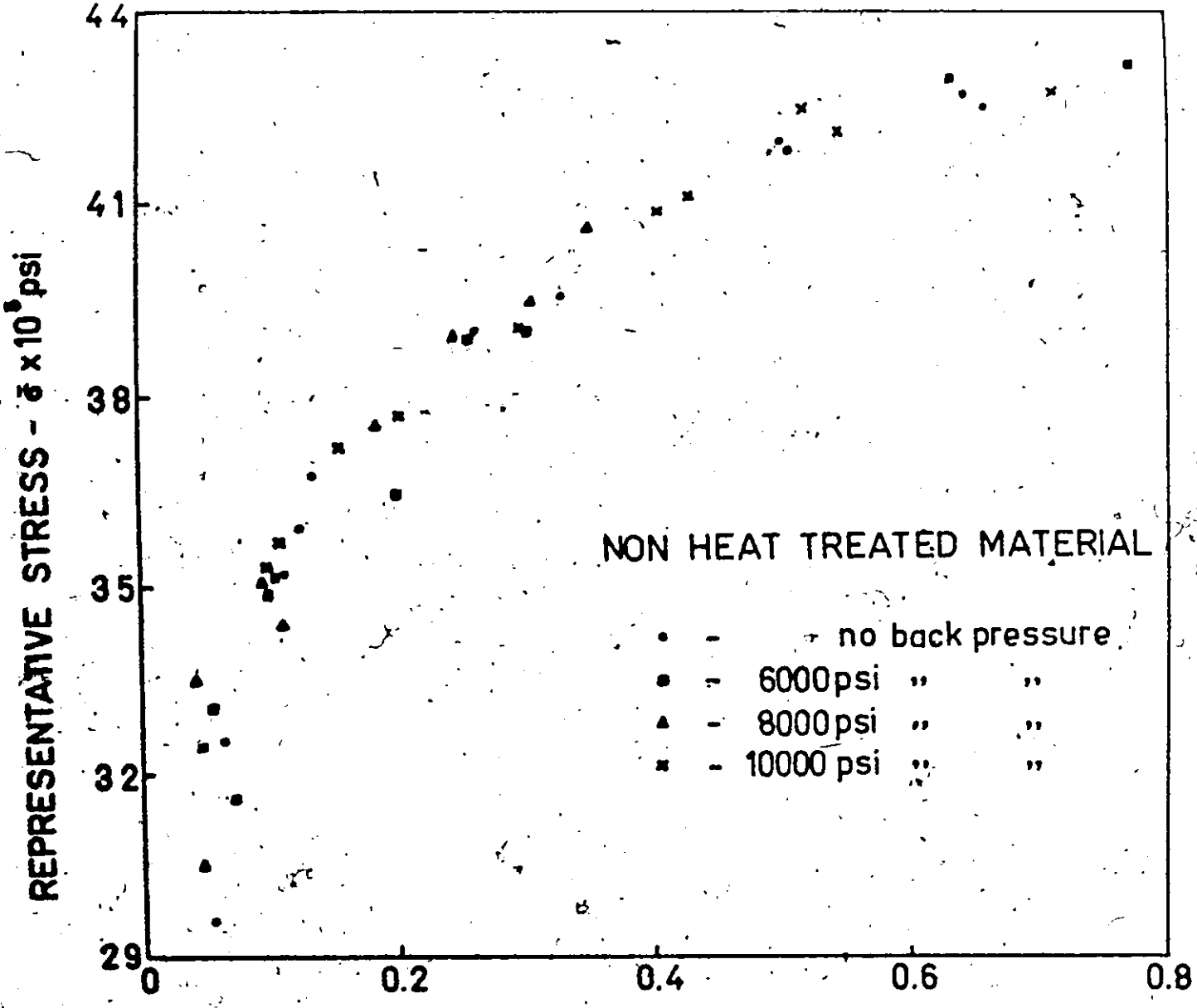

FIG. 3.18 REPRESENTATIVE STRAIN '$\bar{\varepsilon}$'

between the two materials. The pressure differential vs the polar thickness strain plots are as shown in Figs. 3.17 and 3.24.

b) Bulge Profile

The polar height vs polar radius of curvature plots are as shown in Figs. 3.14 and 3.21. On superposing the two plots we see that they are identical, thus verifying their independence from the properties of the metal. To check if the radius of curvature varies with θ, the radius of curvature for $\theta = 0^{o}$ and 90^{o} was measured at the pole for each stage of the bulging. It was observed that at the initial stages of bulging, ρ was constant for the two directions but, at stages near and beyond the point of instability, there was a variation in the values of ρ_0 and ρ_{90}. This variation however was not consistent and was in the maximum range of about 5%. For calculation purposes, the average values were used, and due to the very small variation it could be concluded that, the bulge profile is symmetrical. From measurements it was also observed that the average radius of curvature decreases away from the pole in the early stages of deformation. It becomes constant in the middle stages and increases away from the pole at strains near the instability point. Similar observations have been made by other workers.

If the bulge obtained from the bulge test was a segment of a sphere, then for a spherical bulge of height h, the thickness strain ε_t is given by Equation 3.2.

• - Non Heat Treated Material
× - Heat Treated Material
} no back pressure

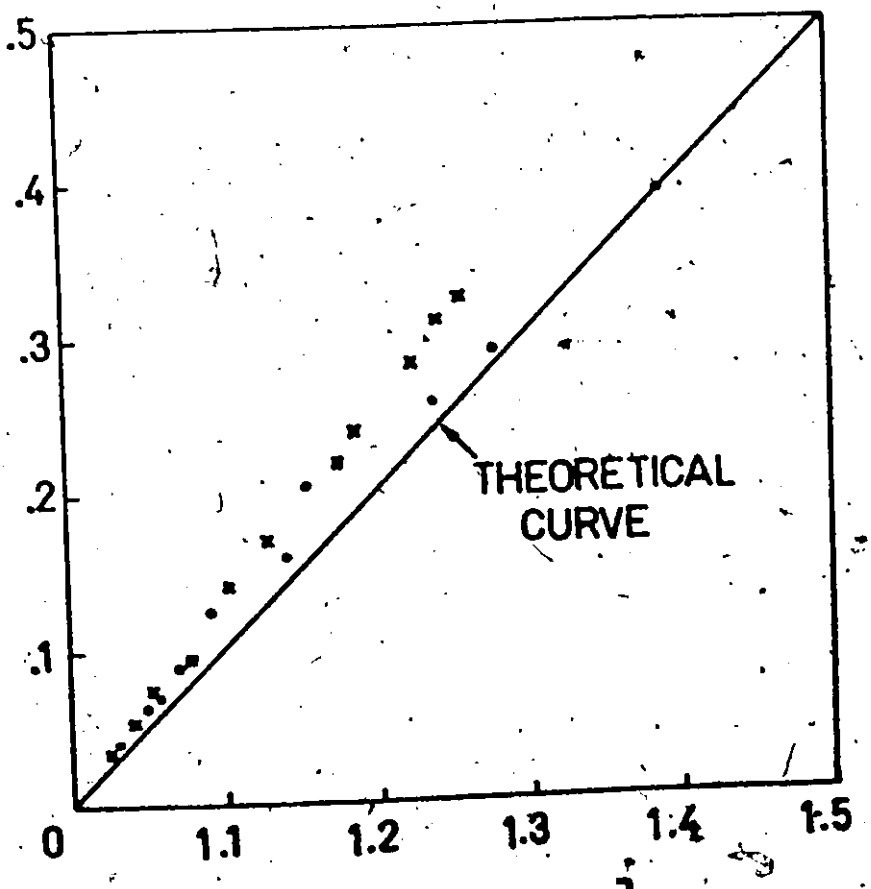

FIG. 3.19

$$\varepsilon_t = \varepsilon_3 = 2 \ln \left(1 + \frac{h^2}{a^2}\right)$$

which can be written as

$$\left(\frac{h}{a}\right)^2 = \left[\text{Exp}\left(\frac{\varepsilon_t}{2}\right) - 1\right]$$

If the bulge is a sphere, the experimental points of $\left(\frac{h}{a}\right)^2$ vs $\left[\text{Exp}\left(\frac{\varepsilon_t}{2}\right) - 1\right]$ should fall on a straight line inclined at 45^0. The theoretical and experimental plots for the two materials are as shown in Fig. 3.19. The differences are clearly apparent. It may be concluded that the bulge is a spherical segment only near the pole.

c) Representative Stress-Strain Curve

It was mentioned in Chapter II, section 2.6, that the effect of anisotropy on the representative stress and strain from the tensile test was less than fifteen percent and hence the calculations were carried out according to Equations (2.15) and (2.16). Similarly the representative stress and strain values for the bulge test at various back pressures were calculated according to Equations (3.31) and (3.32) and the plot is as shown in Figs. 3.18 and 3.25. A least square curve was fitted to the data obtained. The values of A and n, thus obtained are as shown in Table 3.1. It was observed that the values of A and n were practically constant for all back pressures (i.e., p_o = 0, 6,000, 8,000 and 10,000 psi). Hence all the points were

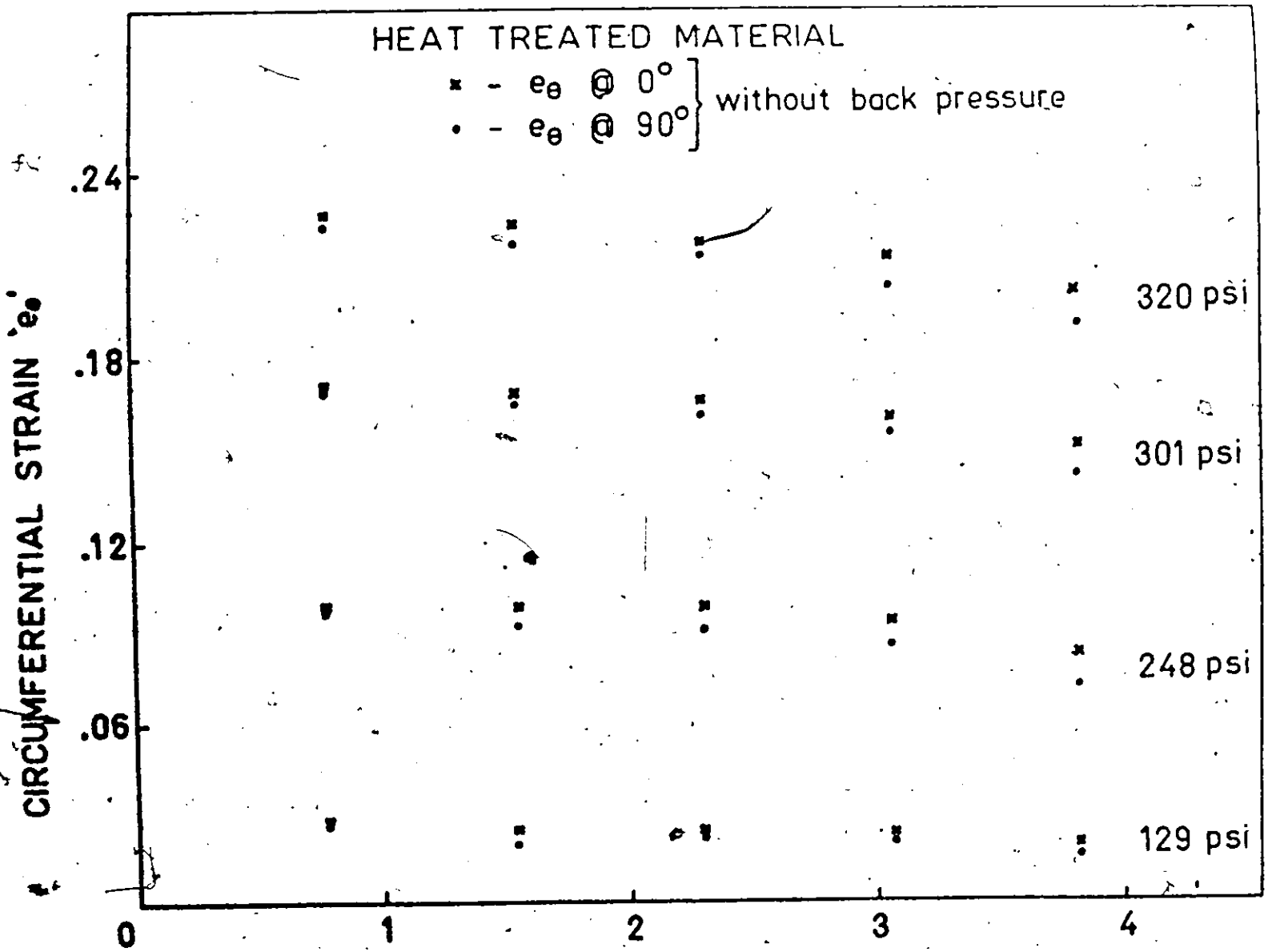
HEAT TREATED MATERIAL
× - e_θ @ 0°
• - e_θ @ 90°
without back pressure
CIRCUMFERENTIAL STRAIN 'e_θ'
.24
.18
.12
.06
320 psi
301 psi
248 psi
129 psi
0
1
2
3
4
CURRENT DIAMETER

FIG. 3.20

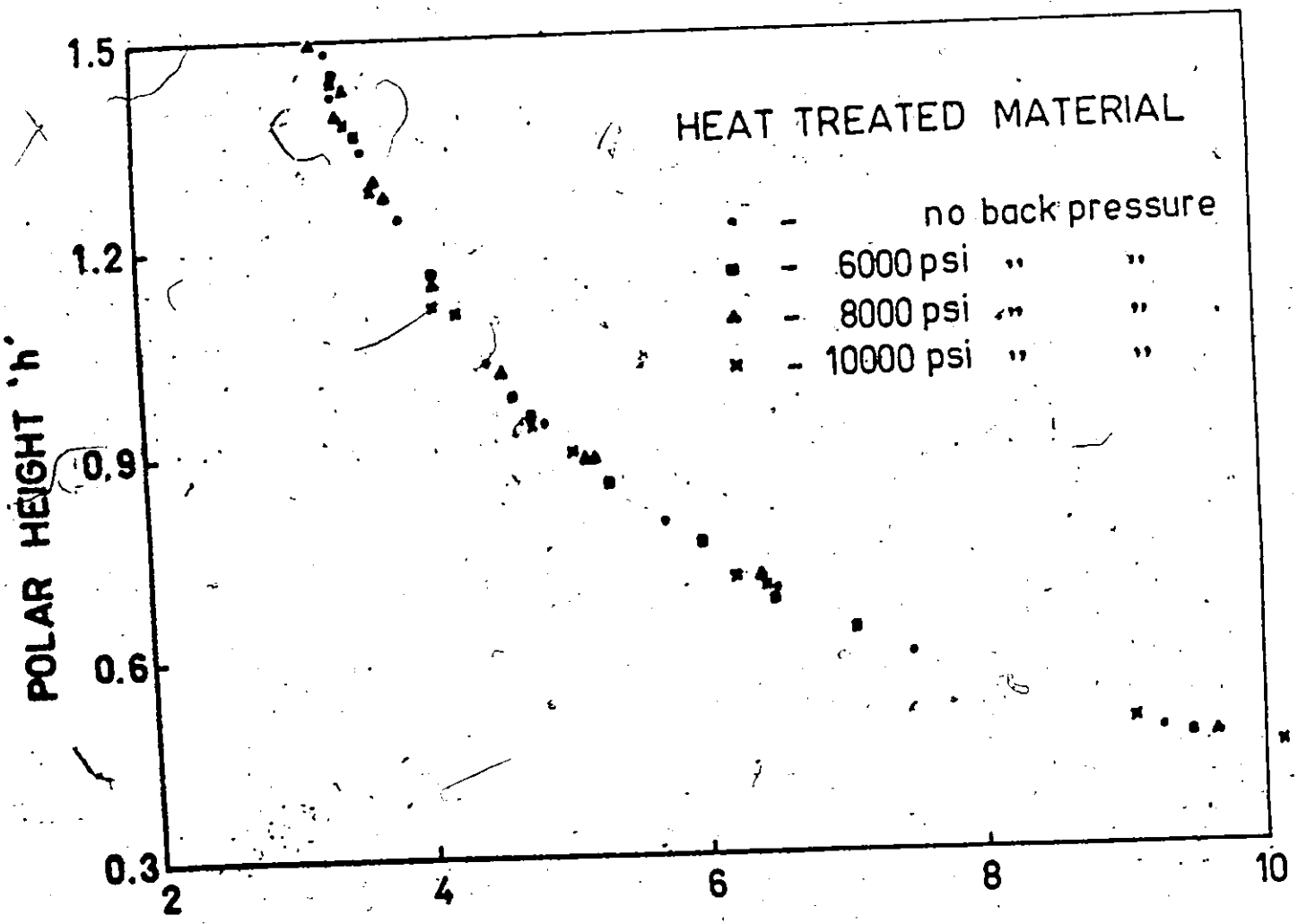

FIG. 3.21 POLAR RADIUS OF CURVATURE 'P'

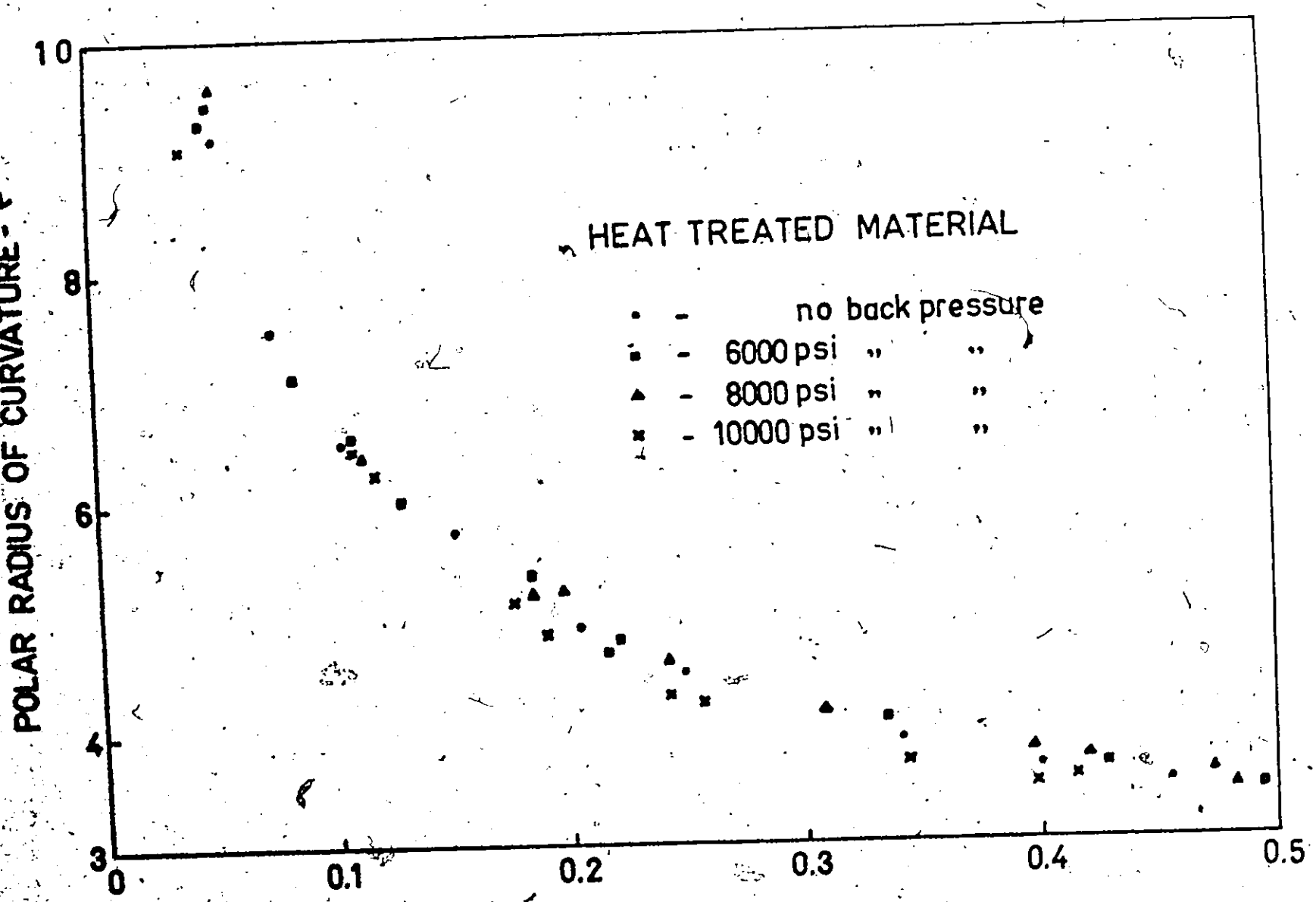
HEAT TREATED MATERIAL
• - no back pressure
▪ - 6000 psi " "
▲ - 8000 psi " "
× - 10000 psi " "
POLAR RADIUS OF CURVATURE - 'ρ'
10
8
6
4
3
0
0.1
0.2
0.3
0.4
0.5
POLAR THICKNESS STRAIN 'εt'

FIG. 3.22

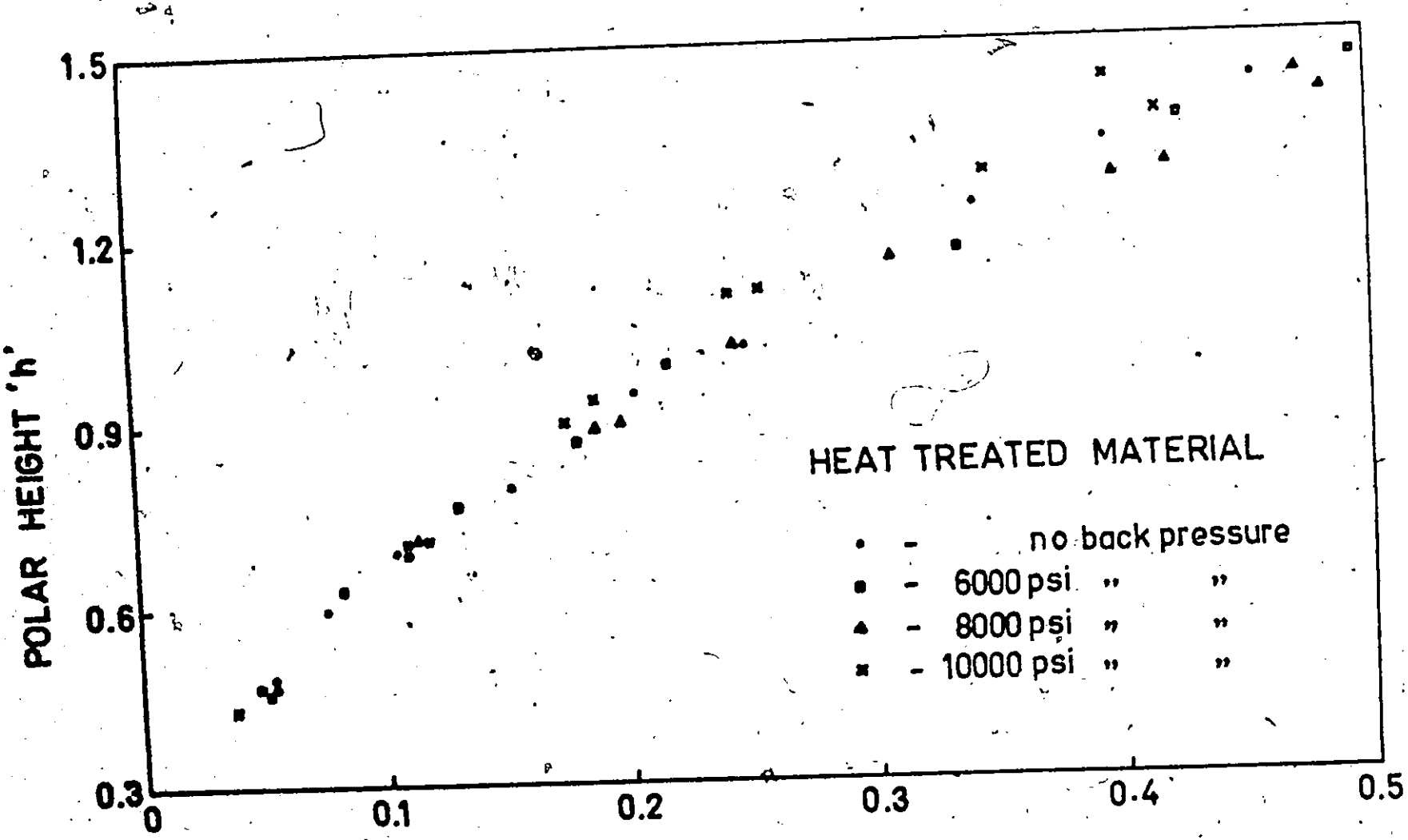

FIG. 3.23 POLAR THICKNESS STRAIN 'ε_t'

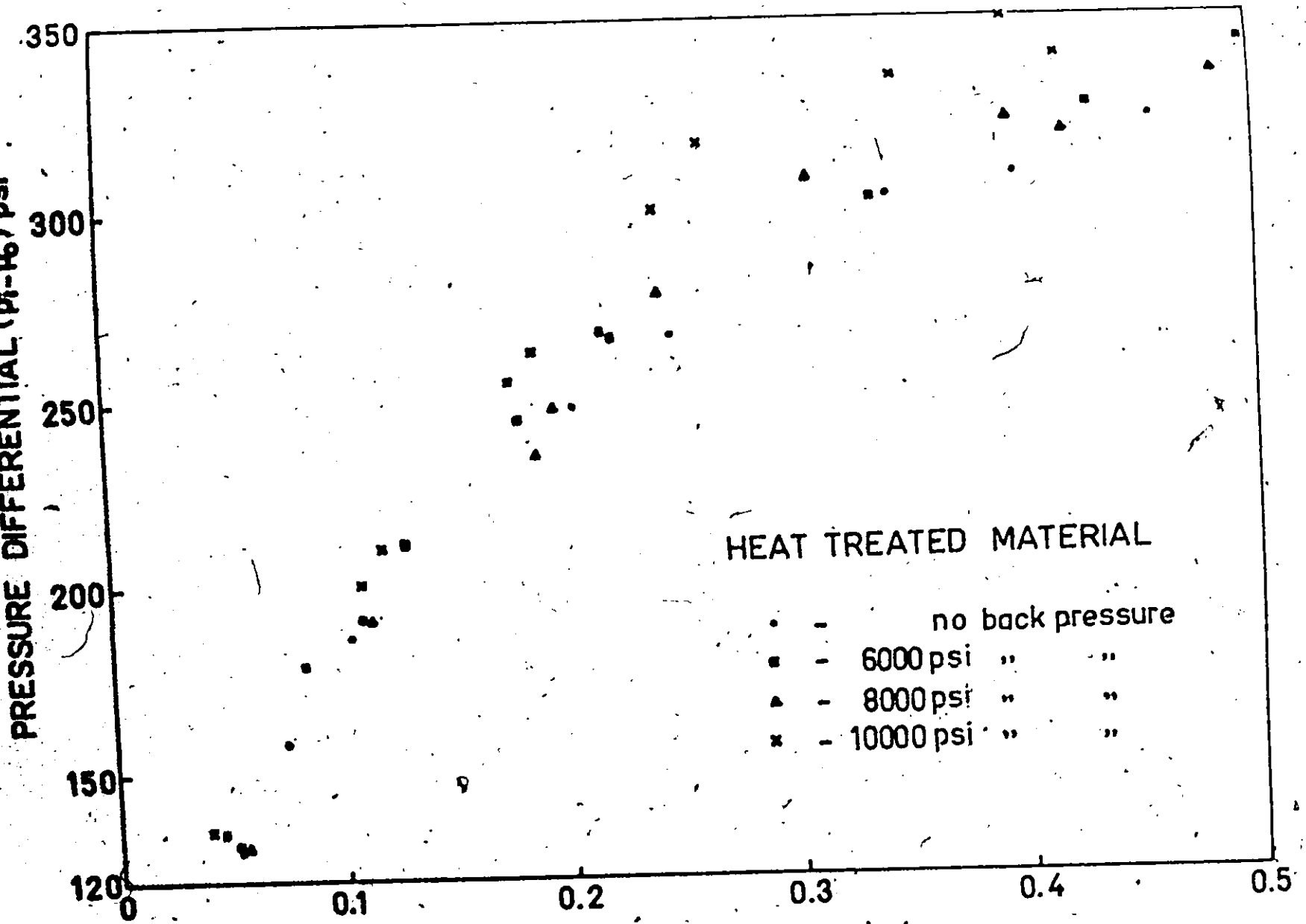
350
300
250
200
150
120
0
0.1
0.2
0.3
0.4
0.5
PRESSURE DIFFERENTIAL ($p_i - R_o$) psi
POLAR THICKNESS STRAIN 'e_t'
HEAT TREATED MATERIAL
• – no back pressure
▪ – 6000 psi " "
▲ – 8000 psi " "
× – 10000 psi " "

FIG. 3.24

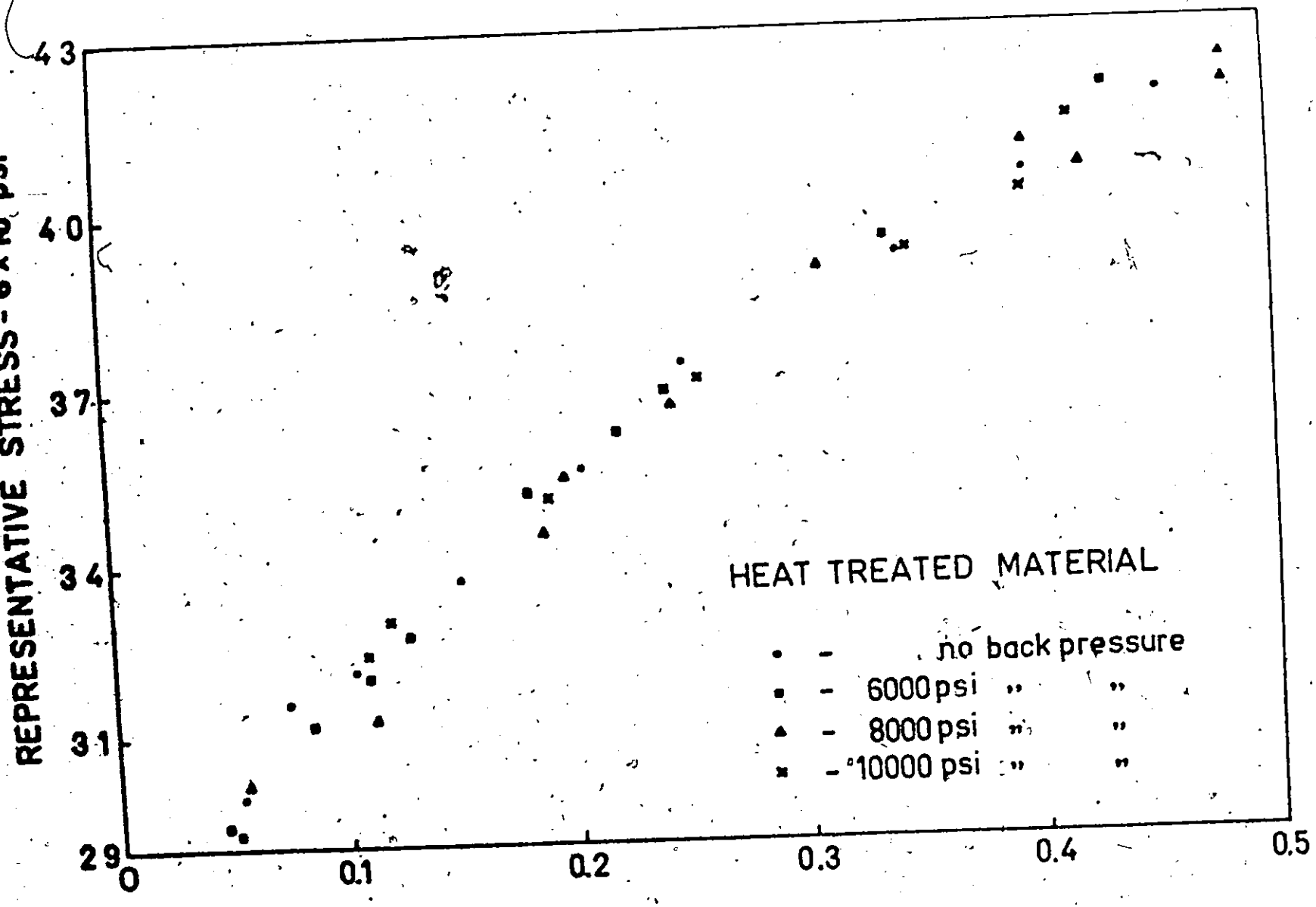
REPRESENTATIVE STRESS - $\bar{\sigma} \times 10^3$ psi
4.3
4.0
3.7
3.4
3.1
2.9
0
0.1
0.2
0.3
0.4
0.5
REPRESENTATIVE STRAIN '$\bar{\varepsilon}$'
HEAT TREATED MATERIAL
• – no back pressure
■ – 6000 psi " "
▲ – 8000 psi " "
× – 10000 psi " "

FIG. 3.25

Table 3.1

The Constants A and n for the Two Materials as Determined from the Bulge Test

Material	A kpsi	n
Non-Heat-Treated	21	.112
Heat-Treated	15	.169

Table 3.2

The Constants A and n for the Two-Materials as Determined from the Bulge Test Using the Bi-axial Test Equipment (Figure 3.10).

Material	A kpsi	n
Non-Heat-Treated	21.75	.096
Heat-Treated	14.75	.155

pooled together and one average value of A and n obtained for the specific material under consideration. The A and n values as obtained by the biaxial test equipment (Fig. 3.10) using the extensometer in conjunction with the spherometer are as shown in Table 3.2 and are in fairly good agreement with the values shown in Table 3.1. Note, this equipment provides no back pressure and thus merely provides a comparison for the bulging behaviour in different diameter dies. On comparing the values of A and n in Table 3.1 to those given in Table 2.3 and Table 2.4 to check if there is any difference in the curves obtained from the bulge test to that of the tension test, it is observed that:

i) for the non-heat-treated metal the A value obtained from the bulge-test is significantly lower than all three values obtained from the tensile tests for the various directions of rolling. Also that the n value from the bulge-test is significantly higher than those obtained from the tension tests.

ii) for the heat-treated metal, the A value obtained from the bulge-test agrees only with one A value of the tension test for $\theta = 0^{o}$, and is significantly different to the other two tension test values. Also, that the n value from the bulge test is close to the n value of the tension test for $\theta = 0^{o}$ but is much higher than the other two values of θ of the tension test. Thus we may conclude that the $\bar{\sigma} - \bar{\varepsilon}$ curve obtained from the

tensile tests and the bulge tests for the two materials are not unique.

Errors in Bursting Test

A few remarks are made here about the source of errors in the tests with back pressure. The only major source of error experienced was the measuring and recording of the maximum pressure differential during the tests. The pressure differential had to be created by closing the valve V_1 (Fig. 3.2) slowly, after having adjusted V_2 to the required back pressure. The relief valve V_2 not being too sensitive, and due to the heating of the oil while flowing past the relief valve, at times a sudden excessive opening of the relief valve was experienced causing a sudden jump in the pressure differential, thereby throwing off the readings. This error was overcome to a great degree by letting the oil cool down between the stages of bulging and also repeating the bulge test in the neighbourhood of the wrong readings. A better way of reducing this error and problem would be the incorporation of a more sensitive pressure relief valve.

CHAPTER IV
CONCLUSIONS

An attempt has been made to study the effects of superimposed hydrostatic pressures on the stress-strain characteristics of zinc and zinc alloy sheets via the circular bulge test. The original theory of Kular [6] has been simplified, and as presented in chapter 3.2., predicts that a superimposed hydrostatic pressure does not influence point of instability, whereas Pugh [12] in his experimental investigations with some hexagonal packed metals demonstrated an existance of a sudden pressure induced transition from brittle to ductile behaviour. Hence the decision to run these experiments.

The main conclusions on the sheets tested were:

1. Superimposed pressures did not influence pressure differential or strain at instability. i.e. no influence on the representative stress-strain curve over the pressure ranges investigated (10,000 psi maximum).
2. The difference in behaviour between the materials tested were as follows:
   (a) The zinc sheet in the preliminary stages of investigations turned out to be defective (localized grooves appearing across the bulged sheet in the direction of rolling very early in the process). Hence further tests on this sheet were abandoned.

(b) Comparison between the non-heat treated and heat treated alloy sheet indicated no great degree of difference in the bulging behaviour. (The producer claimed that the heat treatment of the alloy reduced the grain size thereby increasing the strength and ductility of the sheet. Since the results did not verify this, it was decided to do some preliminary metallurgical work described in Appendix I. The tests did tend to confirm that the heat treatment was incomplete). The non-heat treated sheet indicated a slight degree of instability before fracture while the heat treated sheet fractured under increasing load. But this again was not very significant. A more in-depth comparison is as provided in Chapter 3.5.

3. Tensile tests showed "R" values less than 1, implying a low through thickness strength. Also a great degree of variation of "R" value in the plane of the sheet, indicating a high degree of planar anisotropy. (The pole figures Figs. 2, 3, and 4, Appendix I also tend to confirm planar variations. Based on the work of Robert and Rogers [22], assuming ideal textures a very simple calculation is given in Appendix I, by which R values can be estimated for zinc. However, a

much more complicated technique would be required in the case of the sheets tested in this project since the textures were far from perfect).

4. It is possible to introduce the anisotropic parameters (as measured) into the bulging analysis. However, as mentioned earlier in the text, this complicated the algebra without radically altering the stress-strain characteristics.

5. The load-extension curve as obtained from the tensile test indicated a rather unusual behaviour. i.e. a load maximum was attained without any observable neck developing, and from this point the load extension curve was rather like super-plastic alloys with deformation under a falling load. No pronounced necking was visible in this region until just prior to fracture. The A and n values were found from the tensile test data and are as reported in Tables (2.3) and (2.4) respectively. However, up to the point of maximum load plastic strains were rather small and really not very accurate for the A and n value determination, to extend a linearized fit beyond maximum load is questionable (since constant volume assumption is employed) as we are not sure of what is going on in the material. Hence it would be worthwhile studying this in further depth if such

materials are to be used commercially since it could have implications with regard to creep resistance.

6. The A and n values for the materials were also computed from the bulge test data for tests with and without back pressure and are as reported in Table (3.1). The values thus obtained are more reliable than those obtained from tensile tests as the bulge test is capable of inducing much higher plastic strains without instability. For purpose of comparison some tests were also run on the biaxial test equipment as described earlier in the text, and the A and n values thus obtained are reported in Table (3.2). Correlation of the values of Tables (3.1) and (3.2) as obtained from the two dies of different bulging diameters and measuring techniques is very close.

Final Comments

Use of superimposed fluid pressure to enhance the useful formability was not realised. (at least over the pressure range invistigated - 10,000 psi).

There has been great thrust by producers of zinc and zinc alloys to break more into the non-ferrous market and to compete with aluminium in sheet metal work. Present materials form well enough and in this respect would be comparable with aluminium. the price per pound is also attractive: (ratio - approx. 1:1 in bulk quantity) but strength requirements fall short of expectation. (maximum of 40-45 kpsi tensile strength for zinc alloys as compared

to a maximum of 80-90 kpsi for aluminium alloys). The biggest disadvantage of zinc and zinc alloys being the lack of joining techniques. They can be rivited or soft soldered only whereas aluminium and its alloys can be readily welded without too many complications.

APPENDIX I

As mentioned in the previous chapters, it was decided to test commercially pure zinc and two zinc alloys. The prime reason for the choice of zinc and its alloys as test metals was the fact that some hexagonal packed metals have exhibited sensitivity towards pressure effects. Since zinc and the two alloys fell in this class it was decided to test the same.

The suppliers of the above mentioned metals in sheet form were Matthiessen and Hegeler Zinc Company of La Salle, Illinois. Being a trade secret no information was received from the supplier as to the heat treating procedure of the Heat-Treated zinc alloy. The only comments received were "that the heat treatment made the grain size smaller, thereby increasing the ductility of the material as compared to the Non-Heat-Treated material". On carrying out preliminary tests on the sheets received, it was found out that:

1. The commercially pure zinc sheet was defective and failed prematurely.
2. The Heat-Treated alloy was less ductile than the Non-Heat-Treated alloy.

Thus it was decided to take a brief look into the microstructure of the metals to see if the discrepencies observed at the various stages of experimentation could be accounted for.

Textures in Zinc

It is well known that hexagonal metals in sheet form exhibit

a marked degree of plastic anisotropy. This follows from the fact that plastic anisotropy is associated with the disposition of shear systems relative to the stress axes, and hexagonal metals have a smaller number of slip systems than cubic metals. In zinc the resolved shear stress to effect slip is the smallest on the (0001) plane, the so called basal plane. However, if the Basal plane is unfavourably orientated with respect to the applied stress system, slip can certainly occur on the Prismatic $(10\bar{1}0)$ plane and the Pyramidal $(10\bar{1}1)$ plane. A feature of many hexagonal metals is that deformation can readily occur by twinning, and in zinc this generally occurs on the $\{10\bar{1}2\}$ planes. (Note: explanation of the symbols (0001), $\{10\bar{1}2\}$ etc, known as the Miller indicies can be found in Physical Metallurgy text books such as Reed-Hill [23]. The twinning phenomenon complicates any crystallographic study since the crystal distribution is continuously changing as twinning takes place. It is fair to say that there is a great deal of scope in improving the understanding of texture/mechanical property relationship in hexagonal materials. In what follows a very simple treatment of relating material properties with texture is discussed, this is based entirely on ideal orientations (or textures) without the complicating influence of twinning. Certainly no claim is made that the method could be applied to complicated textures but, that such an approach might reveal certain features about mechanical behaviour and used as an indicator for more complex situations. If the material slipped only on (0001), $(10\bar{1}1)$ or $(10\bar{1}0)$plane in the $\langle 2\bar{1}10\rangle$ direction.

there would be no thinning (or strain of any kind) perpendicular to the basal plane.

For a rolled sheet of zinc, an ideal rolling texture would be where all the basal planes lie in the rolling plane with $[10\bar{1}0]$ in the rolling direction. This would be known as a (0001), $[10\bar{1}0]$ rolling texture. If a pole figure was taken for this ideal texture for the (0001) basal plane, only a black dot would show up at the centre of the figure. Conducting tests in the rolling direction or transversedirection would give infinitely high "R" values for this type of texture, since no thinning would take place in the thickness direction. (This is quite contrary to the values indicated by the experiments R = .2 to .6). Furthermore in this case slip would not occur on the basal plane even though it would normally be the easiest to slip on. This arises because of the unfavourable orientation with respect to the pulling direction and is explained by Schmid law

$$\sigma = \frac{\tau}{\cos \phi \cos \lambda} \qquad (1)$$

where

τ is the critical resolved shear stress on the given plane

σ is the tensile stress

ϕ and λ are respectively the angles between the slip plane normal and tension axes.

Therefore, for pulling in any direction in the plane of rolling ϕ is always 90° ($\cos \phi = 0$) if all the basal planes lie in the rolling plane.

Therefore

$$\sigma = \frac{\tau}{\cos \phi \cos \lambda} = \infty$$

Hence basal slip is unlikely and slip will occur on the pyramidal and prysmatic planes.

Since the ideal (0001) $[10\bar{1}0]$ rolling texture is rather unreal, the basal planes are more likely to be tilted towards the rolling direction at some angle say α. Then for tensile test in the rolling direction

$$\sigma = \frac{T}{\cos \phi \cos \lambda}$$

where

$$\cos \phi = \cos (90 - \alpha)$$

and for tensile test in the transverse direction

$$\cos \phi = \cos 90°$$

i.e. the basal plane normal is perpendicular to the transverse direction.

Hence $\sigma \to \infty$

Therefore, slipping will take place on other planes rather than the basal plane and hence transverse yield strength will be higher.

The shear strain on the active slip system can be resolved in any direction and it is possible to calculate "R" value from the formulae

$$R = \frac{\cos \phi_w \cos \lambda_w}{\cos \phi_T \cos \lambda_T}$$

where

ϕ_w and ϕ_T are the angles between the slip plane normal and the width and thickness directions respectively.

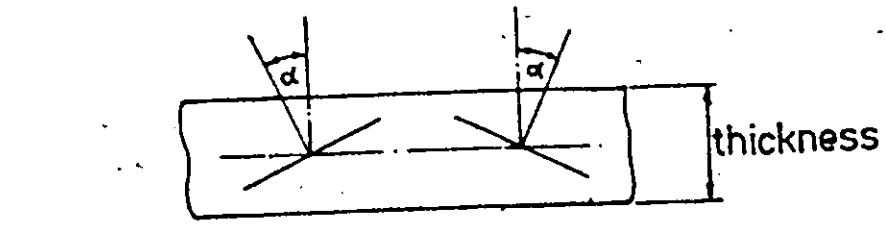
α
α
thickness

(a)

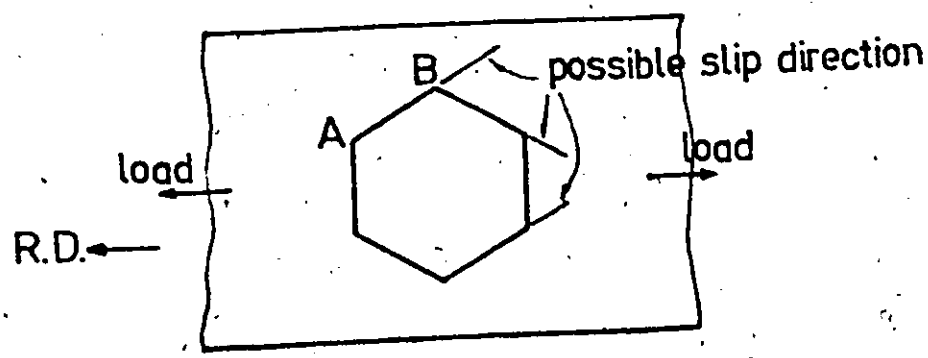
B
possible slip direction
A
load
load
R.D.

(b)

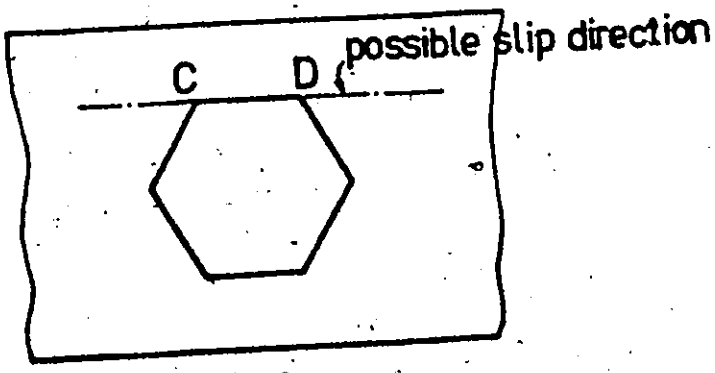
possible slip direction
C
D

(c)

FIG. 1.

λ_W and λ_T are the angles between the slip direction and the width and thickness directions respectively.

(The preceding approach has been used by Rogers and Roberts [22] for a particular ideal textured zinc sheet with surprisingly good results).

A approximate calculation based on ideal textures is performed to provide a means of theoretically computing the most favourable orientation of the basal planes to minimize the applied tensile stress.

Let α be the angle of tilt (Fig. 1. a). Assuming that the crystal rotation is as shown in Fig. 1.b., then considering direction AB, we have

$$AB = \{1^2 + (\frac{1}{\sqrt{3}})^2 + (\tan \alpha)^2\}^{1/2} = \ell \qquad (2)$$

The direction cosines are then

$$\frac{1}{\ell}, \frac{1}{\sqrt{3}\ell}, \frac{\tan \alpha}{\ell}$$

and the angle between AB and the rolling direction is

$$\cos \lambda = C_1 C_1' + C_2 C_2' + C_3 C_3'$$

where

C_1, C_2, and C_3 are the direction cosines of the rolling direction

C_1', C_2', and C_3' are the direction cosines of AB given by Equation (2)

Then

$$\cos \lambda = 1.\frac{1}{\ell} = \frac{1}{(1^2+1/3+\tan^2\alpha)^2}$$

The angle between the slip plane normal and the rolling direction is cos (90 - α) = sin α. Therefore, from Eqn. (1)

$$\sigma = \frac{T}{\cos \lambda \sin \alpha}$$

$$= \frac{(1\ 1/3 + \tan^2 \alpha)^{1/2}}{\sin \alpha} \cdot T$$

$$\frac{d\sigma}{d\alpha} = T \left[1/2\ (1\ 1/3+\tan^2\alpha)^{-1/2} \tan\alpha \sec^2\alpha - (1\ 1/3+\tan^2\alpha)^{1/2} \cos \alpha \right] / \sin^2 \alpha$$

on simplifying (3)

$$\alpha = 47°$$

Hence for α = 47°, σ should be minimum.

The other extreme orientation could be as shown in Fig. 1.c., in which case

$$CD = (1^2 + \tan^2 \alpha)^{1/2} = \ell$$

and on following a similar analysis as in the previous case, we get (4)

$$\alpha = 45°$$

Hence for α = 45°, σ should be minimum.

Pole Figures for the Three Materials Tested

Basal plane (0001) pole figures were taken for the three materials in the "as-received" condition and are shown in Figs. 2, 3, and 4. The numbers on the figures represent the increasing order of intensity of the basal planes i.e. 6 represents the

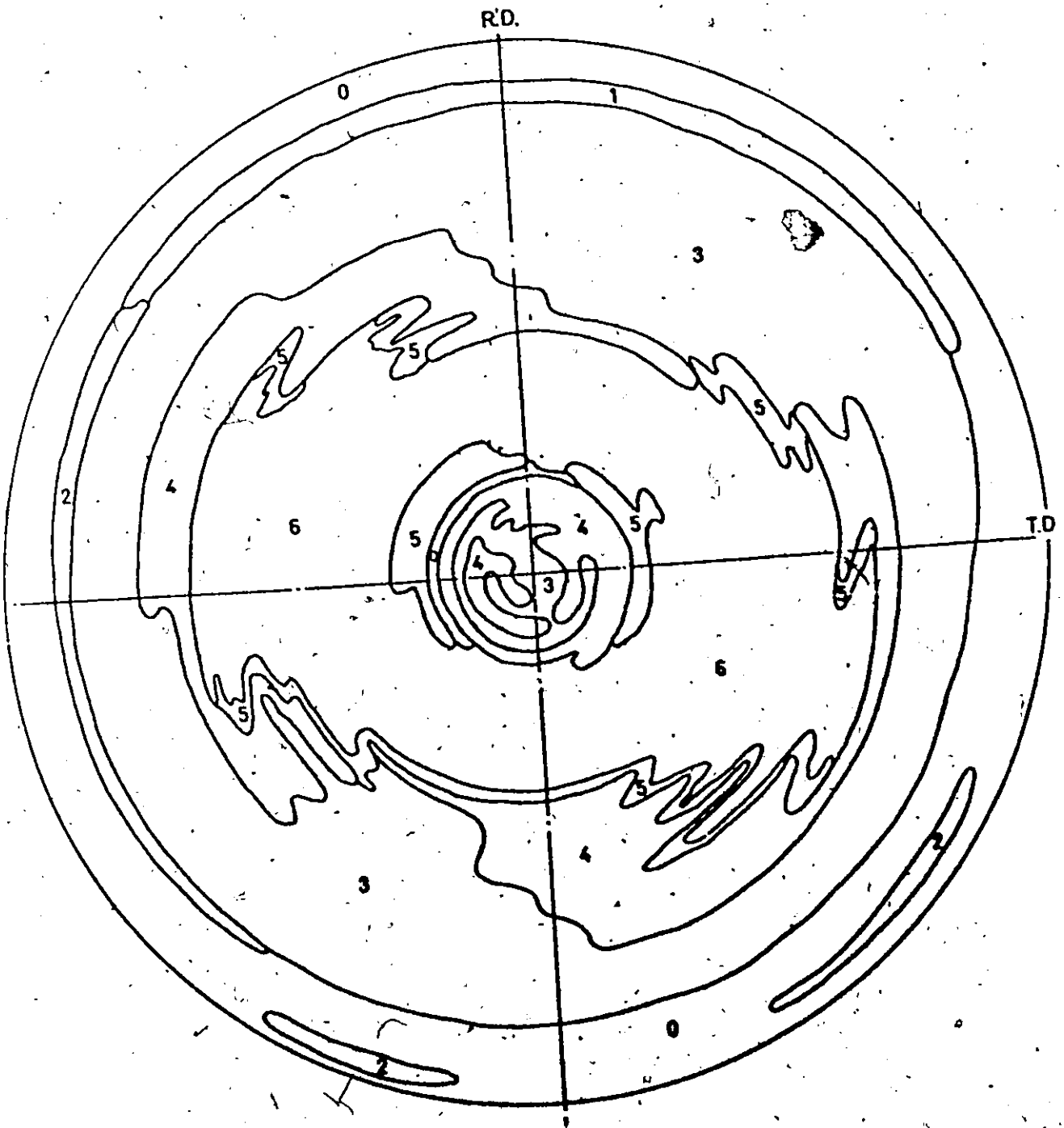

FIG. 2. POLE FIGURE FOR COMMERCIALLY PURE ZINC.

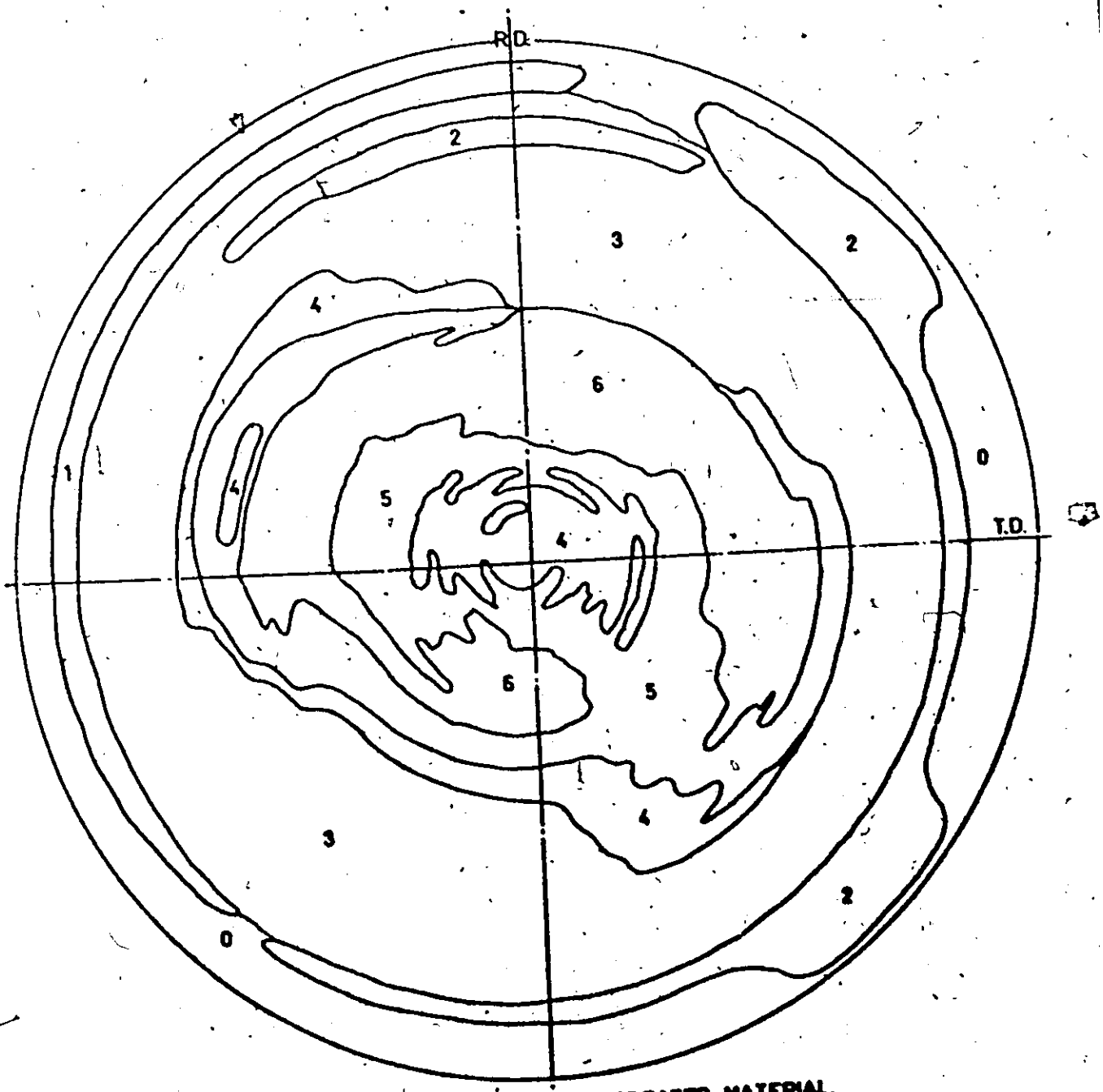

FIG. 3. POLE FIGURE FOR NON-HEAT TREATED MATERIAL.

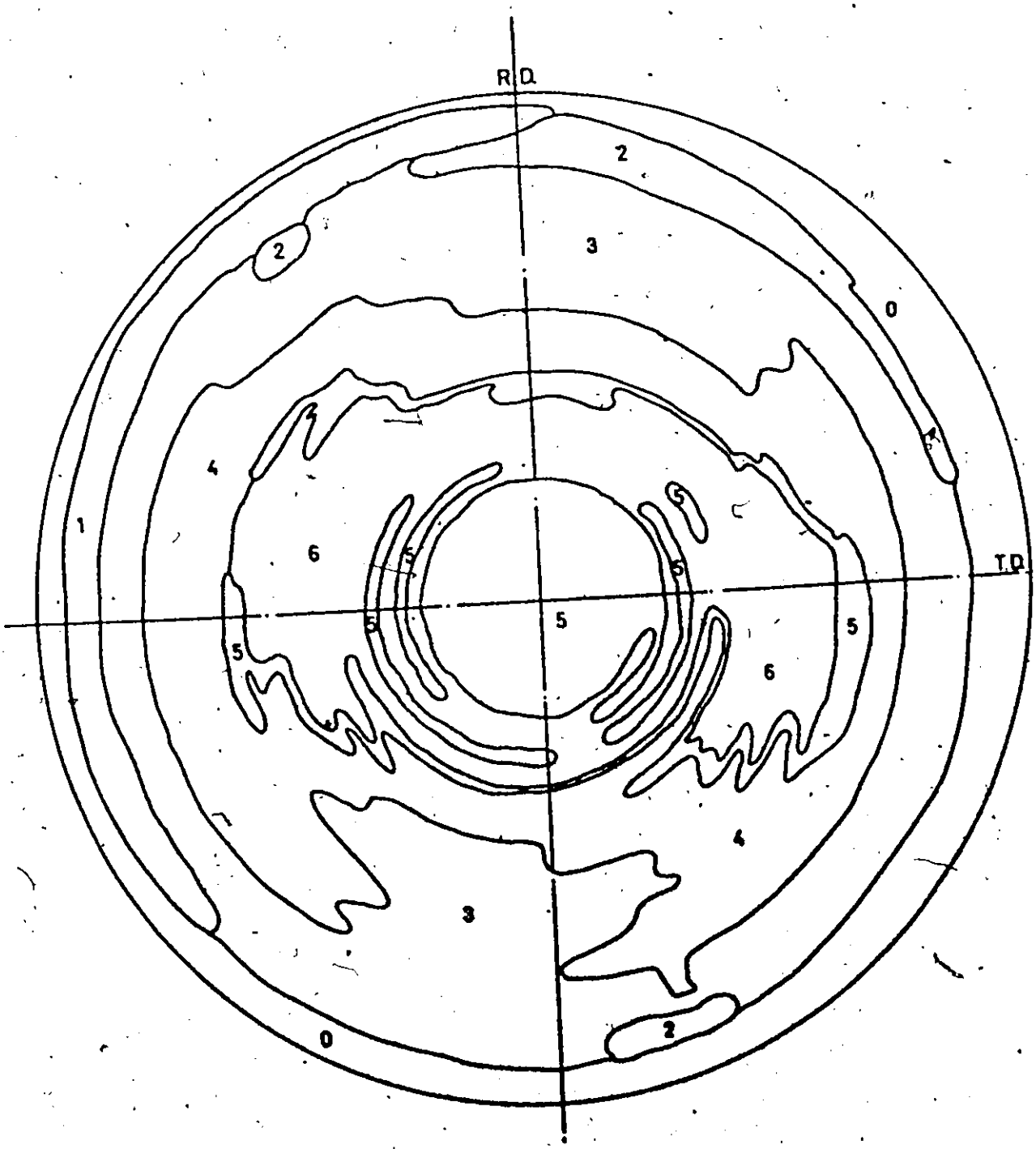

FIG. 4. POLE FIGURE FOR HEAT TREATED MATERIAL.

highest intensity area.

Note that the centre of these figures represents the normal direction of the plane of the rolled sheet. The rolling direction is indicated by R.D. and the transverse direction by T.D. Thus moving out in a vertical direction, on the diagram, from the centre to the extremity represents a rotation of 90° of the sample in the rolling direction. Similarly moving out along a horizontal line represents a 90° rotation in the transverse direction. The maximum intensity of the basal planes spreads more in the transverse direction than in the rolling direction and consequently it can be anticipated that the material will exhibit different material properties in these directions. However, to predict the difference in mechanical properties is complex in this instance since the observed textures are far from ideal.

A possible analytical technique for determining mechanical properties from textures lies in first establishing a three dimensional orientation distribution function of the crystallites and this goes beyond the scope of this present work.

What can be observed in the diagrams of the Non-Heat-Treated and the Heat-Treated alloys, Figs. 3, and 4 respectively, is that the heat treatment has only been a partial one. In other words there has not been a major alteration in the texture through heat treatment. (In the following section a brief discussion is provided of the photomicrographs taken of these samples, and these reveal further information regarding grain size etc.)

One could anticipate from the pole figure diagrams that the variation in mechanical properties of each of the zinc alloys would be similar in nature. For example, if the Non-Heat-Treated material showed a higher yield strength in the transverse direction as compared to the rolling direction, then the Heat-Treated material would show a similar behaviour. This was confirmed by the mechanical tests conducted on the materials and reported in the main text. The variation in "R" values and yield strength with orientation followed the same trend for each of the zinc alloys.

The analysis of the preceding section based on ideal textures, provided a means through which to compute the most favourable orientation of the basal planes to minimize the applied tensile stress. While these results are not strictly applicable to the present materials, since the textures are not ideal, it might be possible to use them in a qualitative manner to say something about the behaviour of the existing materials. From the pole figures of the zinc alloys it can be seen that a high intensity region of the basal planes does occur at approximately 45° orientation (in all directions) from the sheet normal. In this sense the basal planes would appear to be favourably orientated such that twinning would not be a major deformation mode. This was confirmed from the photomicrographs shown in the next section.

It was found impossible to provide a quantitative description of the mechanical properties using the simplified theory of the preceding section. As already indicated it requires a much more

sophisticated analysis to rationalize the correlation between non ideal textures and mechanical properties. Such a study would constitute a thesis project in its own right.

PHOTOMICROGRAPHS

A brief study of the microstructure of the sheets tested was undertaken to see if the variation of the experimental results obtained could be correlated from this study. For example, see if the defect in the zinc sheet could be detected from such an analysis and also at the same time to see why the results of the Heat-Treated Zinc alloy were contradictory to the suppliers comments i.e. "the heat treatment should have reduced the grain size and thereby increased the ductility of the sheet".

Metallographic specimens of the materials were prepaired in the as received condition i.e. sheets before testing, and of the sheets from the region of the pole of the bulge after failure in the bulge test. Typical micrographs are as shown in Figs. 5, 6, and 7.

Fig. 5 is a photomicrograph of zinc-surface parallel to the plane of the sheet-pole of the bulge-near premature fracture area. The study of this micrograph revealed no apparent faults in the microstructure except for the black streaks (lead strings) in the direction of rolling which perhaps could have been the source of premature failure (the specimen during the course of testing always failed prematurely along the direction of rolling at about 5-15% strain).

Figs. 6 and 7, are photomicrographs of the Non-Heat-Treated and Heat-Treated zinc alloys. A brief description with comparisons is as given below.

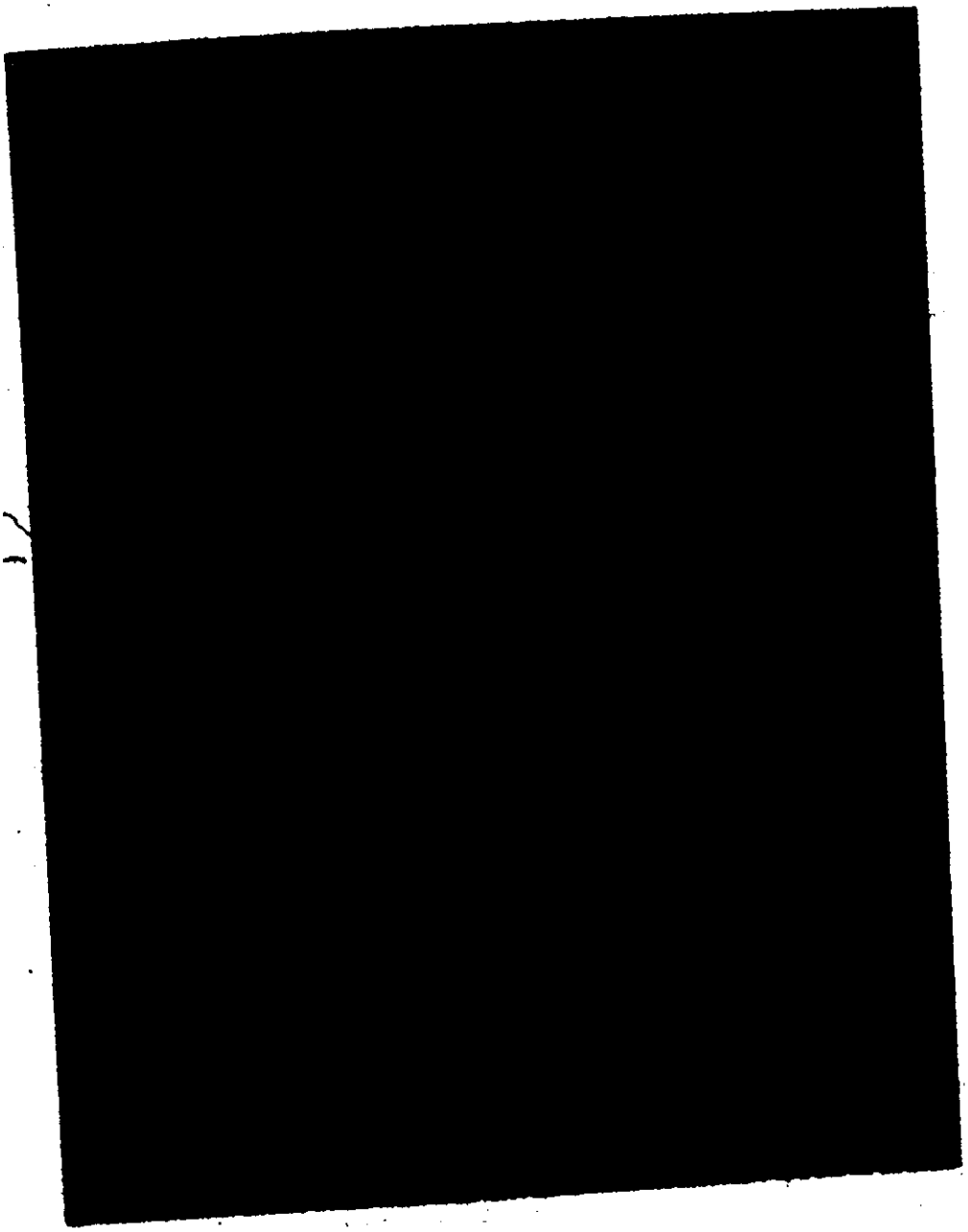

ZINC, MAGNIFICATION x 500.
SURFACE OF SHEET AFTER
BULGING.

FIG. 5.

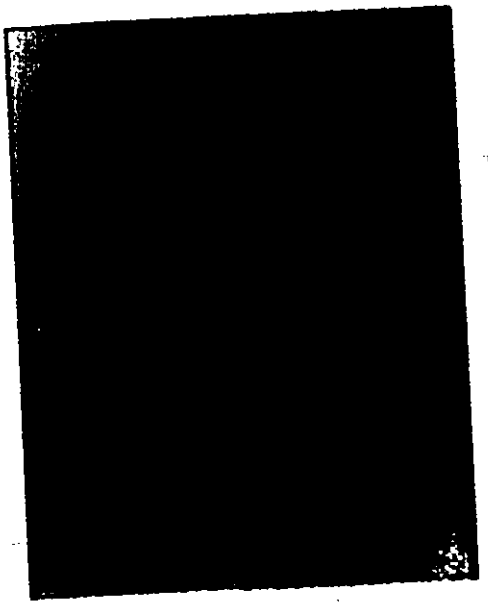

(a)
NON-HEAT TREATED ALLOY 'AS RECEIVED' - SURFACE OF SHEET MAGNIFICATION ×500

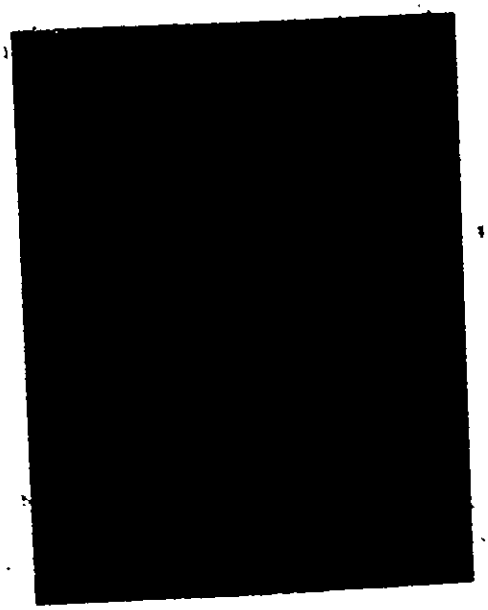

(b)
SAME AS (a) BUT TAKEN IN POLARISED LIGHT

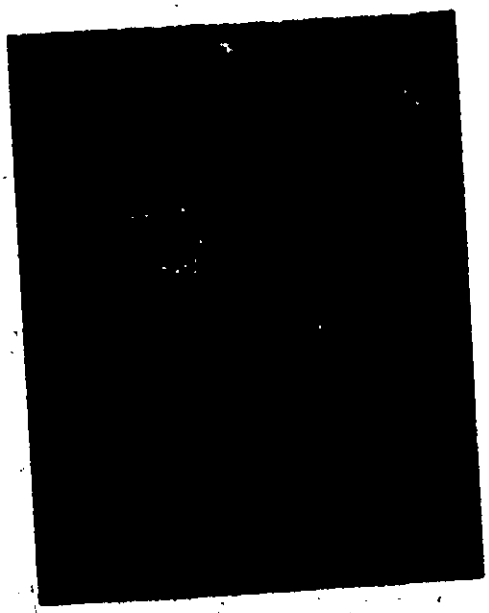

(c)
NON-HEAT TREATED ALLOY, SURFACE OF SHEET AFTER BULGING - MAGNIFICATION ×500

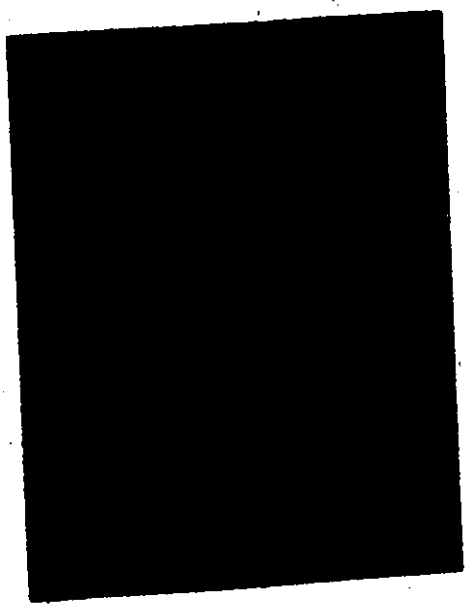

(d)
SAME AS (c) BUT TAKEN IN POLARISED LIGHT

FIG 6.

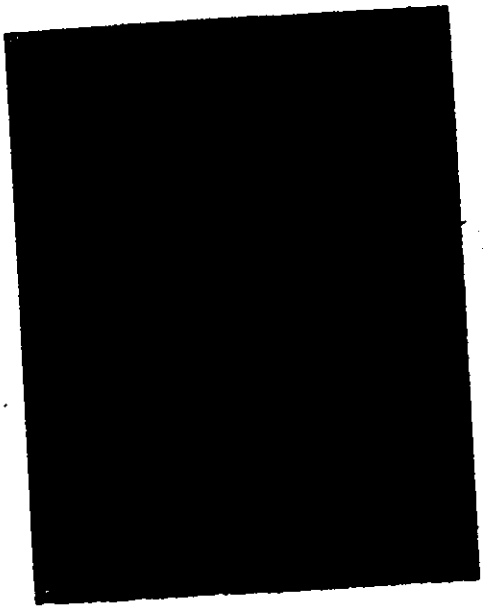

(a)

HEAT TREATED ALLOY 'AS RECEIVED'. SURFACE OF SHEET MAGNIFICATION ×500

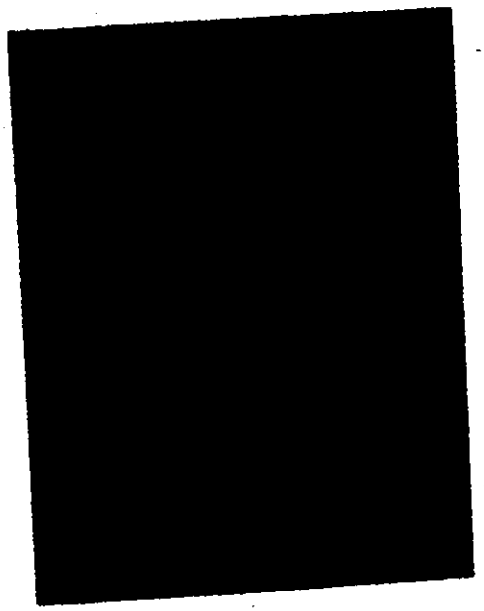

(b)

SAME AS (a) BUT TAKEN IN POLARISED LIGHT.

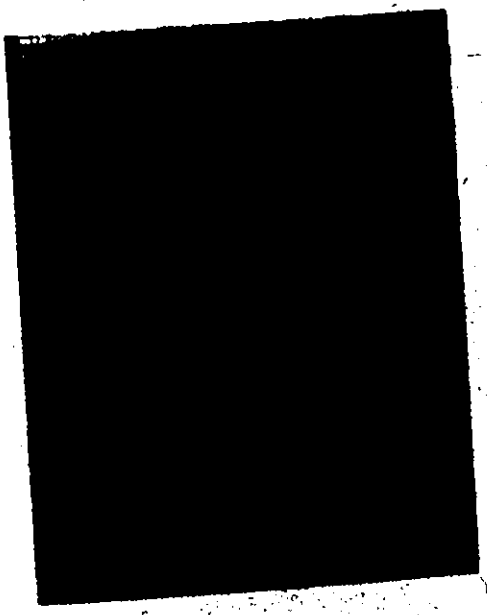

(c)

HEAT TREATED ALLOY, SURFACE OF SHEET AFTER BULGING. MAGNIFICATION ×500

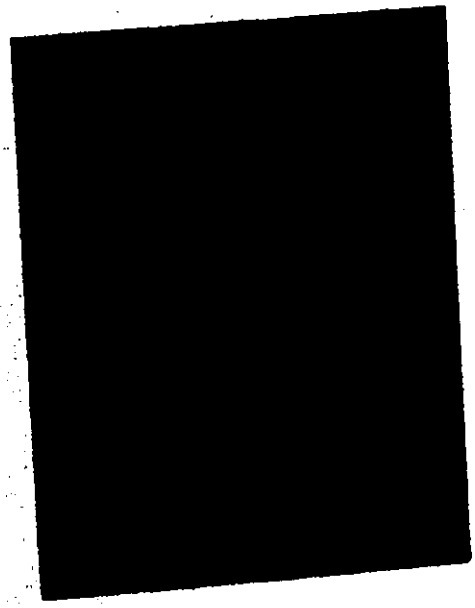

(d)

SAME AS (c) BUT TAKEN IN POLARISED LIGHT.

FIG. 7

Comparing Figs 6(a) and 7(a), the dark streaks and patches are T_iZ_{n15} which tends to limit the grain growth to distances between the steaks, and the rather grainy appearance of the two figures which is also revealed in Figs 6(b) and 7(b) is due to the Z_n-C_u phase in the zinc matrix [24]. Either the heat treatment of the material has been incomplete or to much copper is present. The copper is supposed to be redissolved into the solution on heat treatment and this has not happened. (The similarity of the pole figures, Figs. 3 and 4, also tend to confirm this partial heat treatment). The grain size is better revealed in Figs. 6(b) and 7(b). The grain size in Fig. 7(b) does seem to be smaller than Fig. 6(b) although there is not a significant difference as claimed by the producer. There is also a little evidence of twins in Fig. 6(b) and 7(b) no doubt due to rolling, but this again is not very significant.

On the photomicrographs of the deformed material at the pole of the bulge in Figs 6(c) and 6(d) it is rather difficult to detect the grain size, because of the very grainy appearance, but it is clearly evident that there is a lot more undissolved copper in the Non-Heat-Treated material as compared to the Heat-Treated material. (Difference is more prpnounced in Figs 6(d) and 7(d) as compared to Figs. 6(b) and 7(b). The grain size is clearly revealed in Figs 7(c) and 7(d) and the distances between the black streaks (T_iZ_{n15}) and the width of streaks themselves tend to be bigger in the deformed material as compared to the untested sheets, although the general shape of the grain is expected to be retained due to the biaxial stretching. Similar

effects of the T_iZ_{n15} are also revealed in Figs. 6(c) and 6(d) although there is lack of clarity in this case due to the grainy appearance. There is no significant evidence of further twinning in Figs. 7(c) and 7(d) and due to lack of clarity nothing is revealed in Figs. 6(c) and 6(d). The pole figures reveal the favourable orientation of the basal planes in the undeformed materials and although subsequent plastic deformation will result in some reorientation, it can be anticipated that twinning may not be significant.

References

1. American Society for Metals, Metals Handbook, Vol. IV, Forming, p. 239.

2. Goodwin, G. M., Society of Automotive Engineers, Paper No. 680093, 68.

3. Backofen, N. A., and Keeler, S. P., "Plastic Instability and Fracture in Sheets Stretched over Rigid Punches", Trans. A.S.M., 56, 25-48, 1963.

4. Marciniak, Z. and Kuczyncki, K., "Limit Strains in the Process of Stretch Forming Sheet Metal", Intl. J. Mech. Sci., 9, 609-620, 1967.

5. Sowerby, R. and Duncan, J. L., "Failure in Sheet Metal in Biaxial Tension", Intl., J. Mech. Sci., 13, 217-229, 1971.

6. Kular, G. S., "The Effect of Hydrostatic Pressure on the Onset of Instabilities in Biaxial Tension", Ph.D. thesis, University of Waterloo, 1971.

7. Bridgman, P. W., "Studies in Large Plastic Flow and Fracture", Harvard Univ. Press (1952) Second Ed., 1964.

8. Hillier, M. J., "Tensile Plastic Instability under Complex Stresses", Intl. J. Mech. Sci., 5, 57-67, 1963.

9. Hillier, M. J., "On the Tensile Instability of Orthotropic Plastic Materials", Intl, J. Mech. Sci., 7, 441-445, 1965.

10. Hillier, M. J., "The Effect of Pressure on the Ductility of Thin Sheet Subjected to some Simple Forming Processes", Intl. J. Prod. Res., 3, 341-352, 1964.

11. Pugh, H., Li, D., "Engineering Solids under Pressure", 1970.

12. Pugh, H., Li,D., "Mechanical Behaviour of Materials under Pressure", Elsevier Publishing Co. Ltd., 1970.

13. Sachs, G., Espey G., and Kasik, G. B., "Circular Bulging of Aluminium Alloy Sheet at Room and Elevated Temperatures", Trans. A.S.M.E., 68, 161-173, 1946.

14. Brown Jr., W. F. and Thompson, F. C., "Strength and Failure Characteristics of Metal Membranes in Circular Bulging", Trans. A.S.M.E., 71, 575-585, 1949.

15. Gleyzal, A., "Plastic Deformation of a Circular Diaphragm under Pressure", Trans. A.S.M.E. 70, 288-296, 1948.

16. Hill, R., "A Theory of the Plastic Bulging of a Metal Diaphragm by Lateral Pressure", Philosophical Magazine Series 7, 41 (322), 1133-1142, 1950.

17. El-Sebaire, M. G. and Mellor, P. B., "Prediction of the Limiting Drawing Ratio in the Deep Drawing of a Flat Headed Cylindrical Shell", 7th Biennial Congress of the International Deep Drawing Research Group, Amsterdam, 2.1-2.5, 1972.

18. Johnson, N. and Mellor, P. B., "Plasticity for Mechanical Engineers", D. Von Nostrand Co. Ltd., 1962.

19. Hill, R., "Mathematical Theory of Plasticity", Oxford University Press, 1950.

20. Albertin, P. H., "Development of the Biaxial Stress Test for Sheet Material, Master's thesis, McMaster University, 1972.

21. Baraya, G. L., et al., "Mechanical and Photographic Processes for Producing a Grid of Lines", Intl. J. Mech. Sci., 5, 365-367, 1963.

22. Rogers, D.H., and Roberts, W.T., "Plastic Anisotropy of Titanium and Zinc Sheet-II, Crystallographic Approach", Intl. J. Mech. Sci, 10, p. 221, 1968.

23. Reed-Hill, R.E., "Physical Metallurgy Principles", D. Van Nostrand Company, 1964.

24. American Society of Metals, Metals Handbook, Vol. 7, "Atlas of Microstructures", p. 339.